Miller Communications Systems Ltd.

PERFORMANCE OF NON-COHERENT FREQUENCY HOP/PSEUDONOISE SPREAD SPECTRUM

MARCH 1978

This work is Part I of a three-part study performed under DSS Contract No. OST.77-00094.

Miller Communications
Systems Limited
39 Leacock Way
Kanata, Ontario
K2K 1T1

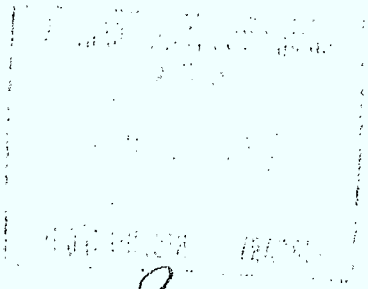

TABLE OF CONTENTS

LIST OF TABLES

LIST OF FIGURES

PERFORMANCE OF NONCOHERENT FREQUENCY HOP/PSEUDONOISE SPREAD SPECTRUM

1.0 INTRODUCTION

The signal design of a spread spectrum system requires tradeoffs between the possible types of antijam modulation, multiple access modulation, data modulation, and error-correction coding. Table 1 presents the choices for each portion of the signal design. While a large number of designs may be generated by taking various combinations, only a few designs are applicable to the given system objectives shown in Table 2. To determine the best signal design to meet these system objectives, Section 2 presents a general comparison of the signal design choices to illustrate under what conditions a given signal design is optimum. Finally, Section 3 presents a system design of the optimized signal.

Table 1. Spread Spectrum Signal Design Options

Antijam/Covert Modulation	Multiple Access Modulation	Data Modulation	Error Correcting Coding
Frequency Hopping (FH)	FDMA	PSK	Block
Time Hopping (TH)	TDMA	DPSK	Convolutional Binary Feedback Decoding
Pseudonoise (PN) DS	CDMA	DQPSK	Viterbi Decoding Binary
Hybrids	WBFH	MCSK	Dual-3 M-ary
FH/PN			
FH/TH	NBFH	MTSK	
FH/TH/PN			

Table 2. Summary of System Objectives

IF FREQUENCY ..... 70 MHz

SPREAD SPECTRUM BANDWIDTH .. 20 MHz

HOP RATE ..... 1000, 100, 50, 10 AND 5 Hz

PN CHIP RATE ..... 25 kHz

DATA RATES ..... 45.45, 50, 75, 110, 150, 300, 1200 AND 2400 bps

ERROR CORRECTION CODING .... NO LESS THAN RATE 1/2

ACQUISITION TIME ..... 15 sec AT S/J_o = 30 dB-Hz

2.0 SIGNAL DESIGN COMPARISONS

Antijam protection is achieved by signalling over a much larger bandwidth than required by the data rate. Frequency hopping can achieve very large antijam processing gain by hopping pseudorandomly over a very large bandwidth. Because the jammer does not have knowledge of which frequency is being used for the signal at any one time, the jammer must jam a large portion of the total bandwidth to ensure a reasonable probability of jamming the signal. Thus, frequency hopping achieves antijam processing gain by jamming avoidance. The synchronization for frequency hopping is a function of hop rate and not the total bandwidth over which the signal is hopped. Therefore, slow hopping requires modest hardware complexity and very modest synchronization accuracies. However, very slow frequency hopping is susceptible to a frequency tracking jammer that intercepts the transmission, performs a fast-frequency search over the total potential bandwidth, and jams a narrowband region around the intercept frequency.

Time hopping can achieve antijam processing by utilizing peak power over a short time slot which is pseudorandomly chosen from the average time between transmission equal to the inverse of the duty cycle. If the ratio of peak-to-average power is equal to the inverse of the duty cycle, then the antijam processing gain is equal to the number of time slots as the frequency hopping processing gain is equal to the number of frequency slots. It should be noted that since the number of time slots is just equal to the peak-to-average power ratio, it is the peak power capability that provides antijam protection. For large antijam processing gains, large peak power is required which is not applicable for satellite transmission.

2.1 Direct Sequency Pseudonoise Modulation

Pseudonoise provides antijam protection by averaging the jamming over its bandwidth. Pseudonoise is particularly effective against tone jamming since, after correlation at the receiver, the tone is converted to wideband noise which is essentially flat over the PN bandwidth R_c where R_c is the PN clock rate. After correlation at the receiver, the

signal bandwidth is reduced to a bandwidth R_b where R_b is the bit rate with a BPF around the despread signal bandwidth. The noise power at the output of the BPF is approximately NR_b/R_c, where N is the jammer power within the PN bandwidth. Thus, the noise power has been reduced by the factor R_b/R_c, which is the antijam processing gain. For extremely wideband interference with noise power spectral density, N_0, the noise power within the PN bandwidth is $N = N_0R_b$. Therefore, the input noise power at the BPF after PN correlation is N_0R_b. Thus, PN has no processing gain in a white noise environment.

Direct sequence PN spreading in conjunction with PSK data modulation is the most common spread spectrum system. The basic modulation is shown in Figure 1 wherein the modulo-2 addition of the PN code and the data biphase modulate an RF carrier. The transmitted signal has a $((\sin x)/x)^2$ spectral shape with the first nulls spaced $2/T_c$Hz apart, where T_c is the PN chip width.

The receiver for this system must acquire and track the PN code before carrier tracking and data demodulation take place. Referring to the receiver shown in Figure 1, a passive correlator is used to acquire the PN code to within a chip time and then an active correlator or a code tracking loop refines the delay estimate. The passive correlator is implemented with a tapped delay line matched filter with taps corresponding to the PN code over the initial time uncertainty. A matched filter can be implemented with either analog or digital devices as discussed in Appendix A. The disadvantage of matched filter acquisition is the relatively large complexity required for large antijam processing gain. Alternately, active correlation requires a search of the initial time uncertainty. For example, consider a simple serial synchronizer which tests each possible PN chip in the total initial time uncertainty to determine where the received PN signal align with the replica PN code in the receiver. Let the time to test each PN chip be denoted by T_s and let $T = 1/R_c$ be the duration of a PN chip. Figures 2 and 3 present[1] the ratio of T_s/T multiplied by the expected signal-to-jamming

Figure 1. Direct Sequence Pseudo-Noise Modulator/Demodulator

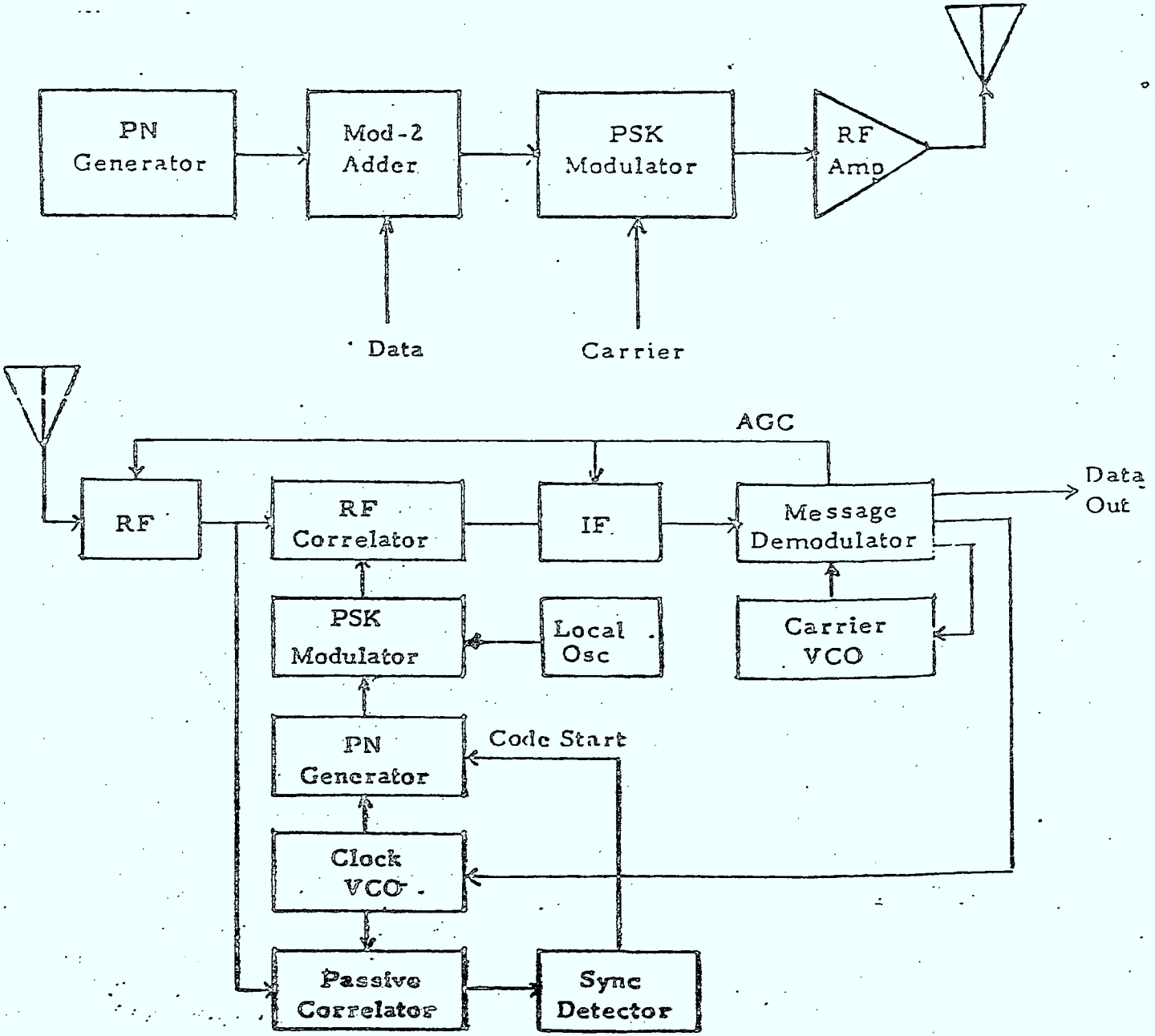

ratio (S/J) versus the probability of false dismissal P_{fd} and probability of false alarm P_{fa}. For example, let $P_{fa} = 10^{-6}$ and the probability of detection $P_d = 1-P_{fd} - 0.9$. Using noncoherent detection shown in Figure 3.

$$\left(\frac{T_s}{T}\right)\left(\frac{S}{J}\right) = 15 \text{ dB } (31.62) \qquad (1)$$

or

$$T_s = 31.62\ (J/S)\ T \qquad (2)$$

The total acquisition time T_A is equal to the number of chips in the initial time uncertainty T multiplied by the time to test each PN chip; thus,

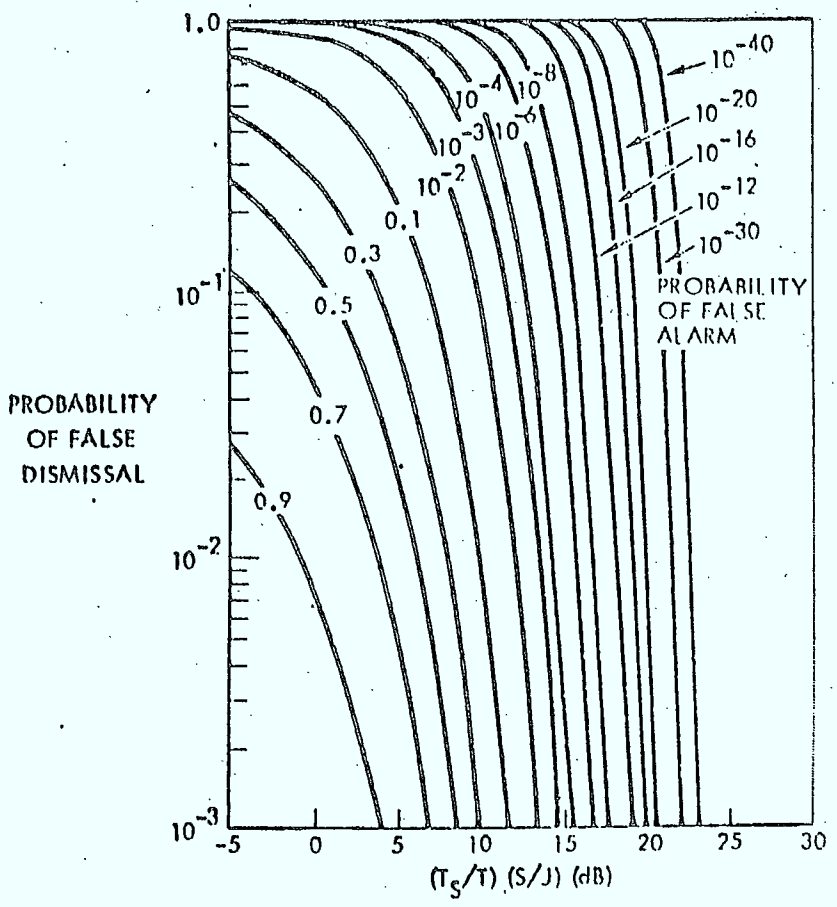

Figure 2. Coherent Detection of Synchronization

1. G.F. Sage, "Serial Synchronization of Pseudonoise Systems," IEEE Transactions on Communication Technology, December 1964, pp.123-127

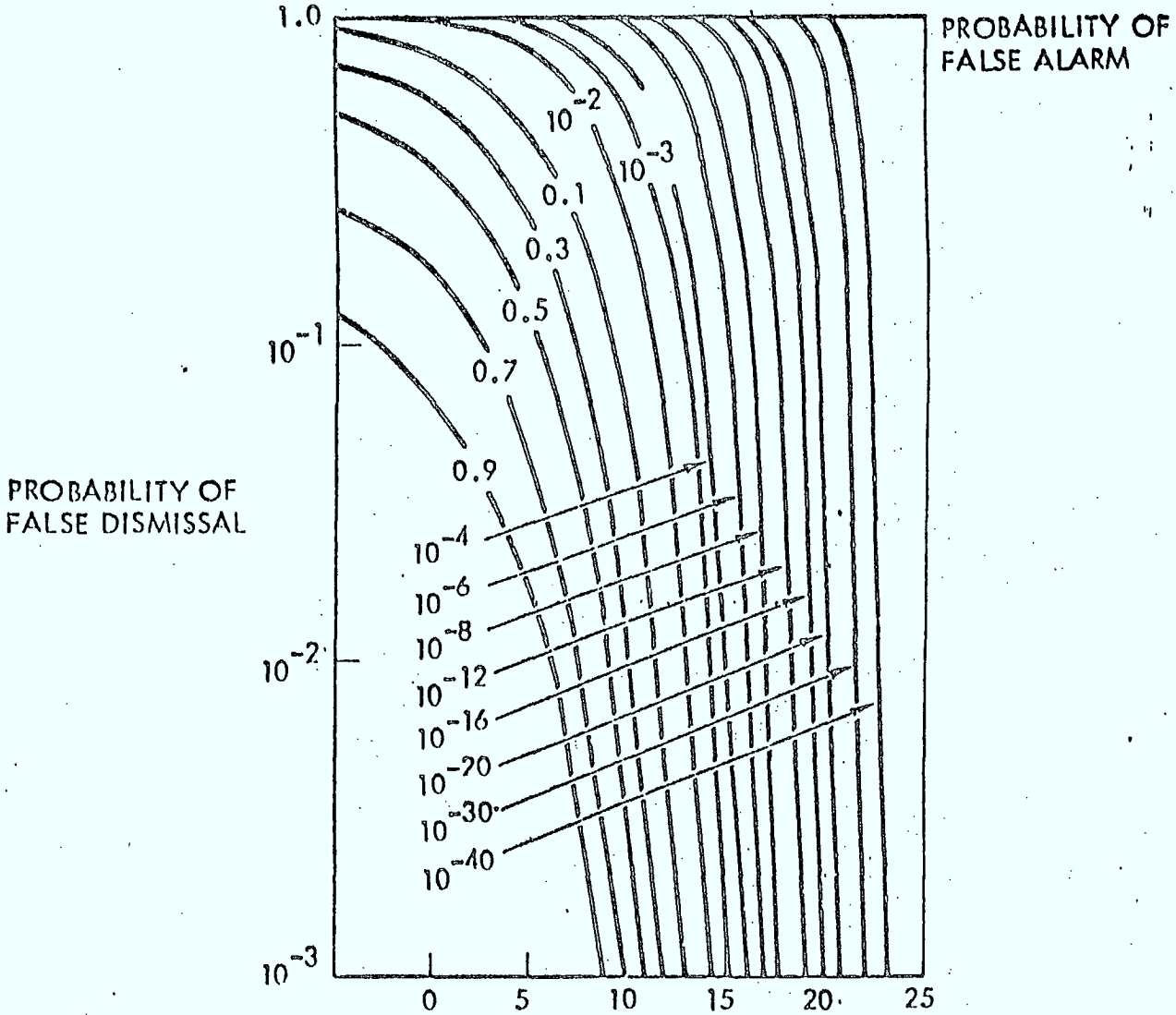

Figure 3. Noncoherent Detection of Synchronization

$$T_A = \frac{\Delta T}{T} T_s \tag{3}$$

But, from Equation (2)

$$T_A = \frac{\Delta T}{T} 31.62\ (J/S)\ T = 31.62\ \Delta T\ (J/S) \tag{4}$$

From Equation (4), it is seen that the total acquisition time is only dependent on the received (J/S) ratio and the initial time uncertainty. The PN code rate cancels since more processing gain, obtained as shown in Equation (1), results in more PN chips in a fixed time uncertainty.

The acquisition time can be improved by using an optimized two-step serial synchronizer. In this case, the first step is a fast search with high false alarm probability and the second step is a slow search that tests the possible sync positions determined by the first step. The probabilities of detection are P_{D1} and P_{D2} in the first and second step, respectively, and the probabilities of false alarm are P_{fa1} and P_{fa2}. Then,

$$P_D = P_{D1} P_{D2} = 0.9$$
$$P_{fa} = P_{fa1} P_{fa2} = 10^{-6} \tag{5}$$

The average time to test a PN chip is

$$T_s = T_{s1} + P_{fa1} T_{s2} = T\ (J/S) \left[N_1 + P_{fa1} N_2\right] \tag{6}$$

where T_{s1} and T_{s2} are times to test a PN chip in the first and second step, respectively. The values of N_1 and N_2 are obtained from Figure 3 as was done in the previous example. To minimize T_s, the quantity in brackets in Equation (6) must be minimized. For the requirements given by Equation (5), the probabilities that minimize T_s are

$$P_{D1} = 0.92, P_{D2} = 0.98$$
$$P_{fa1} = 10^{-1}, P_{fa2} = 10^{-5} \quad (7)$$

For these probabilities

$$T_s = 11.75\ T\ (J/S) \quad (8)$$

or the initial acquisition time is

$$T_A = 11.75\ \Delta T\ (J/S) \quad (9)$$

The optimized two-step synchronizer improved the acquisition time by a factor of 2.7. Additonal improvements can be made on the serial search by using more steps or by using sequential detection, which is essentially an infinite number of steps. Significant improvements beyond the optimized two-step synchronizer are not obtained under typical requirements using these serial methods. Multiple correlators could be used to divide the initial time search among them, but the resulting synchronization time is decreased by the number of correlators while receiver complexity increases at the same rate.

Therefore, PN antijam modulation is limited to processing gain by its inherent long acquisition time for large initial time uncertainties. Also, for PN to obtain processing gain, phase characteristics of the medium must be linear. For propagation through a uniform ionosphere, the phase shift can be written as [1]

$$\beta = \sqrt{(\omega^2 - \omega_p^2)/c^2} \quad (10)$$

where

$$\omega_p^2 = \frac{Nq^2}{E_0 m} = 324\pi^2 N \quad (11)$$

1. H. Staras, " The Propagation of Wideband Signals Through the Ionosphere," IRE Proceedings, Volume 49, July, 1961, p.1211.

and

c = velocity of light in free space (M/sec)

ω = $2\pi f$, radian frequency (rad/sec)

N = free electron density (number/m^3)

q = electron charge (coulombs)

ε_0 = dielectric constant of free space

For propagation through a distance r, the total phase shift is $\Theta = \beta r$. To determine the phase distortion, β can be expanded in a power series about the center frequency ω_c as follows.

$$\Theta = \beta r = r\left\{\beta(\omega_c) + (\omega-\omega_c)\left.\frac{d\beta}{d\omega}\right|_{\omega_c} + 1/2\,(\omega-\omega_c)^2\left.\frac{d^2\beta}{d\omega^2}\right|_{\omega_c} + \ldots\right. \tag{12}$$

$$= \frac{r}{c}\left\{(\omega_c^2-\omega_p)^{1/2} + \frac{\omega_c(\omega-\omega_c)}{(\omega_c^2-\omega_p^2)^{1/2}} - \frac{\omega_p^2\,(\omega-\omega_c)^2}{2(\omega_c^2-\omega_p^2)^{3/2}} + \ldots\right.$$

The first term of the expansion is a fixed carrier phase shift which does not affect the correlation amplitude. The second term represents a fixed delay which the receiver tracks. The third term is the first actual distortion term; thus,

$$\Theta_d(\omega-\omega_c) \approx -\frac{r\omega_p^2(\omega-\omega_c)^2}{2c\,(\omega_c^2-\omega_p^2)^{3/2}} \approx \frac{r\omega_p^2(\omega-\omega_c)^2}{2c\omega_c^3} \tag{13}$$

For notation convenience, let

$$\omega_0 = \omega - \omega_c \tag{14}$$

and

$$D = \frac{r\omega_p^2}{2c\omega_c^3} \tag{15}$$

To determine the antijam loss due to the phase distortion, consider that the transmitted PN spectrum is ideal rectangular bandpass filtered to bandwidth 2B. Then, the ionosphere distorts the phase.

The correlation output can be found by multiplying the filter characteristic times the filter response and then taking the Fourier transform. Thus, the peak correlation R(0) is given by

$$\left|R(0)\right| = \left|\frac{T_c}{2\pi} \int_{-\pi B}^{\pi B} \left[\frac{\sin(\omega_0 T_c/2)}{\omega_0 T/2}\right]^2 e^{jD\omega_0^2} \, d\omega_0\right| \tag{16}$$

where T_c is the PN chip duration. Equation (16) is numerically evaluated (step size $\delta\omega = 2\pi/100T_c$) in Figure 4 for correlation loss (antijam loss.) Note that the loss can increase as the bandwidth becomes wider due to phase cancellation when the distortion is present. The normalization in Figure 4 is the phase distortion at the first null. That is,

$$\Theta_d(2\pi/T_c) = 4\pi^2 D/T_c^2 = \text{Phase Distortion at First Null in Radians} \tag{17}$$

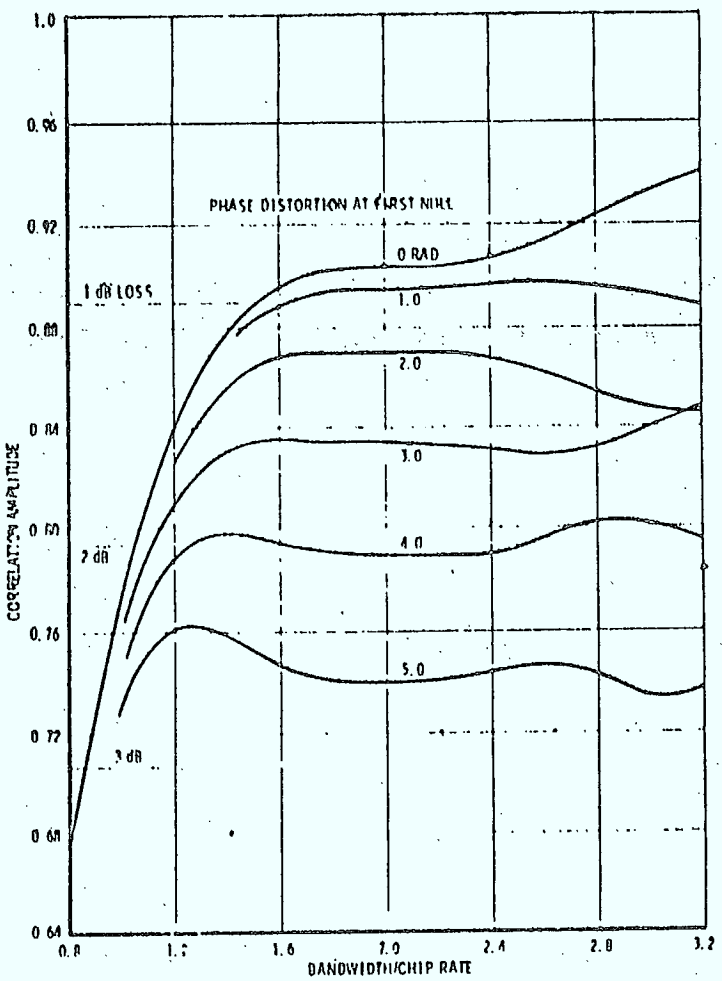

Figure 4. Antijam Loss Due To Phase Distortion and Finite Bandwidth

The antijam loss can be seen in Figure 4 to become significant when the phase distortion becomes greater than one radian. Therefore, the maximum allowed distortion for a PN system might be set at 2 radians. Then,

$$\Theta_d(\omega_0) = 2 = \frac{r\omega_p^2}{2c\omega_c^2}\left(\frac{2\pi}{T_c}\right)^2 \tag{18}$$

or the maximum allowed chip rate $R_c = 1/T_c$ is

$$R_c < \sqrt{\frac{2c\ f_c^3}{\pi r\ f_p^2}} \tag{19}$$

It may be noted[1] that a worst case value of Nr is roughly 2×10^{18} electrons/m^2. Assuming $r = 10^5$m for this worst case, then $N = 2^{13}$ electrons/m^3 and from equation (11), $f_p = 40$ MHz. For UHF at $f_c =$ 300 MHz, the maximum allowable PN chip rate is 5.6 MHz.

The antijam performance of PN/PSK spread spectrum modulation can be compared for various parameters by computing the performance measure G.

$$\text{Performance Measure } G = \left(\frac{W}{R_c}\right)\left(\frac{S}{J}\right)\left(\frac{1}{R}\right) = (E_b/N_o)_{eff}$$

W = Spread Spectrum Bandwidth
R_c = Channel Data Rate (Coded Bits/Sec)
R = Code Rate (1, 1/2)
S = Signal Power
J = Jammer Power

$$J/S = \left(\frac{W}{R_c}\right)\frac{1}{GR} \tag{20}$$

The code rate R included in the performance measure corresponds to error correction coding. Error correction coding provides a powerful technique to improve the capability of data modulation to withstand jamming. The performance improvement using a number of different coding techniques is shown in Figure 5. For a given channel bit error probability, the decoded bit error probability can be determined.

1. Hughes Aircraft Company, "System G21B-Satellite System for Precise Navigation," Final Report (Part 2) SAMSO TR69-4, January 1969, Appendix III.

Figure 5. Hard Decision Coding Performance

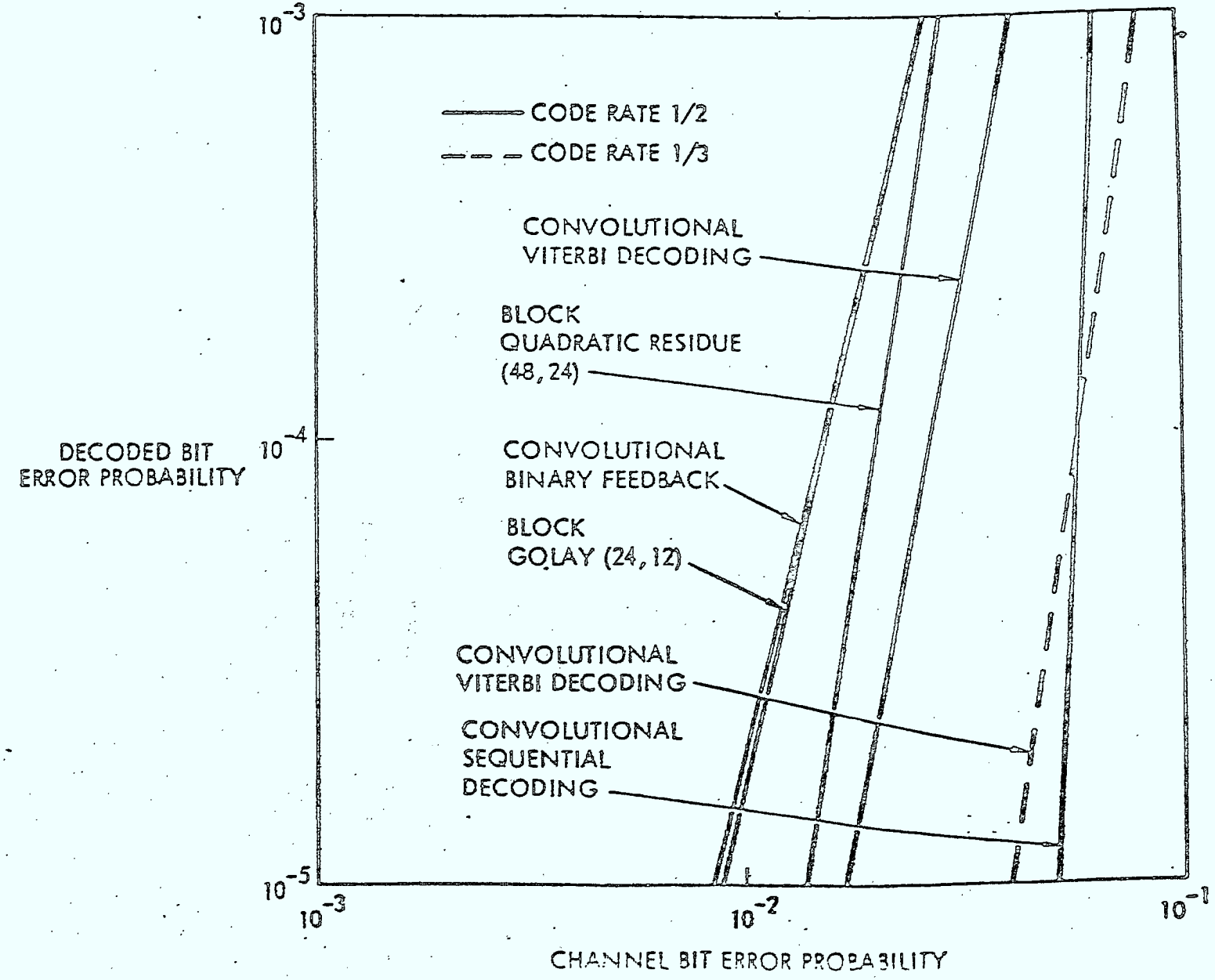

Table 3. Antijam Performance of Direct Sequence Pseudo-Noise

ERROR CORRECTION CODE TECHNIQUE	PULSE JAMMER DUTY CYCLE (%)	PERFORMANCE MEASURE (dB)
NO CODING		
$P_b = 10^{-3}$	100.0	6.8
	0.85	19.2
$P_b = 10^{-5}$	100.0	9.6
	0.0035	39.2
RATE 1/2 BINARY FEEDBACK		
$P_b = 10^{-3}$	100.0	5.7
	23.0	7.9
$P_b = 10^{-5}$	100.0	7.6
	7.2	12.9

For example, with the rate 1/2 convolutional code with binary feedback decoding, to achieve a decoded bit error probability of 10^{-3}, the channel bit error probability need only be 0.0266.

To see how much error correction coding improves the antijam performance, assume that PN/PSK modulation is used against the worst case jammer. The worst case jammer against PN/PSK modulation is a tone at the carrier frequency that is pulsed with duty cycle α. It is assumed that the jammer chooses the duty cycle to maximize the probability of error for the communication system. It is also assumed that a jammer with average power J can pulse with duty cycle α and achieve a peak power of J/α. Appendix B derives the performance of this jammer against PN/PSK modulation. The antijam performance in terms of the performance measure is given in Table 3. For a CW tone (i.e., 100 percent duty cycle), the simple binary feedback decoder only improves the performance by 1.1 dB at $P_b = 10^{-3}$ and 2 dB at $P_b = 10^{-5}$. However, for the worst case duty cycle, the error correction coding improves the performance by 11.3 dB at $P_b = 10^{-3}$ and 26.3 dB at $P_b = 10^{-5}$.

2.2 Frequency Hop Modulation

Frequency hop spreading of the message signal is by transmitting each bit on a different carrier (usually by binary FSK) selected from a wide range of frequencies. The selection process is controlled by a PN sequence as shown in the FH modulator in Figure 6. There are 2^n frequency slots and, for each successive message bit, two slots are selected to denote "1" and "0". Note that, for the communication to be more secure, the 2^n slots are derived from a PN sequence with period much greater than 2^{n-1} by using a long shift register. In the FH receiver shown in Figure 6, the signal is dehopped with a replica sequence. As in the direct sequence PN case, acquisition and tracking of the PN switched signal must be accomplished before the data can be retrieved. Since the bit time is much wider than the reciprocal of the total bandwidth, an FH system is more easily acquired than a PN system.

The data modulations considered for FH and FH/PN antijam modulation

Figure 6.. Frequency Hop Modulator/Demodulator

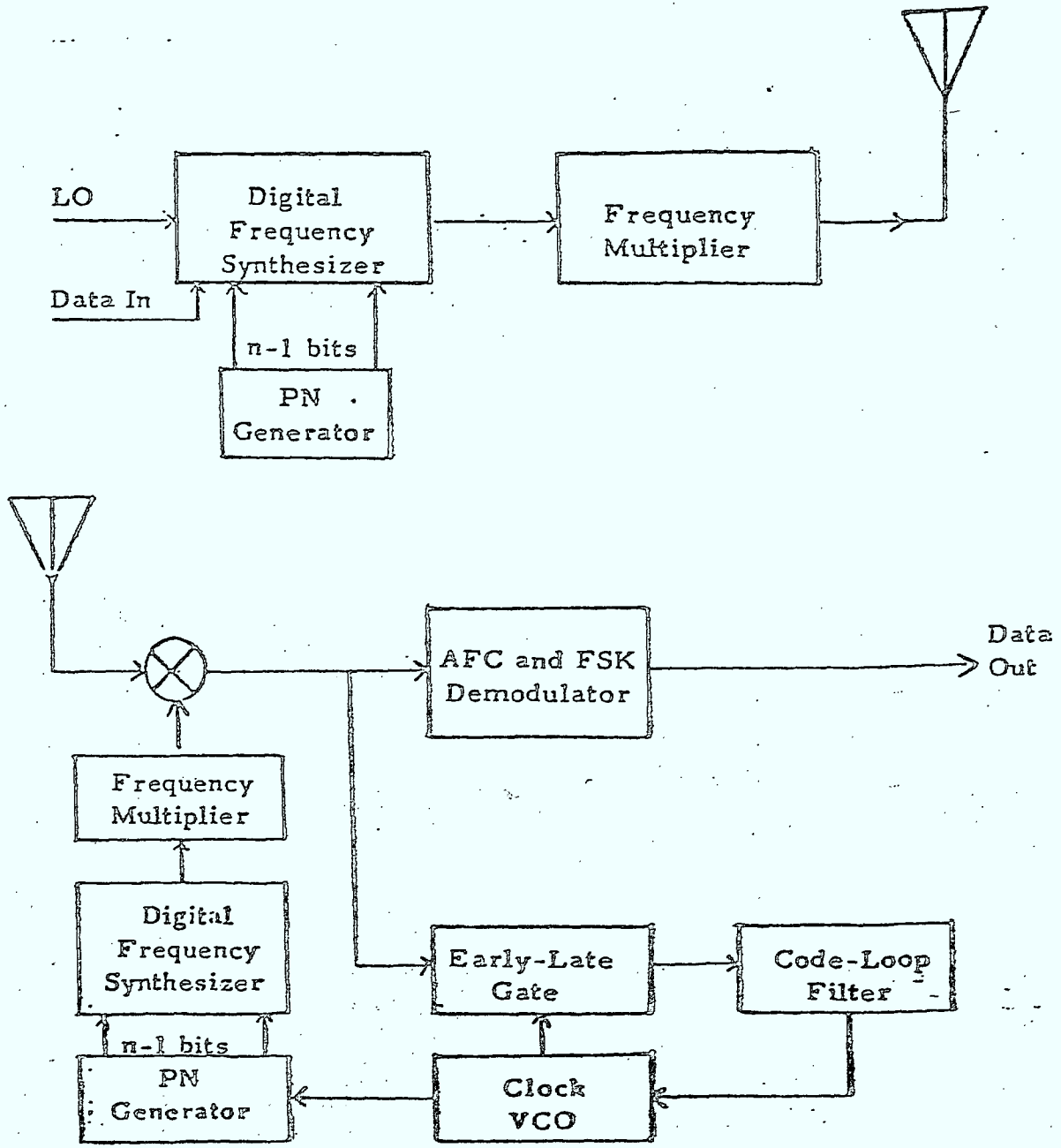

are multiple-frequency-shift-keying (MFSK), multiple-code-shift-keying (MCSK), binary differential phase-shift-keying (DPSK), and differential quadriphase-shift-keying (DQPSK). It should be noted that MFSK and MCSK give equivalent performance if FH/PN is used for antijam modulation.

It is important to note that only noncoherent frequency hopping is being considered since large hopping bandwidths make it impractical to maintain phase coherence across the total bandwidth. Therefore, each hop has an independent phase but the phase is constant over the hop. Constant phase is required for MFSK, MCSK, DPSK, and DQPSK. For DPSK and DQPSK, the hop rate must be slower than the bit rate since one symbol per hop must be used for phase reference. Alternately, a hop rate faster than the bit rate (or symbol rate) is possible with MFSK or MCSK. If several hops must be combined to make to make up a MFSK (MCSK) symbol, then a noncoherent combining loss must be included for this fast frequency hopping (FFH) modulation. The potential antijam/data modulation techniques available are:

FH/MFSK	FH-PN/MFSK (MCSK)
FFH/MFSK	FFH-PN/MFSK (MCSK)
FH/DPSK	FH-PN/DPSK
FH/DQPSK	FH-PN/DQPSK

Partial band noise jamming and partial band multitone jamming are considered as possible jamming types against the potential antijam/data modulation techniques.

For partial band noise, the total jammer power J is assumed spread evenly over a fraction P_J of the spread band W. For B_J equal to the jammer bandwidth, this implies that the fraction of band jammed is (as shown in Figure 7) $P_J = B_J/W$, and the spectral height of the jammer density is $N_J = J/B_J = J/WP_J$.

For partial band multitone, the total jammer power J is evenly divided

- PARTIAL BAND NOISE

$P_J = B_J/W$

$N_J = J/B_J = J.W/P_J$

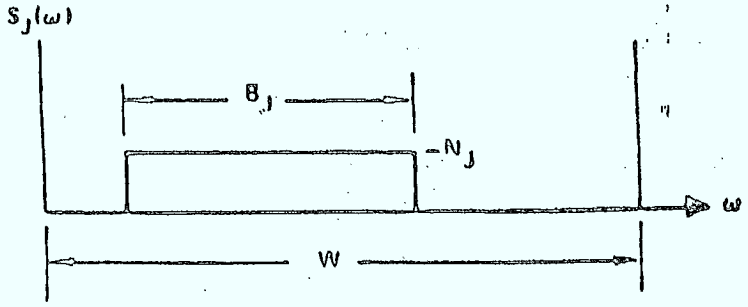

- PARTIAL BAND MULTITONE

DPSK $P_J = \frac{q R_c}{W}$

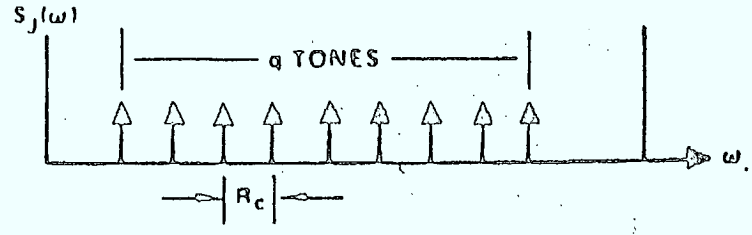

MFSK $\frac{n \text{ TONES}}{B \text{ SLOTS}}$

$P_J = q \frac{R_c}{W} \frac{B}{n}$

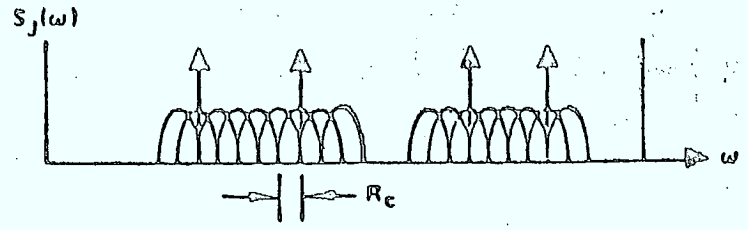

- REPEAT JAMMING — SPATIAL DISCHIMINATION
- PULSE JAMMING — TWT PEAK LIMITING
- SWEPT JAMMING — UPPER BOUNDED BY MULTITONE

Figure 7. Jammer Types

among q jammer tones. For jamming against differential phase-shift-keying (DPSK), the jammer is assumed to place tones at the centers of the DPSK tone slots. The slot widths for DPSK have bandwidth $R_c = 1/T$ (T = symbol duration) and the number of available jamming slots is W/R_c.

This implies that the fraction band jammed is $P_J = qR_c/W$. For jamming against MFSK signals, the jammer has the further option of varying the number of jammer tones within the group of M possible MFSK signals. Assuming the jammer places n tones per group of M and that the spacing between adjacent MFSK tones is $R_c = 1/T$ (T = tone duration), the jammed fraction of the band becomes $P_J = MqR_c/nW$.

The demodulation techniques must be specified to determine the antijam performance. The particular demodulation techniques assumed are not intended to reflect optimum demodulators, but rather realistic mechanizations. When degradation is expected, due to the demodulation technique, these effects are included in the analysis (e.g., quantization if DPSK). Figure 8 illustrates the demodulator which has been assumed for the MFSK signal format. The received signal is assumed to be perfectly dehopped and filtered to the PN bandwidth when FH/PN is used. PN despreading is accomplished, and the resulting baseband signal is filtered at the bandwidth of the M-ary signal immediately filtered at this bandwidth. The baseband M-ary spectrum is then bandpass-limited to provide gain control, and the output is envelope detected by a bank of filters matched to the M modulation frequencies.

At the output of the envelope detectors, three demodulator strategies may be employed for slow frequency hopping. A hard decision may be output, corresponding to the largest envelope; soft decisions may be output, corresponding to the amplitudes of each detector; or list of L decisions, corresponding to the filters having the L largest responses in descending order (rank statistics).

For fast frequency hopping, the output of the envelope detectors is peak

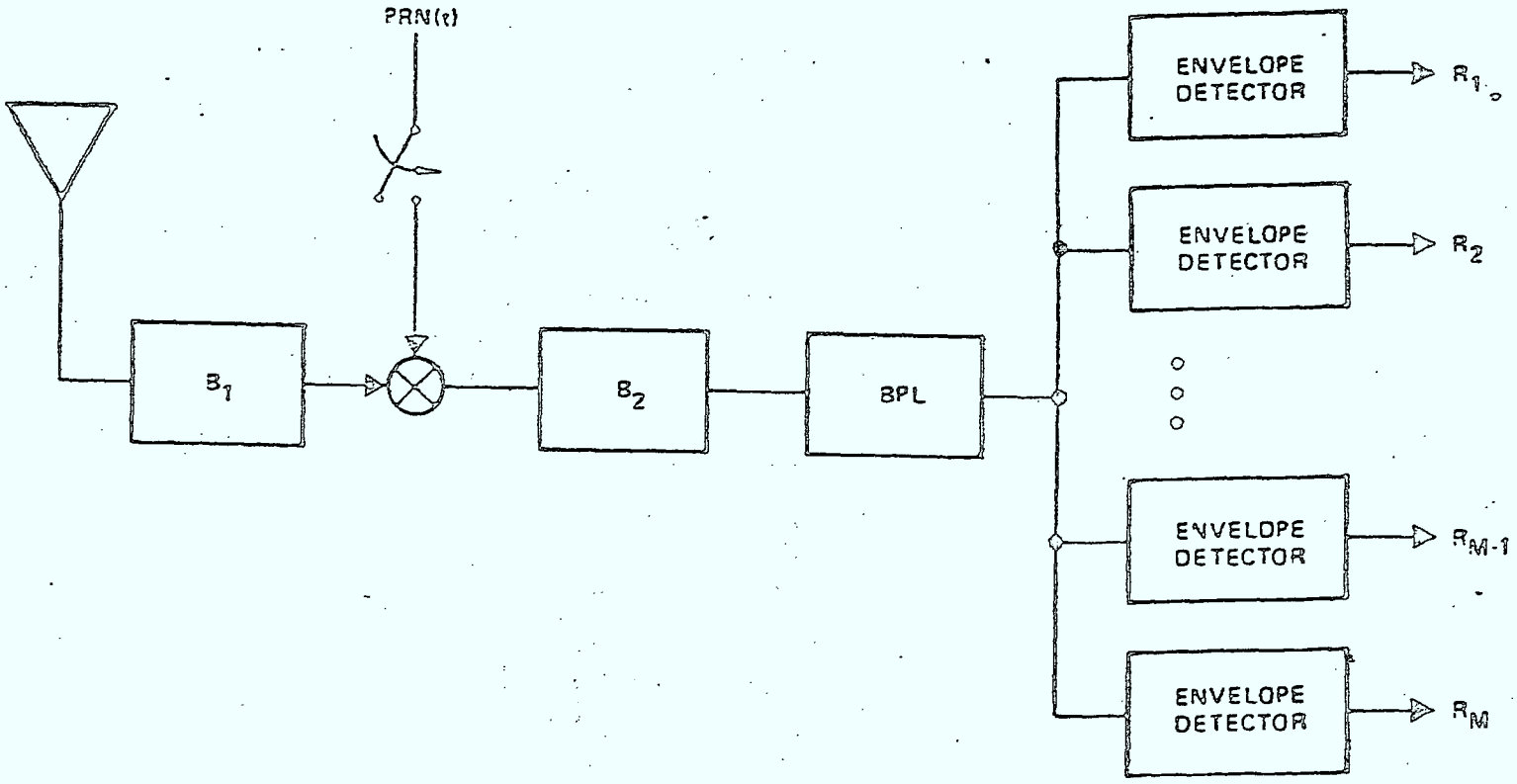

Figure 8. MFSK Demodulation Implementation

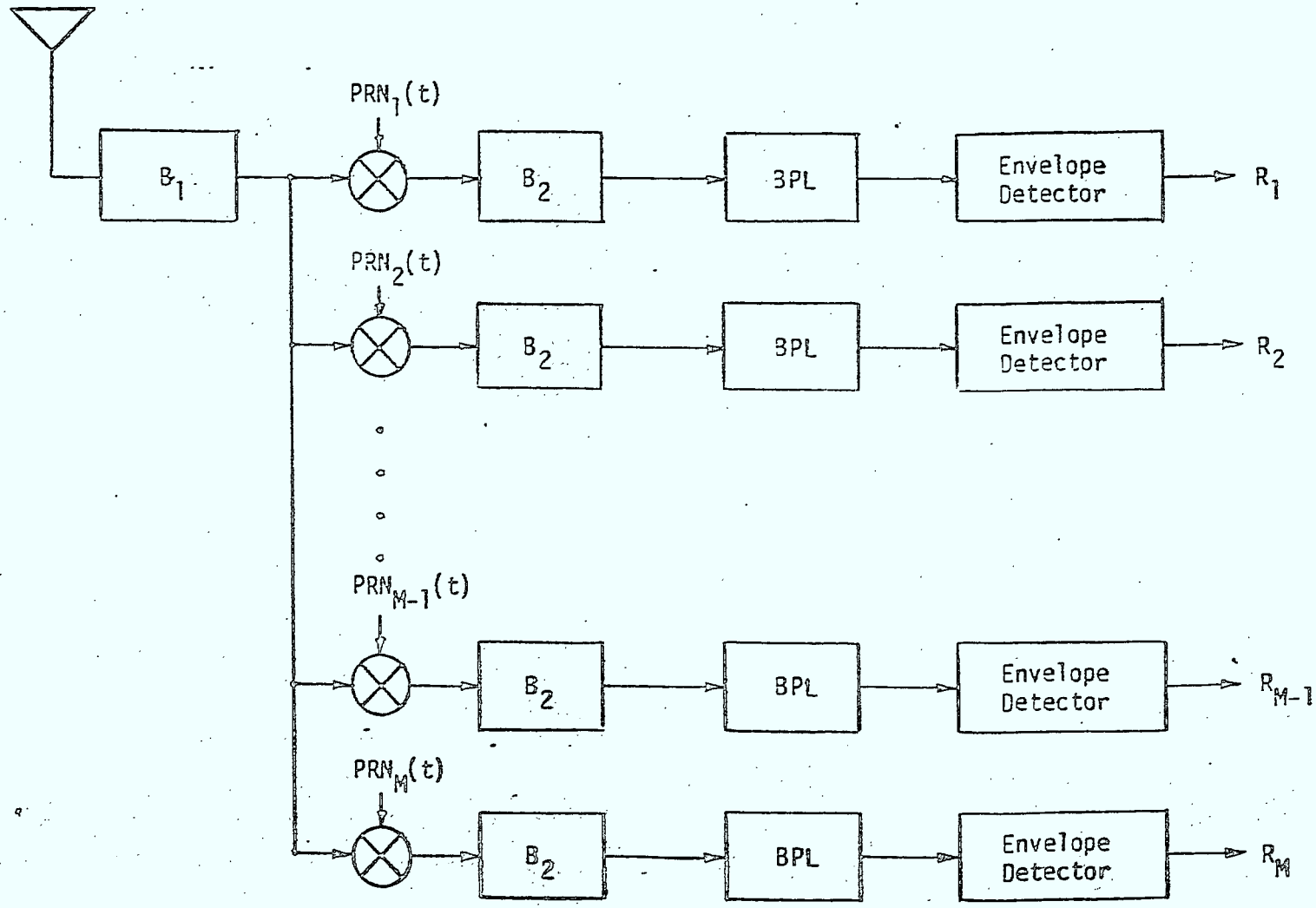

Figure 9. MCSK Demodulation Implementation

clipped and quantized (A/D converted). Let the hop rate be N times faster than the duration of the MFSK signal tone, then the output of the envelope detectors is summed over the N hops. The three demodulator strategies employed for slow frequency hopping can be applied to the resulting sum of the envelope detectors over the N hops.

The functional demodulation implementation of MCSK is presented in Figure 2. The actual implementation may be a single channel time-shared over the M outputs. The received signal is assumed to be perfectly dehopped and filtered to the PN bandwidth. The PN despreading for each of the M signals is assumed to be in perfect synchronization. Each channel is filtered and band-pass limited to provide gain control. The output of each channel is the envelope-detected despread signal. The output of the envelope detectors may be processed by the same three demodulation strategies as with MFSK. In fact, the performance of MCSK is identical to MFSK with partial band noise interference for each of the demodulation strategies.

The DPSK demodulation strategy includes quantizing the phase angle in order to digitally compute the difference between successive symbols. Figure 10 illustrates the DPK demodulation technique. The received signal is frequency dehopped and PN despread. The resulting signal is bandpass-limited and mixed with I and Q signals from a local oscillator. Note that the local I and Q signals are noncoherent with the received signal. Therefore, there is an unknown phase angle ϕ between the received signal and the reference signal. The phase angle ϕ is found in a quantized form from the six angle test statistics SGN ($I \sin \gamma_i$ - $Q \cos \gamma_i$) for $\gamma_i = \gamma_1\ \gamma_2, \ldots, \gamma_6$ shown in Figure 10. Since the argument of the SGN represents $\sin (R-\gamma_i)$, for the received angle R, the total statistic determines whether the received angle R lies above or below the line at angle γ_i. Thus, from the six numbers, a unique segment containing R may be determined.

The choice of 12 segments arises from a symmetry requirement for hard demodulated DQPSK. Given that the true signals lie in segments 3,6,9,12,

the demodulator maps differentially decoded segments 2,3,4 back to a demodulated 3; 5,6,7 to 6; 8,9,10 to 9; and 11,12,1 to 12. In order to ensure this type of symmetry, the total number of segments must be an odd multiple of 4. Thus, the candidates are 4,12,20,28,etc. The number of segments chosen is 12 as a compromise between quantization error in the differential decoding and the cost of mechanization.

For each modulation candidate, analysis has been performed to determine the output bit error rate as a function of the interference parameters[1] [2]. These analytical formulations were then optimized to determine the worst case interference for each modulation candidate. The results are a family of curves of worst case output bit error versus the effective signal-to-interference ratio, effective E_c/N_0, where

$$(E_c/N_0)_{eff} = (\frac{W}{R_c})(\frac{S}{J}) \qquad ((21)$$

The resulting family of curves is given in Figure 11. The MFSK performance shown in Figure 11 is for 8-ary FSK with slow frequency hopping assumed. For reference, the performance of 8-ary FSK, DPSK, and DQPSK in thermal noise is also presented. It may be observed in Figure 11 that, for slow frequency hopping, DQPSK is the best data modulation against the worst case tone jammer. For slow FH-PN, the best data modulation choice is DPSK against the worst case partial band noise or tone jamming, which gives about 1.5 dB better performance than FH/DQPSK against worst case tone jamming. The analytical expressions for calculating performance are summarized in Table 4.

The performance of MFSK and MCSK can be improved by fast frequency hopping (i.e., more than one hop per M-ary symbol)[2]. Fast frequency

1. S.W. Houston, "Tone and Noise Jamming Performance of Spread Spectrum M-ary FSK and 2,4-ary DPSK Waveforms," Proceedings of the IEEE National Aerospace and Electronics Conference, Dayton, Ohio, June 10-12,1975, pp. 51-58

2. A.J. Viterbi and I.M Jacobs, "Advances in Coding and Modulation for Noncoherent Channels Affected by Fading Partial Band and Multiple Access Interference," Advances in Communication Systems, Vol 4, New York: Academic Press, 1975, pp. 279-308.

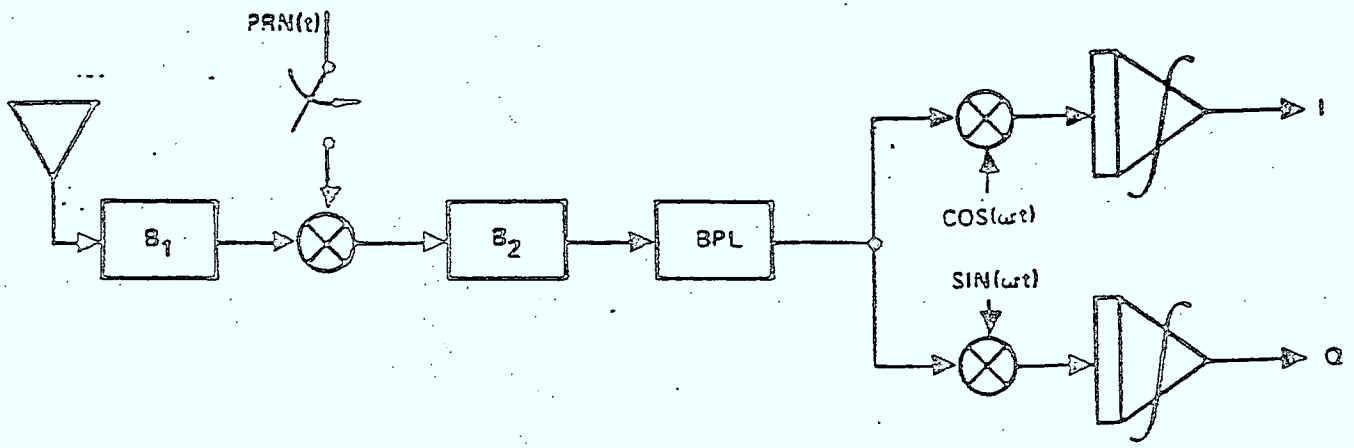

RESOLVE PHASE BY PERFORMING

SGN (I SIN γ_i – Q COS γ_i)

FOR $\gamma_i = \gamma_1 \ldots \gamma_6$, AND

DETERMINING SEGMENT

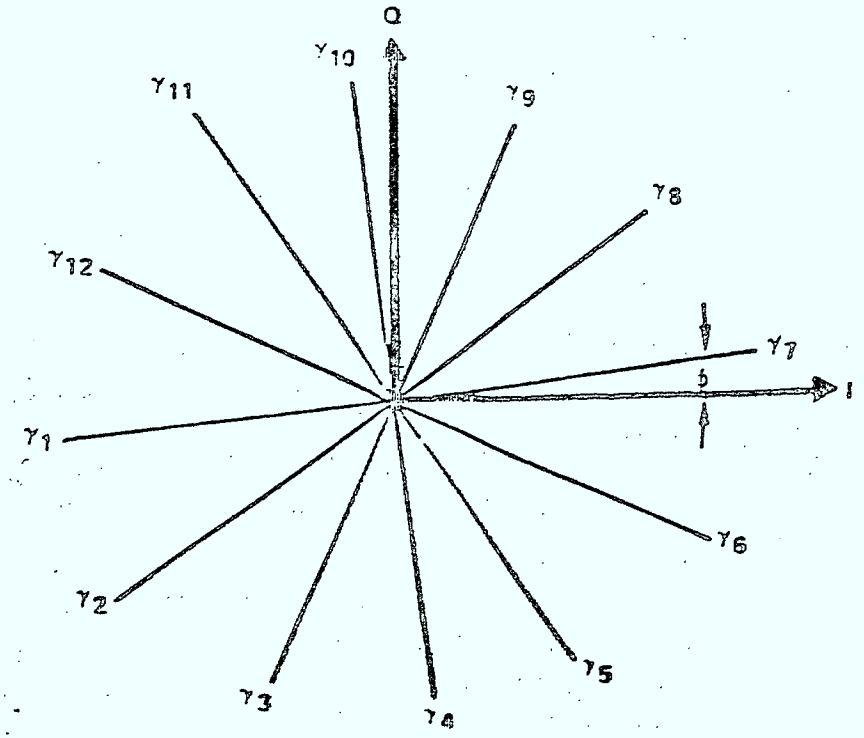

Figure 10. DPSK Demodulation Implementation

hopping is not applicable to DPSK or DQPSK because a reference symbol is required each hop to resolve carried phase. A summary of the performance of 8-ary MFSK against partial band tone and noise interference is illustrated in Figure 12. Depending on the desired bit error probability, there is an optimum choice of N (the number of hops per 8-ary symbol). With partial band noise interference, the optimum value of N is shown for each bit error probability. Note that the composite curve for noise interference is made up of straight line segments. If the value of N was held constant, then the straight line characteristic results. At $(E_c/N_0)_{eff}$ = 7.8 dB, the bit error probabilities of N = 4 and N = 5 are equal; but for larger values of $(E_c/N_0)_{eff}$, N = 5 results in lower bit error probability. This type of result occurs at various values of $(E_c/N_0)_{eff}$ where the optimum value of N changes for partial band noise interference. In general, the optimum value of N for large $(E_c/N_0)_{eff}$ with partial band noise interference is

$$N_{opt} = \frac{(E_c/N_0) \log_2 M}{4} \qquad (22)$$

for any value of M-ary MFSK (MCSK).

For partial band tone interference, the performance of fast frequency hopping is not as well behaved as for partial band noise. The best performance for partial band tone interference is for N = 4, except at very large values of $(E_c/N_0)_{eff}$. Here again, there is an optimum choice of N at any value of $(E_c/N_0)_{eff}$. Note, however, that even values of N perform better than odd values for partial band tone interference.

To illustrate the best choice of N for a pure fast frequency hopping modulation with 8-ary MFSK data modulation, assume that the required channel bit error probability is $P_{cb} = 10^{-2}$. Table 5 presents the required $(E_c/N_0)_{eff}$ to obtain $P_{cb} = 10^{-2}$ for various values of N against partial band tone and noise interference. While N = 4 is the best choice for partial band tone interference, the best choice for partial band noise interference is N = 5. However, to minimize the required $(E_c/N_0)_{eff}$ for the worst case jammer, it may be seen in Table 5 that the best choice is N = 4.

Figure 11. Hard Decision Performance For Slow Frequency Hopping

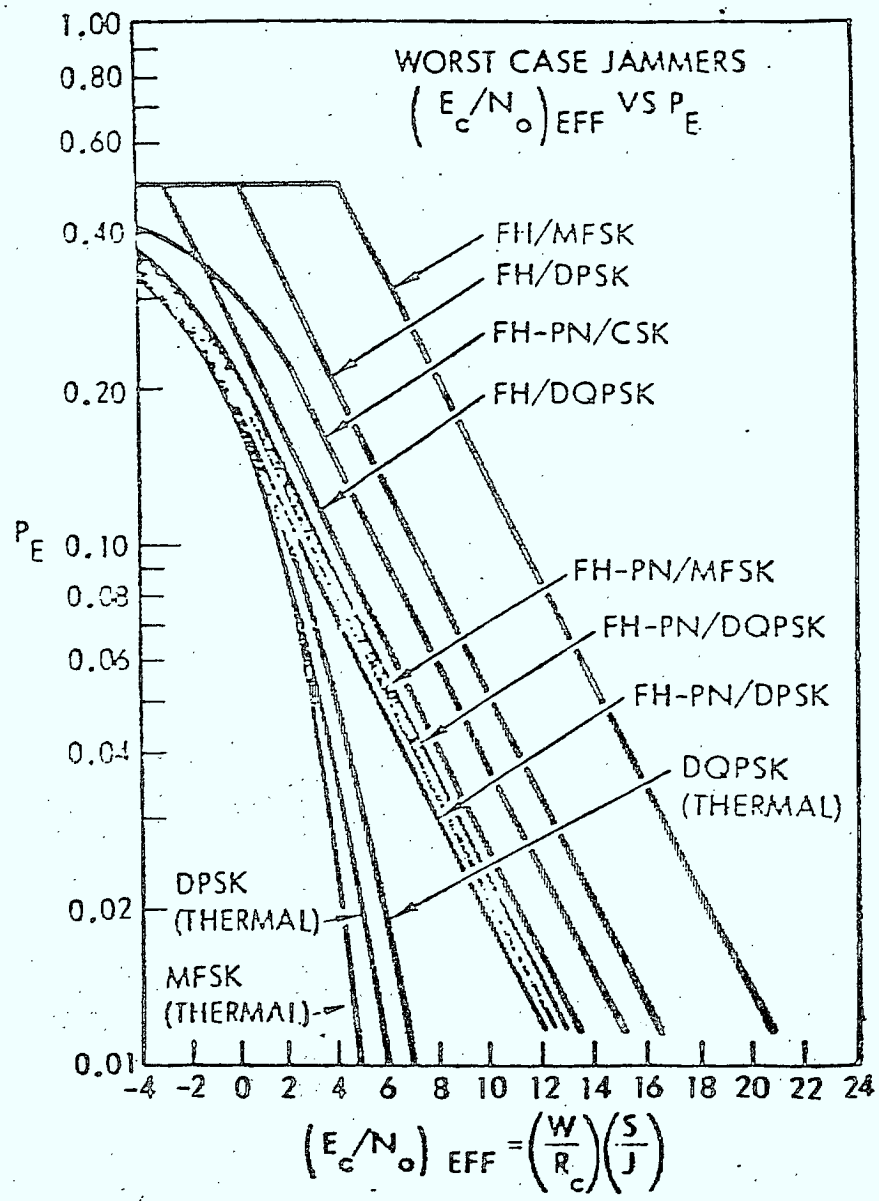

Table 4. Hard Decision Analytical Performance for Slow Frequency Hopping

CHANNEL SIGNAL	JAMMING SIGNAL	BIT ERROR PROBABILITY $P_B(X)$ $X = (E_C/N_o)_{Eff} = (W/R_c)(S/J)$
FREQUENCY HOPPED 8 ARY MFSK	MULTITONE WITH $R_c/3$ TONE SPACING	$P_B(X) = 4/7\,(1 - 1/3X)\,[1 - (1 - 1/3X)^7]$
	MULTITONE WITH $8/3\,R_c$ TONE SPACING (WORST CASE)	$P_B(X) = 4/3X;\ X \geq 8/3$ $P_B(X) = 1/2;\ X \leq 8/3$
	PARTIAL BAND NOISE	$P_B(X) = 0.1954/X;\ X \geq 0.9273$ $P_B(X) = P_F(8, X);\ X \leq 0.9273$
FREQUENCY HOPPED PN/8-ARY MFSK	MULTITONE WITH $1/T_p$ SPACING OR PARTIAL BAND NOISE	$P_B(X) = 0.1954/X;\ X \geq 0.9273;\ 8/3\,R_cT_p << 1$ $P_B(X) = P_F(8, X);\ X \leq 0.9273$
FREQUENCY HOPPED PN/2-ARY CSK	MULTITONE WITH $1/T_p$ SPACING OR PARTIAL BAND NOISE	$P_B(X) = 1/ex = 0.3679/X;\ X \geq 2;\ 2R_cT_p << 1$ $P_B(X) = 1/2\,e^{-x/2};\ X \leq 2$
FREQUENCY HOPPED DPSK	MULTITONE WITH kR_c TONE SPACING (WORST CASE)	$P_B(X) = k/2X;\ X \geq k$ $P_B(X) = 1/2;\ X \leq K$
	PARTIAL BAND NOISE	$P_B(X) = k/2ex = 0.1839k/X;\ X \geq k$ $P_B(X) = 1/2\,e^{-x/k};\ X \leq k$
FREQUENCY HOPPED PN/DPSK	MULTITONE WITH $k\,R_c$ TONE SPACING OR PARTIAL BAND NOISE	$P_B(X) = k/2ex = 0.1839k/X;\ X \geq k$ $P_B(X) = 1/2\,e^{-x/k};\ x \leq k$
FREQUENCY HOPPED DQPSK	MULTITONE WITH $1/2k\,R_c$ TONE SPACING (WORST CASE)	$P_B(X) = k/4x;\ X \geq k/2$ $P_B(X) = 1/2;\ X \leq k/2$
	PARTIAL BAND NOISE	$P_B(X) = 0.212k/X;\ X \geq 1.259k$ $P_B(X) = 2/3\,P_D(4, x/k);\ X \leq 1.259k$
FREQUENCY HOPPED PN/DQPSK	MULTITONE WITH $1/2k\,R_c$ TONE SPACING OR PARTIAL BAND NOISE	$P_B(X) = 0.212k/X;\ X \geq 1.259k$ $P_B(X) = 2/3\,P_D(4, x/k);\ X \leq 1.259k$

Figure 12. Hard Decision Performance of 8-ary MFSK With Fast Frequency Hopping

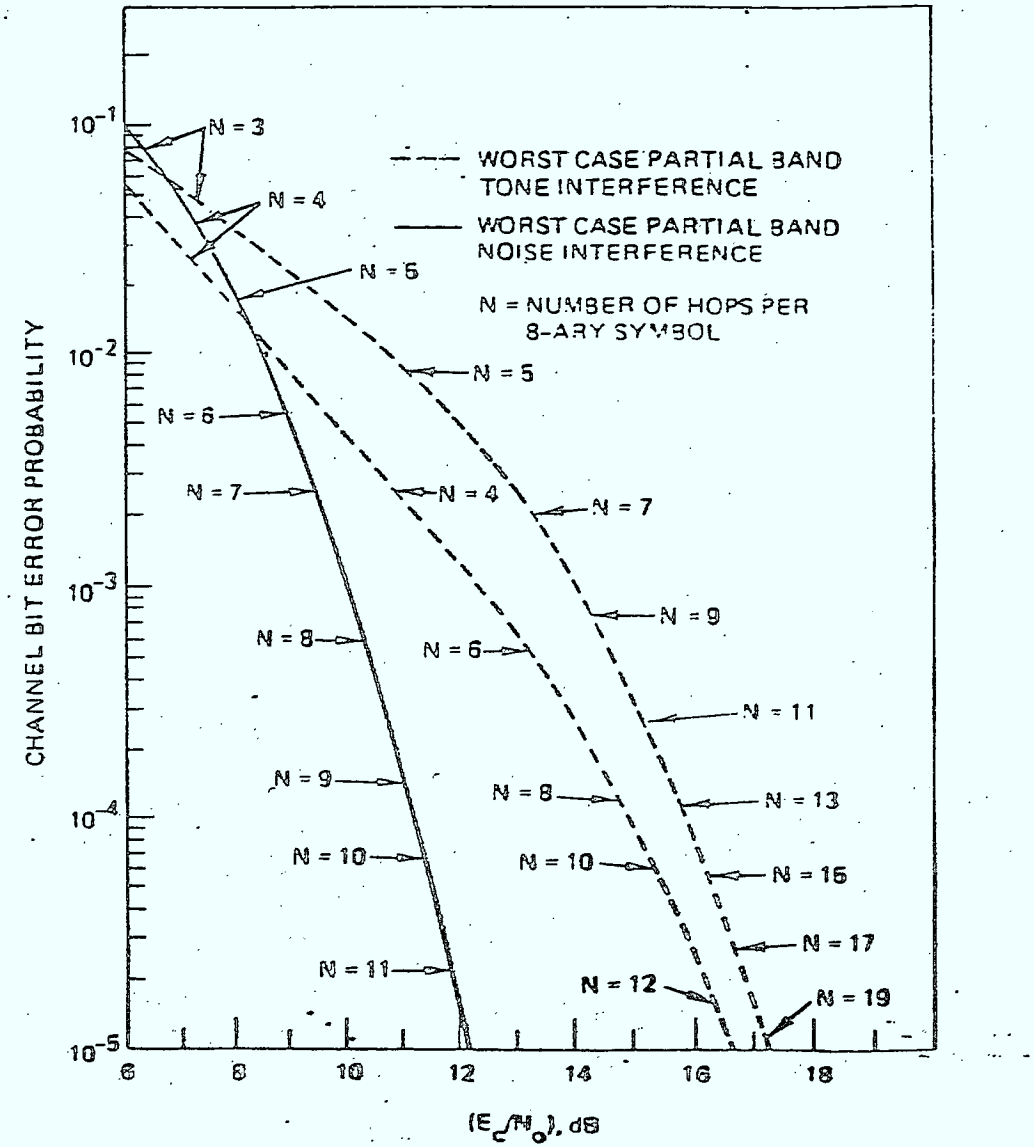

Finally, it is important to note that fast frequency hopping requires noncoherent combining of the signal over N hops. Noncoherent combining has an associated loss in additive white Gaussian noise (thermal).[1] Figure 13 presents the required energy per channel bit to noise spectral density (E_c/N_0) to achieve a given channel bit error probability for 8-ary MFSK. Note that N = 4 requires 1.4 dB larger E_c/N^0 to achieve $P_{cb} = 10^{-2}$ than is required by N = 1. Therefore, there is a large loss in thermal noise performance as N becomes large.

The performance of convolutional coding techniques is presented in Tables 6 and 7 for FH and FH/PN with various data modulations. At 10^{-3} bit error probability, rate 1/3 convolutional coding with Viterbi decoding provides the best performance for reasonable complexity for all data modulations except FFH/MFSK. The improvement in performance with rate 1/3 convolutional coding/Viterbi decoding is even more pronounced at 10^{-5} bit error probability. Note that, at $P_b = 10^{-5}$, the coding gain for all the coding techniques is greater than 26 dB, except FFH/MFSK.

If the data rate is low and small complexity is required, then FFH/MFSK with 8-ary MFSK and N = 4 hops per 8-ary symbol using rate 1/2 convolutional coding and binary feedback decoding is the best signal design. The medium complexity, rate 1/3 convolutional code with Viterbi decoding only provides about 0.8 dB improvement using FH/DQPSK over this choice. For all other conditions considered so far in the discussion, rate 1/3 convolutional coding with Viterbi decoding, using either FH/DQPSK or FH-PN/DPSK, is the best signal design. With Viterbi or sequential decoding using either FFH-PN spread spectrum modulation, the optimum value of N is one. Hence, this is not fast frequency hopping and the performance is the same as FH-PN.

Additional improvements in performance from coding can be obtained if the output of the demodulator is quantized (soft decision) to more than two levels or, for MFSK, if a list-of-L of the largest M envelope detectors is provided to the decoder. Typically, about a 2 dB improvement in

1. W.C. Lindsey, "Error Probabilities for Rician Fading Multichannel Reception of Binary and N-ary Signals," IEEE Trans. on Info. Theory, Vol. IT-10, No. 4, October, 1964, pp. 339-351.

Table 5. Required $(E_c/N_0)_{eff}$ For Bit Error Probability of 10^{-2} For Fast Frequency Hopping

N	Required $(E_c/N_0)_{eff}$ for $P_{cb} = 10^{-2}$	
	Partial Band Noise (dB)	Partial Band Tone (dB)
1	13.2	21.3
2	11.4	11.3
3	9.3	10.7
4	8.7	8.7
5	8.5	10.9
6	8.5	9.8

Figure 13. Hard Decision Performance For 8-ary MFSK With Fast Frequency Hopping In White Gaussian Noise (Thermal)

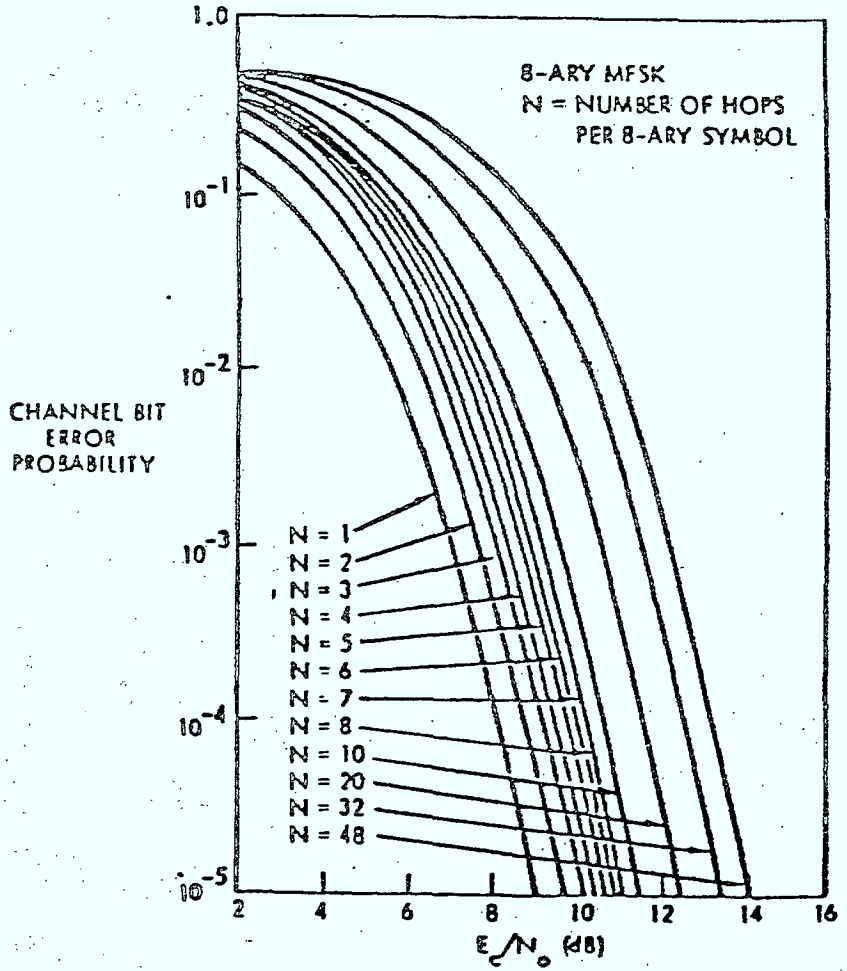

performance is expected from soft decisions. Viterbi and sequential decoding can be implemented to use soft decisions, but binary feedback decoding has not been implemented to date to use soft decisions. Implementing the Viterbi decoder to use soft decisions does not increase its complexity, but sequential decoding complexity increases by $\log_2 Q$, where Q is the number of quantization levels used for the soft decisions (the increase is $\log_2 L$ for List-of-L demodulation).

The performance of the modulation/coding techniques using soft decisions and List-of-L quantization can be approximated (bounded) by using a modification of Gallager's random coding bound. Gallager's function assumed that the decoding rule is matched to the channel statistics. However, for unknown interference, it is desirable: (a) to choose the modulation format and the corresponding demodulation technique, and (b) to optimize the demodulation parameters and the decoder metrics to minimize the probability of error for all possible channel statistics. For each spread spectrum modulation, the worst case interference was determined for the best choice of rate 1/3 Viterbi decoder metrics[1]. The additional coding gain achieved by using soft decisions or List-of-L quantization instead of hard decisions is presented in Table 8. The List-of-4 and List-of-8 quantizations are only applicable to MFSK. Note that, with FH/MFSK, the worst case interference is partial band tones. It was found that the optimum decoder metric was to rank the magnitudes of the tones (i.e., List-of-L quantization) rather than assigning metrics to the individual quantization levels of each filter (i.e., 8-level soft decisions). In fact, with List-of-8 quantization, the required $(E_b/N_0)_{eff}$ to achieve a given bit error probability is 4.8 dB less than required for hard decision. Note that, even with the greater coding gains achieved with soft decisions and List-of-L quantization by FJ/DPSK and FH/MFSK than with FH/DQPSK, the required $(E_b/N_0)_{eff}$ for a given bit error probability with rate 1/3 Viterbi decoding is

1. G.K.Huth, "Optimization of Coded Spread Spectrum System Performance," IEEE Trans. on Comm., Vol. COM-25, No. 8, August, 1977, pp.763-770.

Table 6. Hard Decision Coded FH Performance

Error Correcting Code Technique	Required $(E_b/N_0)_{eff}$ Worst Case Jamming			
	FH/DPSK (dB)	FH/DQPSK (dB)	FH/MFSK (dB)	FFH/MFSK (dB)
No Coding				
$P_b = 10^{-3}$	27.0	24.1	31.2	12.2
$P_b = 10^{-5}$	47.0	44.1	51.2	16.5
R = 1/2 Convolutional Binary Feedback				
$P_b = 10^{-3}$	15.7	12.9	20.0	10.6
$P_b = 10^{-5}$	20.8	17.9	25.0	11.9
R = 1/2 Convolutional Viterbi Decoding				
$P_b = 10^{-3}$	13.8	10.9	18.0	10.1
$P_b = 10^{-5}$	17.7	14.8	21.9	11.1
R = 1/3 Convolutional Viterbi Decoding				
$P_b = 10^{-3}$	12.6	9.8	16.9	11.1
$P_b = 10^{-5}$	15.5	12.7	19.8	11.9
R = 1/2 Convolutional Sequential Decoding				
$P_b = 10^{-3}$	11.9	9.1	16.2	9.7
$P_b = 10^{-5}$	12.8	9.9	17.0	9.8

Table 7. Hard Decision Coded FH/PN Performance

Error Correcting Code Technique	Required $(E_b/N_0)_{eff}$ Worst Case Jamming			
	FH-PN/DPSK (dB)	FH-PN/DQPSK (dB)	FH-PN/MFSK (dB)	FFH-PN/MFSK (dB)
No Coding				
$P_b = 10^{-3}$	22.6	23.3	22.9	11.2
$P_b = 10^{-5}$	42.6	43.3	42.9	12.1
R = 1/2 Convolutional Binary Feedback				
$P_b = 10^{-3}$	11.4	12.0	11.7	10.6
$P_b = 10^{-5}$	16.4	17.0	16.7	11.6
R = 1/2 Convolutional Viterbi Decoding				
$P_b = 10^{-3}$	9.5	10.0	9.7	9.7
$P_b = 10^{-5}$	13.4	14.0	13.6	11.1
R = 1/3 Convolutional Viterbi Decoding				
$P_b = 10^{-3}$	8.3	8.9	8.5	8.5
$P_b = 10^{-5}$	11.2	11.8	11.4	11.4
R = 1/2 Convolutional Sequential Decoding				
$P_b = 10^{-3}$	7.6	8.2	7.9	7.9
$P_b = 10^{-5}$	8.4	9.0	8.7	8.7

Table 8. Rate 1/3 Viterbi Decoding/Coding Gain Over Hard Decisions

Modulation	Coding Gain (dB) Over Hard Decisions		
	Soft Decision (8-Level)	List of 4	List of 8
FH/DPSK	3.4	---	---
FH/DQPSK	1.2	---	---
FH/MFSK	1.7	3.7	4.8
FH-PM/DPSK	1.5	---	---
FH-PM/DQPSK	1.3	---	---
FH-PM/MFSK	1.6	0.8	0.8

still less for FH/DPSK. The required $(E_b/N_0)_{eff}$ for FH/DQSK is 3.5 dB less than required for FH/MFSK and 0.6 dB less than required for FH/DPSK. With FH-PN spread spectrum modulation, however, FH-PN/DPSK and FH-PN/MFSK require $(E_b/N_0)_{eff}$ within 0.1 dB of each other and require about 0.8 dB less $(E_b/N_0)_{eff}$ for a given bit error probability than FH-PN/DQPSK. For FH-PN/MFSK, List-of-L quantization is not as effective as soft decisions because the worst case interference is partial band noise.

2.3 Baseline Signal Design

As a result of the comparison of PN, FH, and FH-PN spread spectrum modulation with various data modulation, the most promising signal design for the required wide variations in data rates and hop rates is FH-PN/MCSK. The performance of FH-PN/MCSK against the worst case jammer is analyzed in Appendix C. A summary of the performance as a function of hops per symbol, bits per symbol, code rate (binary feedback decoding) is presented in Table 9.

The optimum partial jam band α in Table 9 is given in percent where there has been no restriction placed on α. The results in Table 9 show that increasing the number of hops per symbol and employing rate 1/2 coding increases the optimum jam band, while increasing the bits per symbol decreases the optimum jam band. Note, however, that with M = 16, N = 8 and rate 1/2 coding, the jammer is forced to jam the total band.

A comparison of PN/PSK and FH-PN/MCSK is presented in Table 10. At a bit error probability of 10^{-3}, the performance measure for PN/PSK is 4.5 dB better than FH-PN/MCSK. However, at 300 MHz, the largest PN chip rate is about 5 MHz under the worst case ionosphere. Alternately, the FH-PN/MCSK modulation can be used at the 20 MHz allocated bandwidth. Therefore, the FH-PN/MCSK outperforms the PN/PSK modulation by about 1.5 dB for worst case ionosphere. The performance difference is probably not enough to warrant a design choice on this basis. Other advantages of the FH-PN/MCSK modulation include more

Table 9. Antijam Performance For Multiple Code Shift Keying

Hops/Symbol	Bits/Symbol	Code Rate	Percent Partial Jam Band	Performance Measure G (dB)
1, 1/2, 1/3, 1/4, 1/6, 1/12, 1/24	2	1	0.50	23.7
		1/2	13.4	12.4
	3	1	0.48	22.9
		1/2	12.7	11.7
	4	1	0.48	22.6
		1/2	12.9	11.3
2	2	1	6.40	16.7
		1/2	33.0	12.6
	3	1	4.60	16.4
		1/2	23.6	12.3
	4	1	3.24	16.7
		1/2	16.6	12.6
4	2	1	36.2	12.2
		1/2	83.2	11.6
	3	1	30.4	11.2
		1/2	69.6	10.6
	4	1	25.6	10.7
		1/2	58.4	10.1
8	4	1	72.4	9.2
		1/2	100.0	10.4

Table 10. Performance Comparison of PN/PSK and FH-PN 4-ary MCSK

	FREQUENCY HOPPING PSEUDO-NOISE	DIRECT SEQUENCE PSEUDO-NOISE
MODULATION	NONCOHERENT 4-ARY MCSK	COHERENT QPSK
REQUIRED $\left(\frac{W}{R_c}\right)\left(\frac{S}{J}\right)$		
$P_b = 10^{-3}$ UNCODED	23.7 dB	19.2 dB
$P_b = 10^{-3}$ CODED	12.4 dB (15.0 dB)	7.9 dB
SYNCHRONIZATION	UNCERTAINTY PN CHIP RATE	UNCERTAINTY PN CHIP RATE (SPREAD BANDWIDTH)
MULTIPLE ACCESS BY CDMA	ORTHOGONAL FREQUENCY SLOTS	ORTHOGONAL PN CODES (LIMITED BY SELF NOISE)
SPREAD BANDWIDTH AT 400 MHz CARRIER	200 MHz	5 - 10 MHz (1.5 dB LOSS AT 10 MHz)

rapid synchronization and better multiple access capability. In fact, the capability of frequency hopping to selectively reject certain frequency bands and to require only a small instantaneous bandwidth makes the FH-PN/MCSK modulation very attractive in this case where the frequency allocation is distinct slots.

3.0 MULTIPLE RATE FH-PN/MCSK SYSTEM DESIGN

The most promising signal design to meet the system objectives presented in Table 2 is FH-PN/MCSK. In this section, a system design is described to meet the multiple data rates and hop rates given in Table 2.

3.1 FH-PN/MCSK Modulator

The block diagram of the FH-PN/MCSK is shown in Figure 14. The incoming data is rate 1/2 convolutional encoded for binary feedback decoding at the receiver. Figure 15 illustrates the rate 1/2 convolutional encoding process. The input data is shifted into a shift register and an output register. The data in the shift register is sampled by five taps and modulo-2 added to the input data. The result of the modulo-2 addition is also stored in the output register. The output register is shifted out at twice the input data clock rate.

After the input data has been convolutional encoded, the coded data is interleaved. The interleaving is used to disperse the errors in data bits on a single jammed frequency hop among the data bits from unjammed frequency hops to achieve the full power of the binary feedback decoder. When the hop rate is faster than the MCSK symbol rate, then interleaving is not required for the jamming, but there are correlated errors between data bits from the same MCSK symbol. Therefore, to obtain the full power of the binary feedback decoder, data bits from the same MCSK symbol should be separated with 22 data bits from other MCSK symbols.

The 4-ary MCSK modulator groups two coded data bits that have been interleaved to chose which 4-ary code symbol should be transmitted. Each 4-ary MCSK symbol consists of four binary bits as shown in Table 11. The binary sequence resulting from the MCSK modulator is shown in Figure 14 to be modulo-2 added to the PN sequence. In order to combine the PN modulation and the MCSK modulation in this fashion, the PN chip rate must be an integer multiple of the MCSK binary sequence rate for all input data rates. Actually, this will be shown to have a number of implementation advantages in the demodulator as well as the modulator simplification. In addition, there is an anti-intercept advantage by having synchronous data and pseudonoise chips. If the data and pseudonoise chips are synchronous, then the data bits are completely hidden by the randomness of the PN code. This implies that the data cannot be extracted without first obtaining detailed knowledge of the specific PN sequence being used.

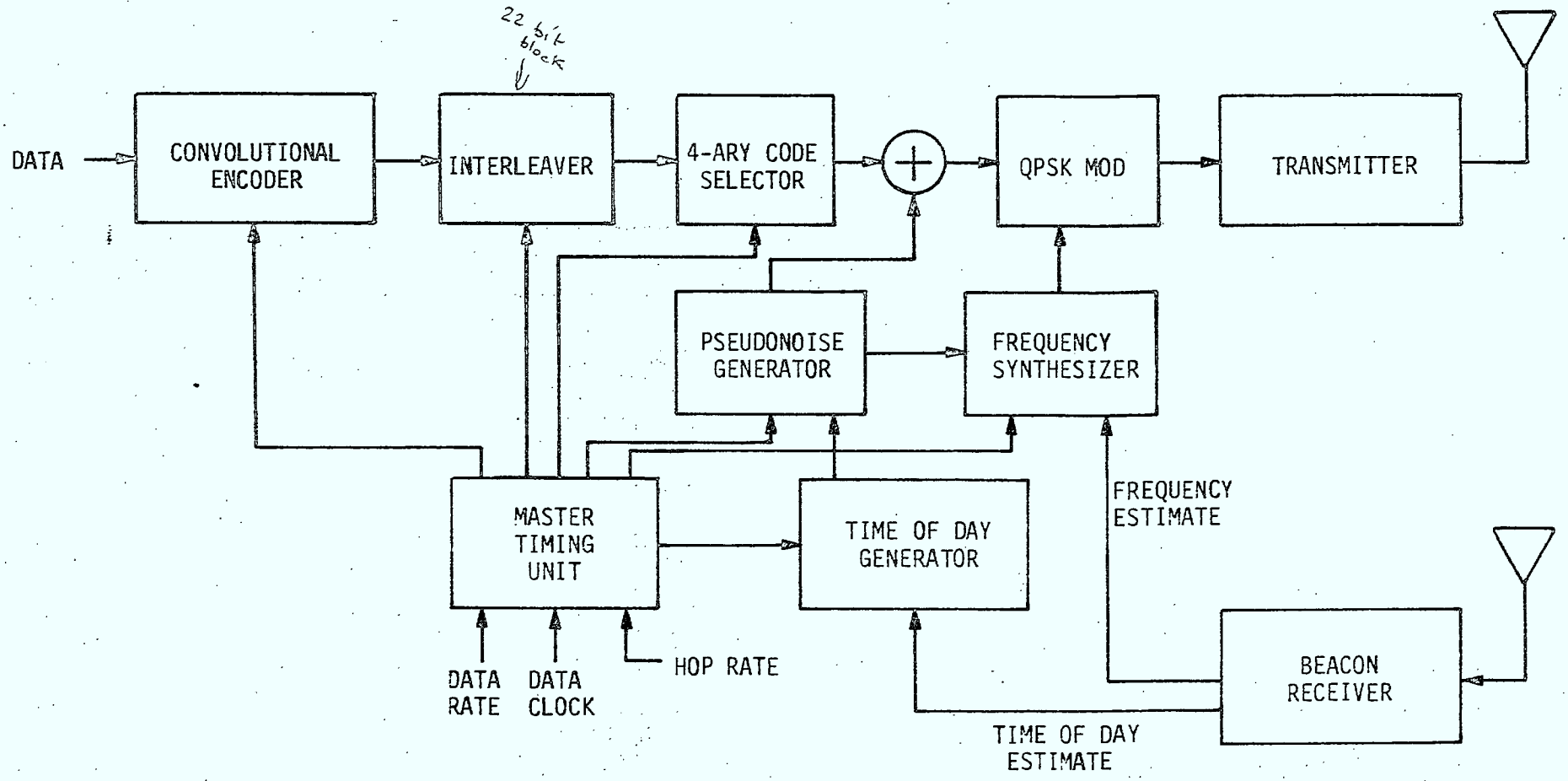

Figure 14. Frequency Hop-Pseudonoise 4-ary Multiple Code Shift Keying Modulator

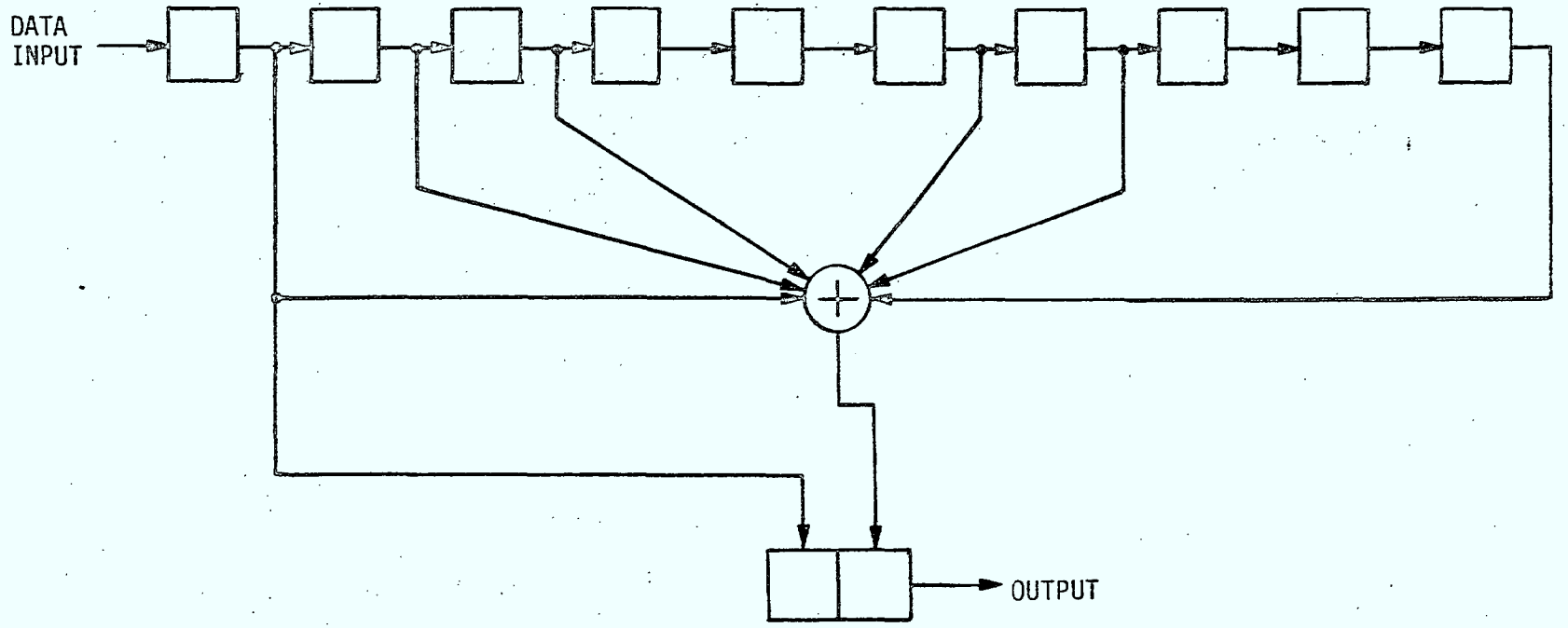

Figure 15. Rate 1/2 Constraint Length 10 Convolutional Encoder

Table 11. 4-ary MCSK Symbols

Input Data	Output 4-ary MCSK Symbols
0 0	1 0 0 0
0 1	0 1 0 0
1 0	0 0 1 0
1 1	0 0 0 1

Following the modulo-2 addition of the encoded data and the PN, the resulting digital data stream is quadriphase-shift-keying (QPSK) modulated on to the frequency hopped carrier. For the high data rates (e.g., 1200 bps and 2400 bps), the 50 msec frequency settling time of the frequency hopper becomes a large portion of an MCSK symbol. Therefore, it is important to have the frequency hopping synchronous with the data and PN. With all the timing synchronous, the demodulator can be significantly simplified. In order to have all the rates synchronous, the PN code rate should be 24 kbps (or 12 ksps for QPSK symbols). Then to accommodate the data rates of 50, 75, 150, 300, 1200, and 2400 bps, the hop rates should be chosen to be 1200, 600, 300, 150, 25, 5 hps.

The antijam performance of the modulator system design that is described above is presented in Tables 12-14. For comparison, Tables 15-17 present the antijam performance with no error correction coding. The antijam performance is calculated using the derivation in Appendix C with correction for nonoptimum frequency hop spacing. The antijam performance measure G is given by

$$G = (E_b/N_0)_{eff} = \left(\frac{S}{J}\right)\left(\frac{W}{C}\right)\left(\frac{B}{R_s}\right)\left(\frac{\ell}{R}\right) \qquad (23)$$

where

S = signal power
J = jammer power
W = the total hopping bandwidth (20 MHz)
C = the frequency hop spacing (25 kHz)
B = PN code rate (12 ksps)
R_s = MCSK symbol rate, (200, 300, 600, 1800, 4800, 9600, sps)
ℓ = bits per MCSK symbol (2)
R = error correction code rate (1/2)

Note that the data rate R_b (i.e., 50, 75, 150, 300, 1200, 2400, bps) is

$$R_b = R_s R/\ell. \qquad (24)$$

Table 12.

Antijam Performance of FH-PN/4-ary MCSK
Rate 1/2 Encoded/Binary Feedback Decoded

Data Rate (bps)	Hop Rate (hps)	N Hops/Symbol	C Chips/Symbol	Partial Band α	$(E_b/N_0)_{Eff}$ (dB)	J/S (dB)
50	1200	24	240	1.0	15.0	37.8
	600	12		1.0	13.3	39.5
	300	6		1.0	12.1	40.7
	150	3		0.609	11.7	41.1
	25	1/2		0.134	12.4	40.4
	5	1/10		0.134	12.4	40.4
75	1200	16	160	1.0	13.9	37.4
	600	8		1.0	12.5	38.6
	300	4		0.823	11.6	39.5
	150	2		0.333	12.6	38.5
	25	1/3		0.134	12.4	38.7
	5	1/15		0.134	12.4	38.7

Table 13.

Antijam Performance of FH-PN/4-ary MCSK
Rate 1/2 Encoded/Binary Feedback Decoded
(continued)

Data Rate (bps)	Hop Rate (hps)	N Hops/Symbol	C Chips/Symbol	Partial Band α	$(E_b/N_0)_{Eff}$ (dB)	J/S (dB)
150	1200	8	80	1.0	12.5	35.5
	600	4		0.823	11.6	36.4
	300	2		0.333	12.6	35.4
	150	1		0.134	12.4	35.6
	25	1/6		0.134	12.4	35.6
	5	1/30		0.134	12.4	35.6
300	1200	4	40	0.823	11.6	33.4
	600	2		0.333	12.6	32.4
	300	1		0.134	12.4	32.4
	150	1/2		0.134	12.4	32.4
	25	1/12		0.134	12.4	32.4
	5	1/60		0.134	12.4	32.4

Table 14.

Antijam Performance of FH-PN/4-ary MCSK
Rate 1/2 Encoded/Binary Feedback Decoded
(continued)

Data Rate (bps)	Hop Rate (hps)	N Hops/Symbol	C Chips/Symbol	Partial Band α	$(E_b/N_0)_{Eff}$ (dB)	J/S (dB)
1200	1200	1	10	0.134	12.4	26.6
	600	1/2		0.134	12.4	26.6
	300	1/4		0.134	12.4	26.6
	150	1/8		0.134	12.4	26.6
	25	1/48		0.134	12.4	26.6
	5	1/240		0.134	12.4	26.6
2400	1200	1/2	5	0.134	12.4	23.6
	600	1/4		0.134	12.4	23.6
	300	1/8		0.134	12.4	23.6
	150	1/16		0.134	12.4	23.6
	25	1/96		0.134	12.4	23.6
	5	1/480		0.134	12.4	23.6

Table 15.

Antijam Performance of Uncoded FH-PN/4-ary MCSK

Data Rate (bps)	Hop Rate (hps)	N Hops/Symbol	C Chips/Symbol	Partial Band α	$(E_b/N_0)_{Eff}$ (dB)	J/S (dB)
50	1200	48	480	1.0	14.9	39.9
	600	24		1.0	13.2	39.6
	300	12		1.0	11.9	40.9
	150	6		0.645	11.4	41.4
	25	1		0.005	23.7	29.1
	5	1/5		0.005	23.7	29.1
75	1200	32	320	1.0	13.8	37.3
	600	16		1.0	12.4	38.7
	300	8		0.860	11.4	39.7
	150	4		0.363	12.2	38.9
	25	1*		0.0048	22.9	28.2
	5	1/5*		0.0048	22.9	28.2

*8-ary MCSK

Table 16.

Antijam Performance of Uncoded FH-PN/4-ary MCSK
(continued)

Data Rate (bps)	Hop Rate (hps)	N Hops/Symbol	C Chips/Symbol	Partial Band α	$(E_b/N_0)_{Eff}$ (dB)	J/S (dB)
150	1200	16	160	1.0	12.4	35.6
	600	8		0.860	11.4	36.6
	300	4		0.363	12.2	35.8
	150	2		0.064	16.7	31.3
	25	1/3		0.005	23.7	24.3
	5	1/15		0.005	23.7	24.3
300	1200	8	80	0.860	11.4	33.6
	600	4		0.363	12.2	32.8
	300	2		0.064	16.7	28.3
	150	1		0.005	23.7	21.3
	25	1/6		0.005	23.7	21.3
	5	1/30		0.005	23.7	21.3

Table 17.

Antijam Performance of Uncoded FH-PN/4-ary MCSK
(continued)

Data Rate (bps)	Hop Rate (hps)	N Hops/Symbol	C Chips/Symbol	Partial Band α	$(E_b/N_0)_{Eff}$ (dB)	J/S (dB)
1200	1200	2	20	0.064	16.7	22.3
	600	1		0.005	23.7	15,3
	300	1/2		0.005	23.7	15.3
	150	1/4		0.005	23.7	15.3
	25	1/24		0.005	23.7	15.3
	5	1/120		0.005	23.7	15.3
2400	1200	1	10	0.005	23.7	12.3
	600	1/2		0.005	23.7	12.3
	300	1/4		0.005	23.7	12.3
	150	1/8		0.005	23.7	12.3
	25	1/48		0.005	23.7	12.3
	5	1/240		0.005	23.7	12.3

Therefore, to calculate the J/S ratio,

$$J/S = \left(\frac{W}{C}\right)\left(\frac{B}{R_b}\right)\left(\frac{1}{G}\right) \tag{25}$$

where G is given in Tables 12 through 17 as $(E_b/N_0)_{eff}$.

Comparing Table 12 with the uncoded results in Table 15, it may be observed that the antijam performance is about equal for fast frequency hopping. This occurs because fast frequency hopping is very effective against jamming, and a simple binary feedback decoder does not improve the performance. However, when there is one or less hops per symbol, the binary feedback decoder improves antijam performance by about 11 dB over the uncoded performance. Consequently, the signal design with coding gives about the same antijam performance regardless of the hop rate. Alternately, the uncoded signal design results in very degraded antijam performance when the hop rate is one or less hops per symbol.

Table 12 also illustrates the effect on antijam performance due to noncoherent combining losses over several hops. For example, at a data rate of 50 bps, the 150 hps hop rate forces the jammer to jam the total hopping band. Increasing the hop rate above 150 hps still forces full band jamming, but there are more hops combined to form an MCSK symbol. The resulting antijam performance degradation is due to the increased number of hops noncoherently combined.

Referring again to Figure 14, synchronization between terminals is improved by using a beacon receiver to distribute time and frequency information to all the users in the network. Actually, the beacon receiver is shown in Figure 14 only to represent a function. The time and frequency information could also be obtained from a master terminal that transmits synchronization information to all network terminals. Another technique to maintain reasonably small time and frequency uncertainties is to use a very stable oscillator in each terminal.[7] In any case, the transmit frequency must be controlled to within 20 Hz for the lowest data rate of 50 bps or a MCSK symbol rate of 200 sps and the slowest hop rates (i.e., less than 200 hps). If the transmit frequency throughout the net cannot be held to this accuracy, then the receiver must perform a frequency search. Similarily, the time of day must be known to within 10 msec to minimize the PN code acquisition at the receiver.

The time of day (TOD) generator in Figure 14 is a counter of the same length as the PN generator. Since the PN code must have a period of two days,

the number of stages in the PN shift register must be at least 32 for a 24 kcps code rate. Let the TOD generator and the PN generator be all ones at the same time. To synchronize the PN code with the net, the 32 bit TOD estimate is received. Both the TOD generator and the PN generator are set to all ones and then clocked at a high speed until the TOD generator agrees with the TOD estimate. Using this technique, the terminal could be synchronized with the net in less than 2 minutes using a 35 MHz clock rate. If faster synchronization is required, either a faster clock rate can be used or more states of the PN generator corresponding to states of the TOD generator need to be stored. If more states of the generators are stored, then synchronization is found by calculating which stored state of the TOD generator is just less than the received TOD estimate. After choosing the correct stored state for the TOD generator, the corresponding PN generator state is loaded, and the two generators are clocked at a high speed until the TOD generator agrees with the TOD estimate. Synchronization with the net can be obtained in less than one second if 128 states of the two generators are stored and a 35 MHz high speed clock is used.

Using the concept of the beacon receiver, each terminal (when transmission is required) receives the TOD estimate and frequency estimate and updates its PN generator and frequency synthesizer. After updating the PN generator and frequency synthesizer, the terminal can transmit its message; and the receiving terminal, since it has also updated its PN generator and frequency synthesizer, will be able to synchronize with the transmitter in a very short time. It may be seen that if a very accurate oscillator is used to drive the TOD generator and frequency synthesizer, then net synchronization may be required only very infrequently.

Note that if the hopped carrier frequency is determined by the last 10 bits of the PN generator, then the frequency synthesizer only loads the contents from the PN generator every 20, 40, 80, 160, 960, or 4800 clock pulses corresponding to hop rates 1200, 600, 300, 150, 25, or 5 hps, respectively. Therefore, when the states of TOD and PN generators are stored, the number of clock pulses (until the frequency synthesizer should be loaded) must also be stored for each hop rate. Hence, after the TOD and PN generators have been updated to the stored TOD state (just less than the TOD estimate), then the TOD generator and PN generator are clocked. The number of pulses stored for the chosen hop rate and the frequency synthesizer is loaded. From that point on, the frequency synthesizer is loaded every so many clock pulses,

according to the hop rate, and the correct frequency will be transmitted corresponding to the state of the PN generator.

To selectively avoid certain frequencies in the frequency hopper, the 10 bit representations of these frequencies are stored. At each time the state of the PN generator is to be sampled by the frequency synthesizer, the last 10 bits of the PN generator are compared against the stored frequencies to be avoided. If the last 10 bits of the PN generator correspond to an undesirable frequency, then the contents of the PN generator are not loaded into the frequency synthesizer, and the frequency being transmitted is not changed.

3.2 FH-PN/MCSK Demodulator

The block diagram of the FH-PN/MCSK demodulator is shown in Figure 16. Net synchronization is achieved by the demodulator using a beacon receiver or similar equipment in the same way as the modulator. If a modulator and demodulator are collocated, then a single beacon receiver can be used to achieve net synchronization for both functions. The demodulator, as shown in Figure 16, consists of a RF receiver with an output at IF wide enough to pass the PN QPSK without significant filtering losses. Since the satellite channel bandwidth is 25 kHz, the receiver IF bandwidth can also be 25 kHz. The RF receiver also performs the AGC which should be fast enough to act independently on each frequency hop. If the AGC time constant is much less than the frequency hop duration, then a jammer cannot suppress the signal in multiple hops by jamming a single hop with a large power and then letting the AGC decay over several hops, thereby suppressing the signal in these subsequent hops. Therefore, the AGC time constant must be much less than 800 msec for the fastest hop rate 1200 hps. Most likely, the AGC time constant would not be changed for the slower hop rates. However, for the slow rate of 5 hps, the AGC time constant used for 1200 hps is probably too short.

The FH-PN modulation is removed following the RF receiver. After the spread spectrum modulation is removed, the MCSK data is left modulated on an IF frequency. This IF frequency is corrected to within at least 20 Hz over the frequency hop band by an Automatic Frequency Control (AFC) loop which fine tunes the frequency synthesizer. The 20 Hz requirement corresponds to the smallest MCSK symbol rate of 200 sps. Ignoring noise, it can be seen[1] that an unnormalized discriminator can be formed by

$$\hat{\omega} = I\frac{dQ}{dt} - Q\frac{dI}{dt} \qquad (26)$$

---

1 J.H. Park, Jr., "An FM Detector for Low S/N,", IEEE Trans. on Comm. Tech., Vol. COM-18, April, 1970, pp 110-118.

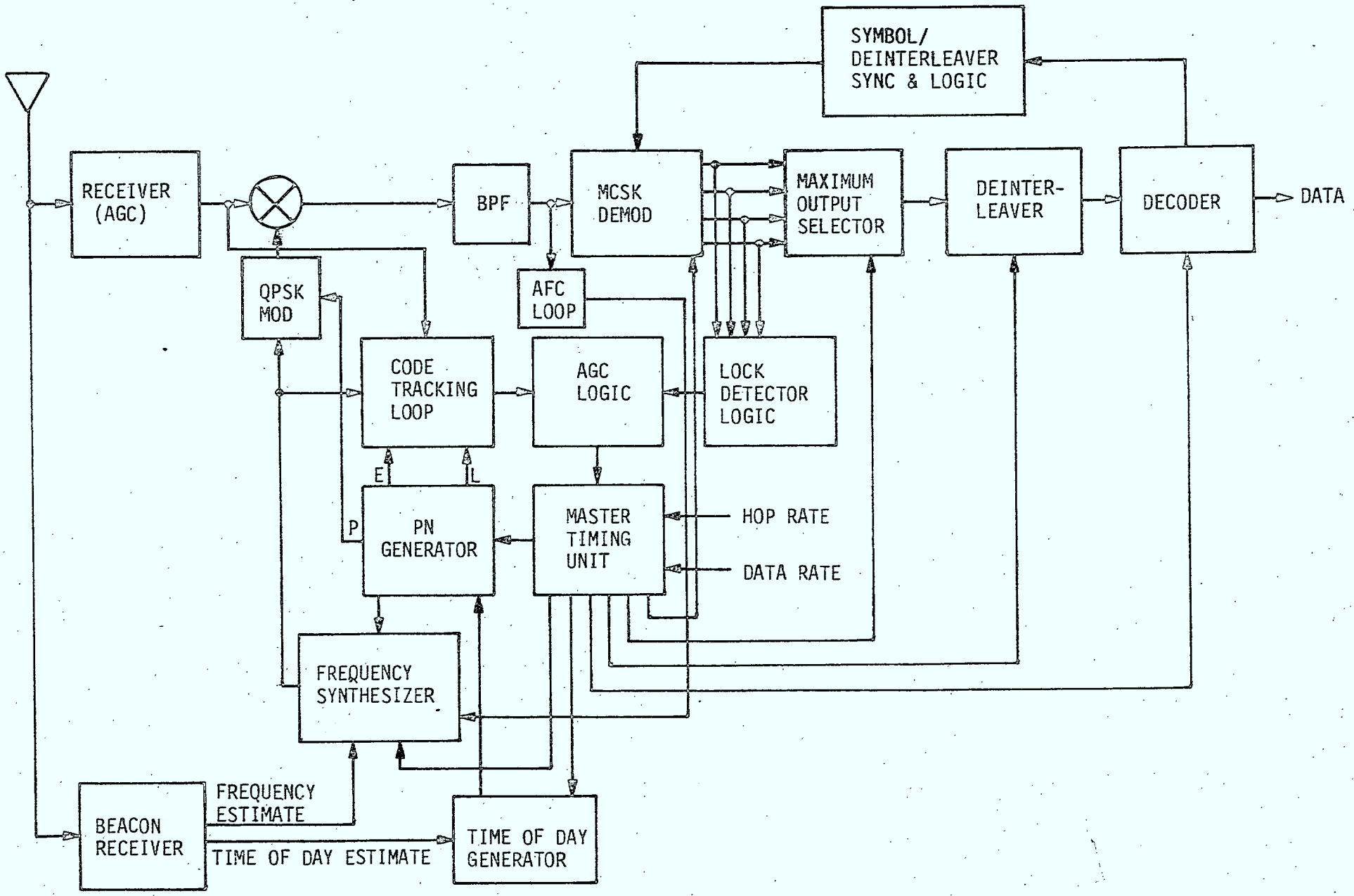

Figure 16. Frequency Hop-Pseudonoise 4-ary Multiple Code Shift Keying Demodulator

Approximating the time derivatives by finite time differences of Δ, then neglecting the scaling by $1/\Delta$, (26) becomes

$$\hat{\omega} = I(t-\Delta)Q(t) - I(t)Q(t-\Delta). \tag{27}$$

Thus, for a frequency error ω_e,

$$\begin{aligned} I(t) &= \cos(\omega_e t+\phi) \\ Q(t) &= \sin(\omega_e t+\phi) \end{aligned} \tag{28}$$

substituting these values into (27) gives

$$\begin{aligned} \hat{\omega}_e &= \cos(\omega_e t-\omega_e\Delta+\phi)\sin(\omega_e t+\phi)-\cos(\omega_e t+\phi)\sin(\omega_e t-\omega_e\Delta+\phi) \\ &= 1/2[\sin(2\omega_e t-\omega_e\Delta+2\phi)+\sin(\omega_e\Delta) \\ &\quad - \sin(2\omega_e t-\omega_e\Delta+2\phi)-\sin(-\omega_e\Delta)] \end{aligned} \tag{29}$$

$$\hat{\omega}_e = \sin(\omega_e\Delta) \tag{30}$$

Therefore, a control proportional to frequency error can be obtained if $|\omega_e\Delta|<1$. Note that (27) is not affected by biphase data modulation unless a data bit transition occurs within the delay Δ.

If noise is present, the mean of $\hat{\omega}_e$ is still given by (30), but there is a signal-to-noise ratio penalty due to the multiplication of wideband noise processes in (27). To avoid this severe penalty, the delay Δ can be realized by low pass filters, as shown in Figure 17. As an example of the frequency error characteristic that can be achieved for the low pass filter discriminator, a Manchester coded data spectrum was used to calculate the discriminator characteristic (output signal amplitude versus input frequency) illustrated in Figure 18. While Manchester coded data has a different spectrum than convolutional encoded MCSK data, the Manchester coded data example indicates the results that can be expected for the convolutional encoded MCSK data. Figure 18 illustrates the output amplitude $\hat{\omega}_e$ versus the frequency error ω_e normalized by the 3 dB cutoff frequency ω_c of the low pass filter. The discriminator characteristic is shown for $\omega_c T = 2.8\pi$ (the optimum product of ω_c and the data bit duration T for Manchester coded data at low values of E_b/N_0)[1] and $\omega_c T = 5.6\pi$. The equivalent linear gain K_ϕ (the slope of the

---

1 M.K. Simon and W.C. Lindsey, "Optimum Performance of Suppressed Carrier Receivers with Costas Loop Tracking," IEEE Trans. on Comm., Vol COM-25, No. 2, February, 1977, pp 215-227.

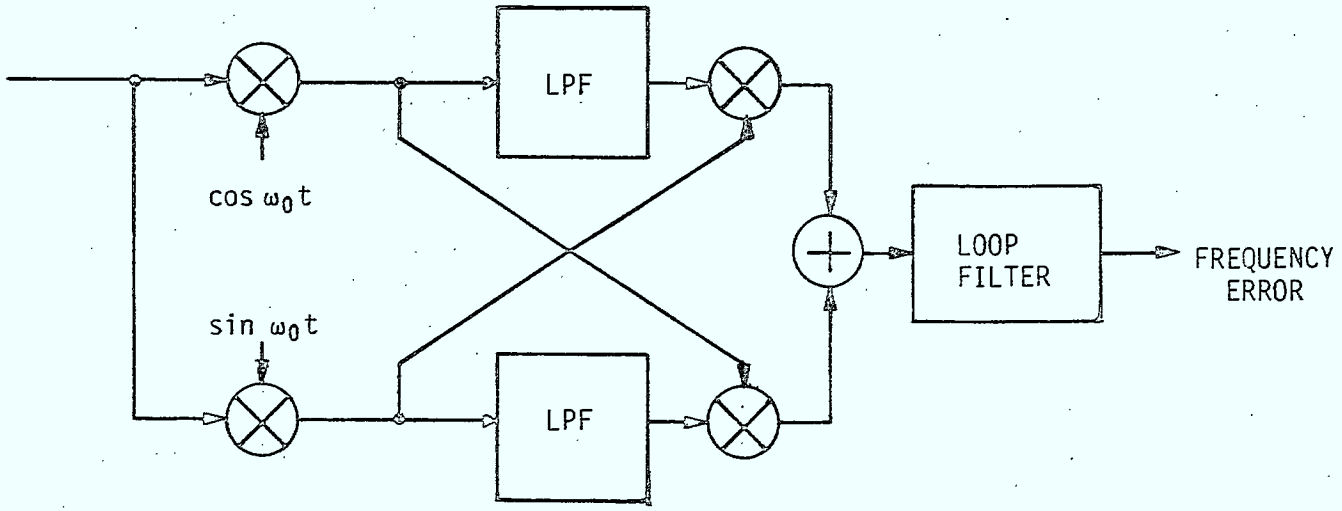

Figure 17. Automatic Frequency Control (AFC)

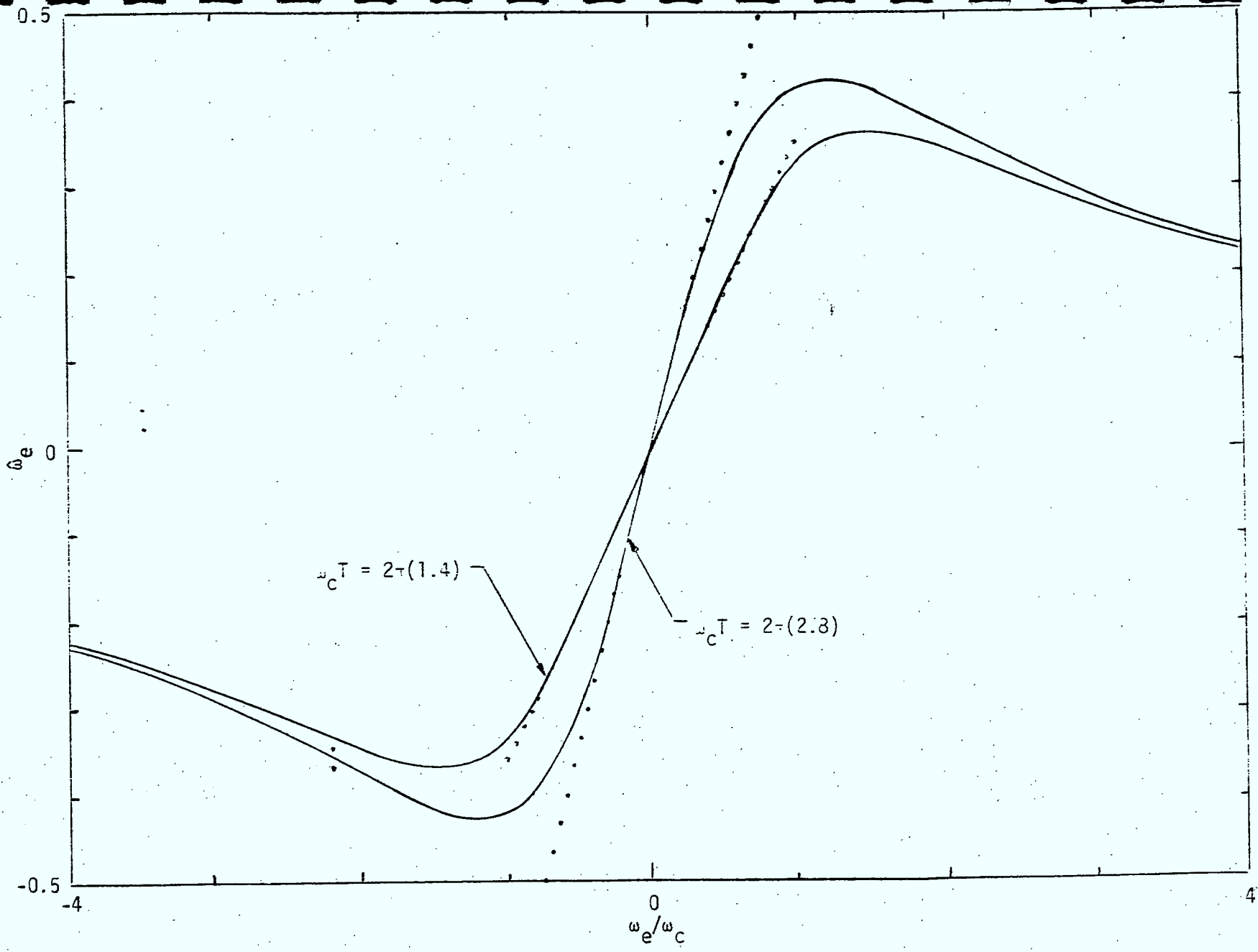

Figure 18. AFC Discriminator Characteristics

discriminator at zero frequency) is indicated in Figure 18 by dotted lines. Thus, assuming $\omega_e/\omega_c T$ to be small, then

$$\hat{\omega}_e = K_\phi \frac{\omega_e}{\omega_c} \tag{31}$$

Figure 19 is a plot of K_ϕ versus $f_c T = \omega_c T/2\pi$. Note from Figures 18 and 19, both the equivalent linear gain and the approximate region of linearity are functions of $\omega_c T$. In fact, at the optimum low pass filter design point ($f_c T = 1.4$), the normalized linear slope is 0.3535 rather than the more commonly assumed value of unity, which would be the case in the limit of infinite low pass filter bandwidth. This reduced value of equivalent linear gain comes about because of the low pass filtering of the Manchester coded data modulation. Alternately, increasing the low pass filter bandwidth increases the noise in the loop. As the low pass filter bandwidth becomes very large, there is again a severe signal-to-noise ratio penalty due to the multiplication of wideband noise processes. The loop filter for the AFC loop should be a two-pole low pass filter to make the closed loop response second order. A second order AFC loop will allow tracking a step function in frequency with zero frequency error. With only a simple imperfect integrating filter typically used in a Costas loop, the AFC closed loop response is only first order. A first order AFC loop will not track a step function in frequency with zero frequency error. The residual frequency error is proportional to the amplitude of the frequency step divided by a factor that is a function of the loop bandwidth, the natural frequency of the loop, and the equivalent linear gain.

After the AFC loop has reduced the frequency uncertainty below 20 Hz, the MCSK symbols are demodulated. Figure 20 presents one of four channels of the optimum 4-ary MCSK demodulator.[1] The cos $\omega_0 t$ and sin $\omega_0 t$ functions are supplied by the AFC loop. The MCSK code symbol is PSK modulated onto the cos $\omega_0 t$ and sin $\omega_0 t$ functions and multiplied by the received signal. The results of the multiplication are integrated over the 4-ary MCSK symbol duration (i.e., the four binary digits that represent one 4-ary MCSK symbol). Note that if the MCSK symbol duration is more than one frequency hop, then the frequency settling time ε is blanked out of the integration and the integration time T is equal to the duration of the frequency hop. In this case, following the integration, the results are squared and quantized where the quantized samples from each half of the demodulator are added together, and then the results are summed over the N frequency hops making up the 4-ary

---

1 A.J. Viterbi, Principles of Coherent Communication, McGraw-Hill, New York, 1966.

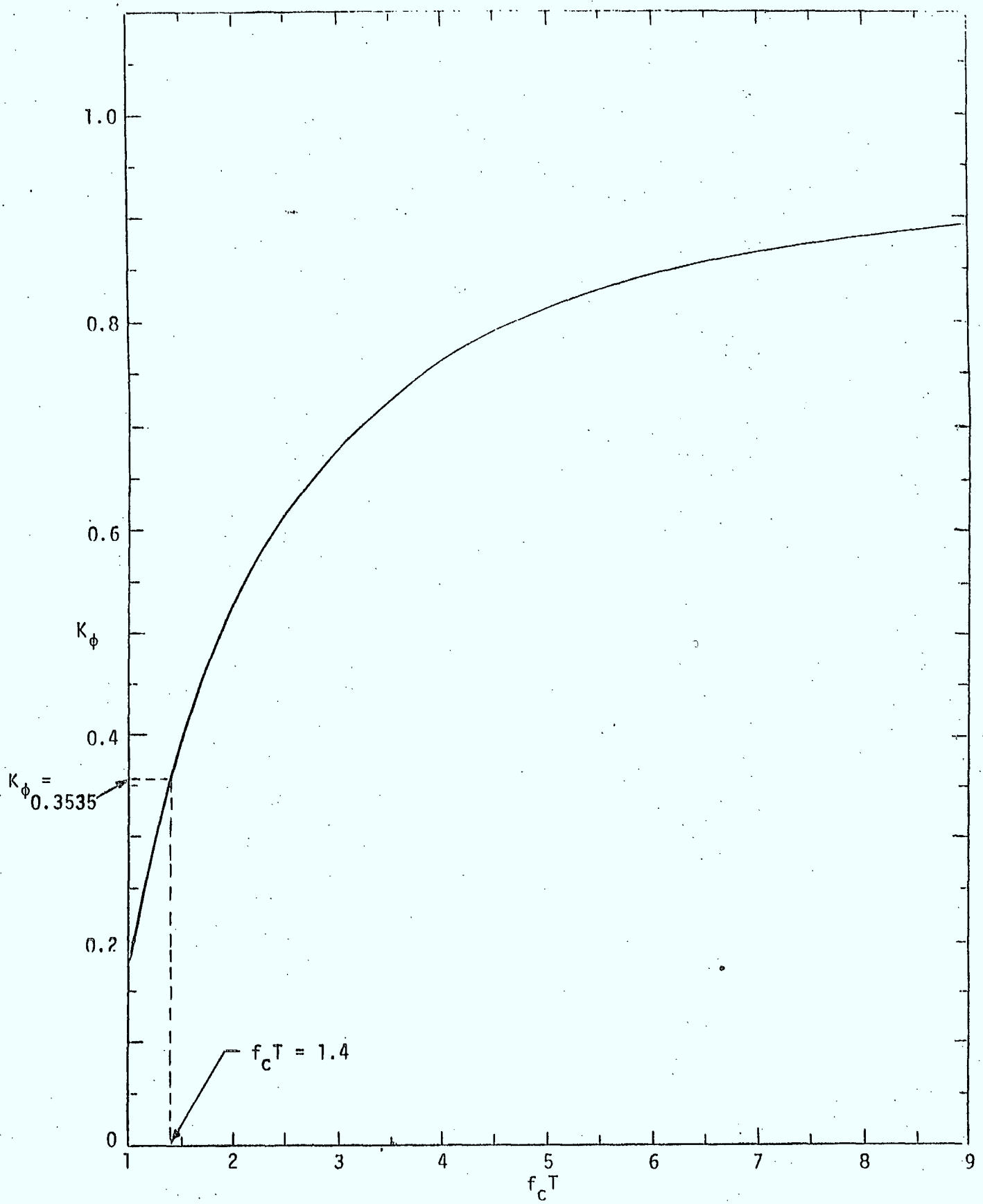

Figure 19. Discriminator Linear Gain vs. Ratio of Arm Filter 3 dB Cutoff Frequency to Data Rate

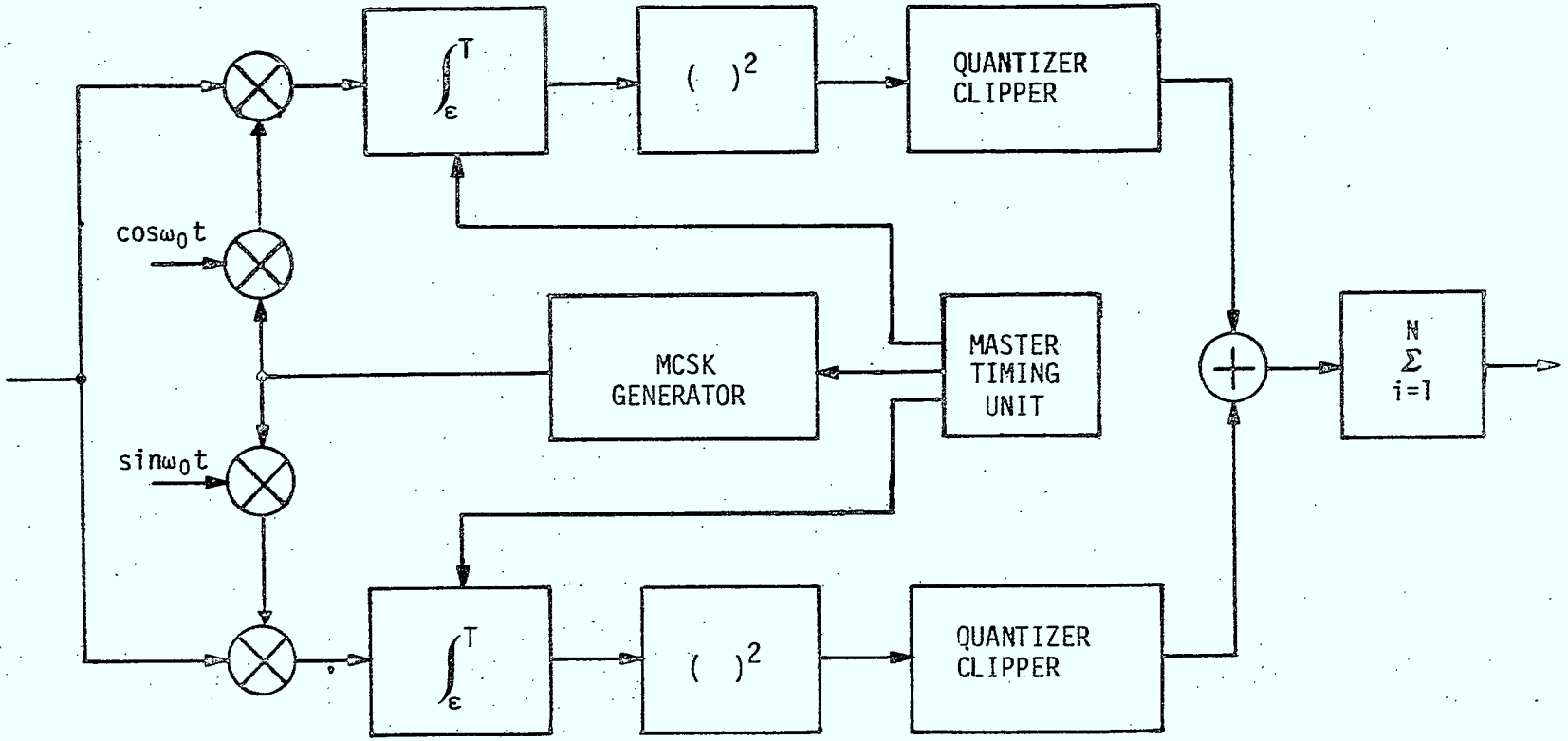

Figure 20. One Channel of Multiple Code Shift Keying Demodulator

MCSK symbol. If the MCSK symbol duration is equal to or less than the frequency duration, then the frequency settling time is not included in the integration, but the integration time T is equal to the MCSK symbol duration. In this case, there is no need for the summation over N hops since N is one or less. The timing for the MCSK generator comes from the Master Timing Unit (MTU) and is shifted at four times the input data rate of the modulator. Note that for data rates 1200 bps and 2400 bps with rate 1/2 convolutional encoding,the MCSK symbol is divided up into five chips to match the PN code rate. The fifth chip is equal to zero for each of the MCSK symbols.

The quantizer used in each half of the MCSK demodulator channels serves two purposes. First, the quantizer provides the output in a digital form so that summation over several hops and comparison of magnitudes of the other channels can be done by digital devices or by a microprocessor. The second purpose is to provide clipping of the received signal so that a large jamming signal cannot influence more than a single frequency hop. To insure protection against a large jamming signal, the maximum quantization level is set equal to the expected signal level. Thus, a large jammer will perhaps suppress the true signal below the maximum quantization level, but the jammer itself cannot produce a larger quantized output than the expected signal level on unjammed frequency hops.

There are four channels identical to the channel shown in Figure 20 that make up the MCSK demodulator. The outputs of the four channels are compared to determine which channel has the maximum output. The channel with the maximum output is then decoded by providing to the interleaver the two bits that identify the channel.

If the MCSK code in Table 11 is used, then each code word is a cyclic shift of first code word. This type of modulation code is denoted as a multiple cyclic code-shift-keying (MCCSK). The advantage in demodulator implementation using a MCCSK code is that a single channel can be easily time-shared rather than requiring the four channels shown in Figure 20. The MCCSK demodulator is illustrated in Figure 21. For simplicity, only one storage position is shown for each chip. However, as discussed in Appendix A, each chip would be represented by several samples, where each sample would be stored in the shift register. For example, suppose that each chip is represented by two samples and each sample is quantized to eight levels (i.e., three bits),then the register would have 24 stages. Table 18 illustrates the operation of the MCCSK demodulator when the received frequency and phase

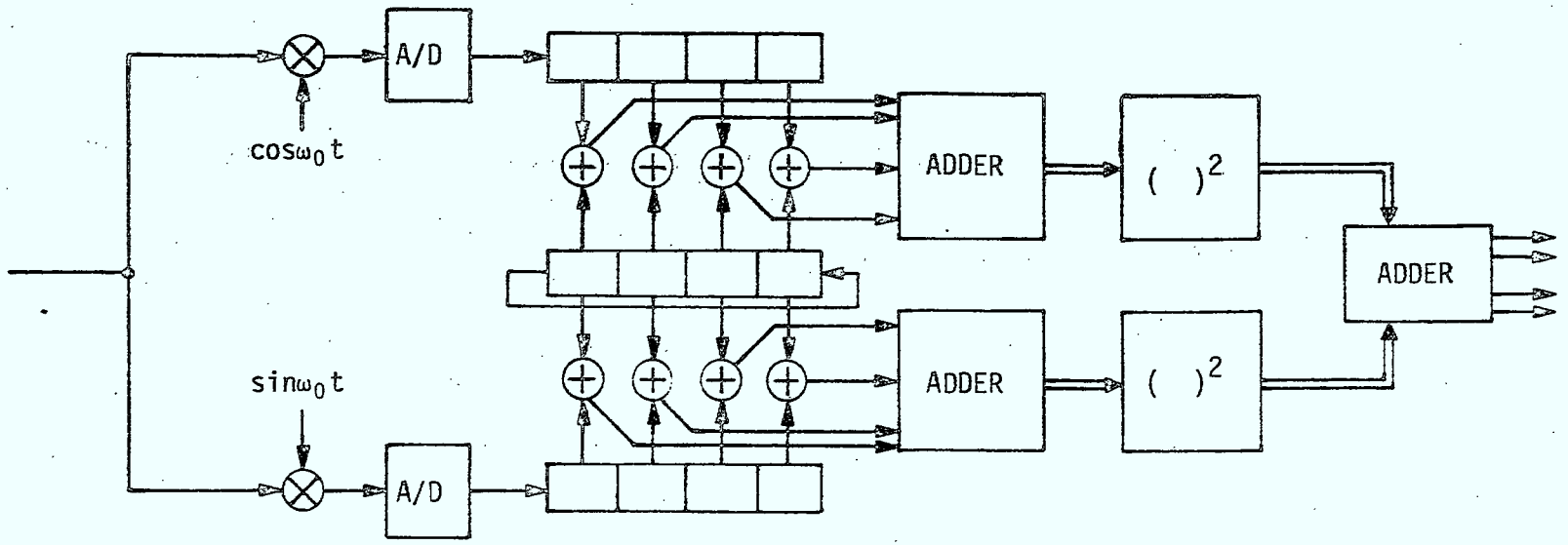

4-ARY MCCSK CODE

00	1000
01	0100
10	0010
11	0001

Figure 21.

Single Channel Digital Implementation of 4-ary Multiple Cyclic Code Shift Keying (MCCSK) Demodulator

Table 18. MCCSK Demodulation Example

Received Quantized Sequence	110	101	010	001	000	011	100	010	Total
Code Word 1000	000	000	111	111	111	111	111	111	
Modulo 2 Addition	110	101	101	110	111	100	011	101	
Octal Conversion and Normal Addition	6	5	5	6	7	4	3	5	41
Code Word 0100	111	111	000	000	111	111	111	111	
Modulo 2 Addition	001	010	010	001	111	100	011	101	
Octal Conversion and Normal Addition	1	2	2	1	7	4	3	5	25
Code Word 0010	111	111	111	111	000	000	111	111	
Modulo 2 Addition	001	010	101	110	000	011	011	101	
Octal Conversion and Normal Addition	1	2	5	6	0	3	3	5	25
Code Word 0001	111	111	111	111	111	111	000	000	
Modulo 2 Addition	001	010	101	110	111	100	100	010	
Octal Conversion and Normal Addition	1	2	5	6	7	4	4	2	31

matches either cos $\omega_0 t$ or sin $\omega_0 t$. The received quantized sequence is input into the 24 stage shift register by the A/D (i.e., sampler and quantizer). The quantization is that the smallest signal is 000 and largest signal is 111, with the signal levels in between denoted by the normal binary representation of the numbers from zero to seven. The quantized sequence is modulo 2 added to the MCCSK code words where a "1" in the code is represented by six zeros and a "0" in the code is represented by six ones. The results of the modulo 2 addition for each sample are added together to determine the maximum output. In Table 18, for convenience, the three bits representing each sample is converted to normal numbers and added together. The results of the addition in Figure 21 are squared and added to the results of the other half of the demodulator. It was assumed in Table 18 that only one half of the demodulator had a nonzero quantized sequence while the other half had a zero quantized sequence. For the zero quantized sequence, the output for each MCCSK code word is 14. Therefore, the output is $(41)^2+(14)^2=1877$ for the 1000 code word, $(25)^2+(14)^2=821$ for the 0100 and 0010 code words, and $(31)^2+(14)^2=1157$ for the 0001 code word. The maximum output corresponds to the 1000 code word and 00 would be the decoded binary digits input to the interleaver.

During synchronization of the PN generator, the outputs of the MCSK demodulator are used to determine when the local PN sequence is synchronized with the received PN sequence. After the PN generator has been coarsely synchronized with the network, the PN generator is stepped in half PN chip increments through the remaining time uncertainty. As the PN generator is delayed one half of a PN chip, the local frequency synthesizer will remain or the current frequency one half of a PN chip longer than normal. Eventually, the frequency generated by the frequency synthesizer will be the same as the received frequency long enough for the AFC loop to lock and refine the frequency uncertainty. The MCSK demodulator will attempt to decode the transmitted code word, but if the local PN sequence is not synchronized with the received PN sequence, then the outputs of each of the channels of the MCSK demodulator will be approximately the same. Therefore, the PN generator is continued to be stepped through the time uncertainty until one channel output of the MCSK demodulator is significantly larger than the other three channels. When this occurs, then the PN generator is considered synchronized, and the code tracking loop is enabled. Since the frequency hopping and the PN generator timing are also synchronous with the MCSK symbol rate, decoder

rate, and the data rate, only the timing ambiguity needs to be resolved, but additional time tracking loops are not required. Another approach to synchronizing the local PN sequence with the received PN sequence is to use a digital matched filter. Figure 22 presents a digital matched filter implementation of QPSK modulated PN. To use the digital matched filter for synchronization, the signal from the RF receiver is mixed with the unmodulated frequency from the frequency synthesizer. The bandwidth of the filter following the mixer must be 25 kHz during synchronization to pass the PN QPSK modulation. The frequency synthesizer is stepped in increments equal to one fourth of the duration of a frequency. One fourth steps are used in this case to minimize the degradation due to an error in the beginning of a frequency hop as well as the misalignment of the PN sequence. As the frequency synthesizer is set to a new frequency hop starting time, the PN sequence is loaded into the digital matched filter. The received PN sequence is loaded into the digital matched filter and clocked in relation to the stored local PN sequence. When the stored PN sequence is synchronized with the received PN sequence, a large correlation value occurs at the output of the digital matched filter, and the PN generator is started with the state corresponding to the stored local PN sequence. Since the frequency synthesizer was stepped relative to the stored local PN sequence in the digital matched filter, the 10 bits corresponding to the frequency selected for the frequency synthesizer by the PN generator and the number of clock pulses to be input into the PN generator before the frequency is changed must be stored along with the state of the PN generator for the local PN sequence in the digital matched filter.

The use of the digital matched filter as described allows very fast acquisition because the total time uncertainty is searched in increments of one fourth of the frequency hop duration. Thus, for slow hop rates, the allowed time uncertainty can be quite large, and there is less requirement for the beacon receiver for net synchronization. For example, a clock with only moderate stability can be used to provide the time of day estimate.

The digital matched filter illustrated in Figure 22 operates very similar to the MCCSK demodulator. In fact, the matched filter for PN synchronization can be reconfigured after the code tracking loop is locked to perform the MCCSK demodulation. The only difference between the MCCSK demodulator and the PN synchronized matched filter is the use of $\cos(n\pi/2)$ and $\sin(n\pi/2)$ weighting functions which are slightly more complicated than the MCCSK demodulator. Table 19 presents the modulation angles for each pair of chips from the PN

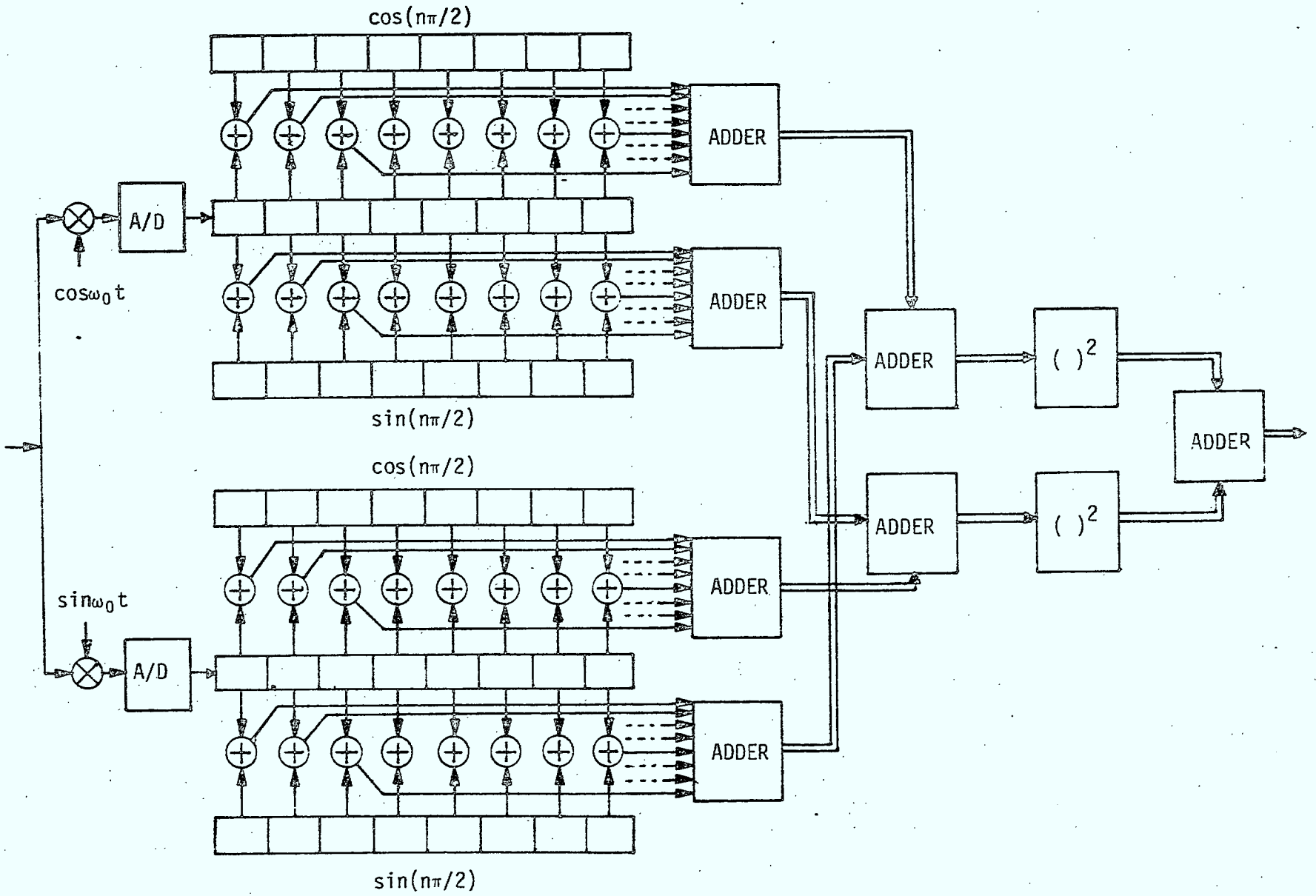

Figure 22. Matched Filter Implementation of QPSK Modulation

generator. Note that the $\cos(n\pi/2)$ and $\sin(n\pi/2)$ functions are three valued, while the MCCSK code chips were only two valued.

Table 19. QPSK PN Modulation/Demodulation

PN chips	Modulated Angle	Demodulator Functions	
		$\cos(n\pi/2)$	$\sin(n\pi/2)$
00	0^o	1	0
01	90^o	0	1
10	270^o	0	-1
11	180^o	-1	0

The value of zero for the demodulation functions means that the modulo 2 addition as shown in Table 18 is not performed and does not contribute to the sum for the output. If the samples are quantized to eight levels (i.e., three bits), then 000 is modulo 2 added to each sample when the demodulator functions are equal to 1 and 111 is modulo 2 added to each sample when the demodulator functions are equal to -1. For PN synchronization, at least four samples per PN chip should be used. With four samples per PN chip, the worst case signal degradation due to misalignment of the local and received PN sequences is 1.2 dB. There is also 0.25 dB degradation due to eight level quantization analog voltages, and there is a worse case degradation of 1.2 dB due to misalignment of the frequency hops if the matched filter must extend beyond a single frequency hop duration. Note that if more than one frequency hop must be included within the correlation time, then the correlation must be computed by sections of a digital matched filter where each section is matched to a single frequency hop, as discussed in Appendix A in connection with doppler.

After the PN generator has been synchronized with the received PN sequence, then synchronism is maintained by a code tracking loop. There are two types of PN code tracking loops: the delay lock loop (DLL) and the tau-jitter loop (TJL). The DLL is shown in Figure 23. The received signal is assumed to consist of a signal component and a bandlimited white Gaussian noise component $n_i(t)$ with the two-sided spectral density of $N_0/2$. The signal component is

$$\sqrt{2P_s}\, s(t-T) \cos(\omega_0 t+\phi) \qquad (32)$$

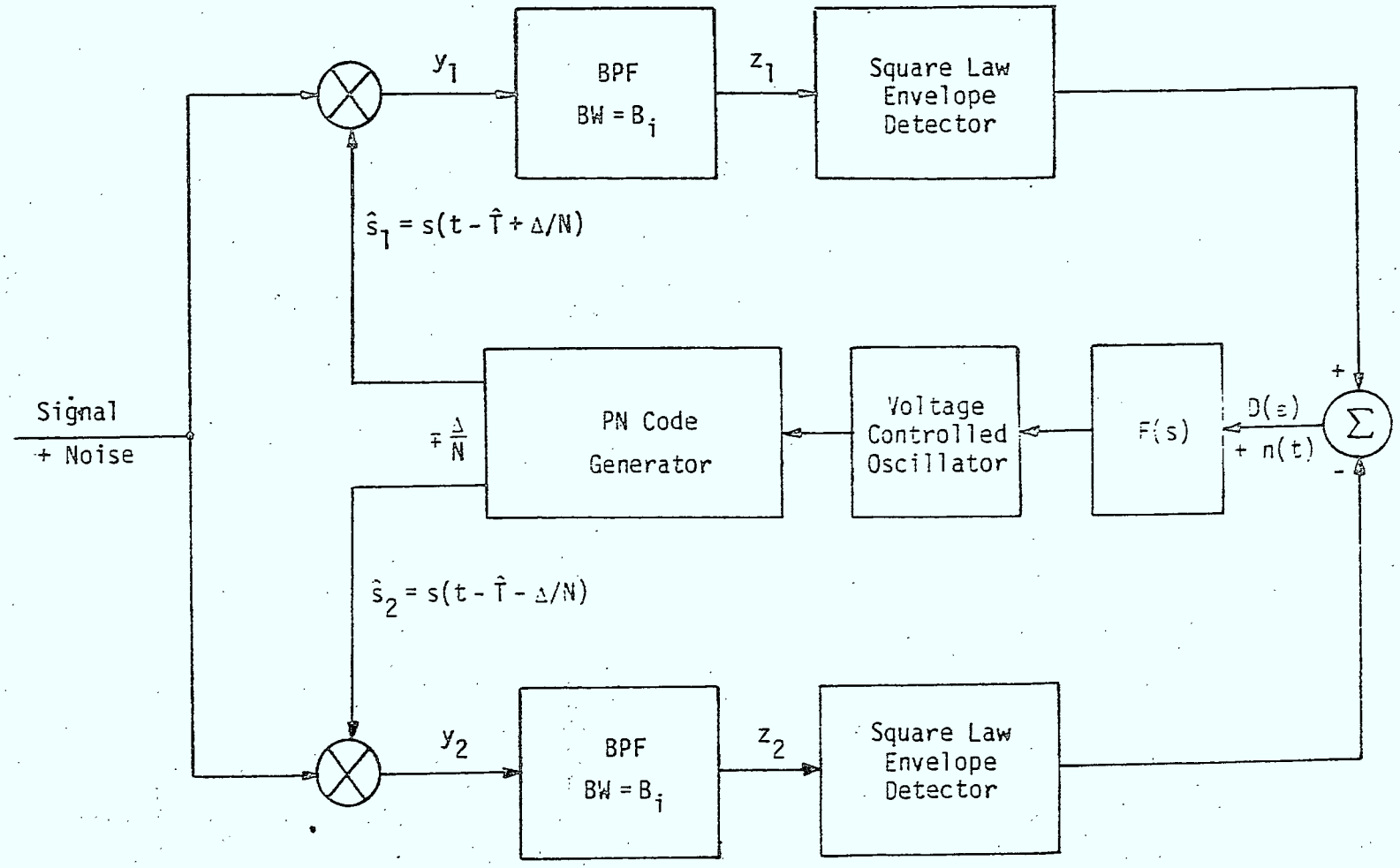

Figure 23. Block Diagram of the Delay Lock Loop

where s(t) is a PN code with a long period and ±1 amplitude, P_s is the average signal power, ω_0 is the carrier frequency including any doppler, T is the difference between the local PN and the receiver PN sequence, and ϕ is a random phase uniformly distributed between 0 and 2π. The received signal is multiplied at the phase detector with a delayed and an advanced replica of the signal component. The amount of correlator spacing is assumed to be $\pm\Delta/N$, where Δ is the chip time and N is any number larger than or equal to 2.

The outputs of the phase detectors assume the form

$$y_{12} = \sqrt{2P_s}\, s(t-T)\, s(t-\hat{T}\pm\frac{\Delta}{N}) \cos(\omega_0 t+\phi) + \text{Noise} \qquad (33)$$

where $\hat{T}$ is the estimated value of T. The delay error is denoted by $\varepsilon = T-\hat{T}$. The error is assumed to be in the region $|\varepsilon|<\Delta/N$.

Assuming that the bandpass filters are ideal rectangular filters with bandwidth B_i and that there is no distortion of the signal by the filters, the normalized mean square delay error can be shown to be

$$\sigma_T^2 = \frac{1}{N}\left[\rho_i^{-1} + (\rho_i)^{-2}\,\frac{N}{N-1}\right]\frac{B_L}{B_i} \qquad (34)$$

where $\rho_i \triangleq P_s/(N_0 B_i)$ is the signal-to-noise ratio at the output of the arm filter and where B_L is equivalent noise bandwidth of the loop. A finer analysis has been performed by Simon[1] which analyzes the effects of the bandpass filter on the signal and considers real filters rather than ideal rectangular filters. For optimized parameters, Simon shows that (34) is optimistic by about 0.9 dB. However, (34) is very easy to compute and can be used for initial design tradeoffs.

One of the disadvantages of the DLL is that in order to achieve the predicted performance at low signal-to-noise ratios, extreme care must be taken to balance the gains and bandwidths of the two arms of the DLL. The balance of the two arms becomes more difficult when the DLL must operate over a moderately large temperature range. To overcome these problems, the TJL is used. The TJL presented in Figure 24 was analyzed by Hartmann[2] and Simon[1].

---

1 M.K. Simon, Noncoherent Pseudonoise Code Tracking Performance of Spread Spectrum Receivers, IEEE Trans. on Comm., Vol. COM-25, No. 3, March, 1977, pp. 327-345.

2 H.P. Hartmann, Analysis of a Dithering Loop for PN Code Tracking, IEEE Trans. on Aerospace and Electronic Systems, Vol. AES-10, No. 1, January, 1974, pp. 2-9.

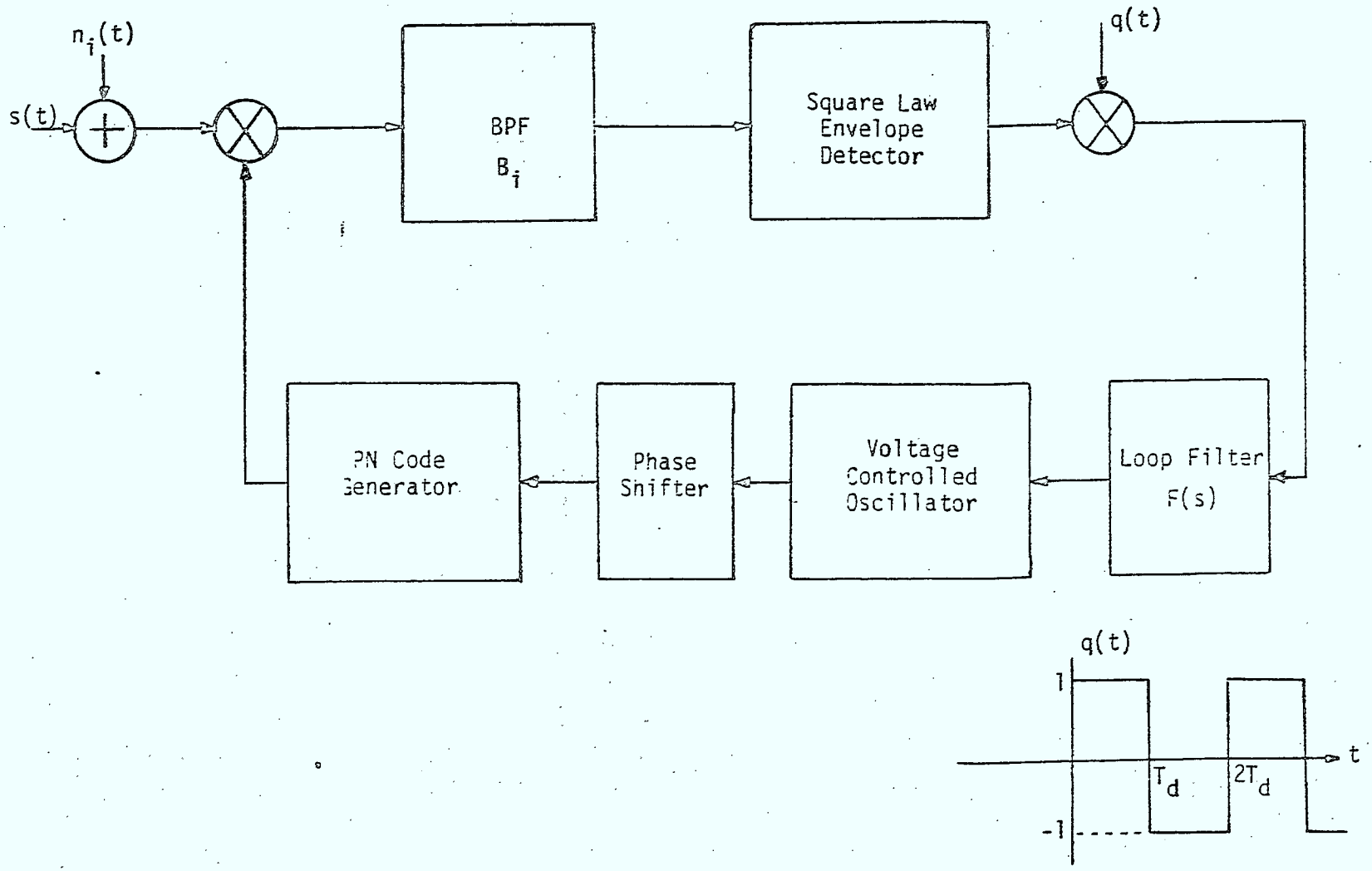

Figure 24. Block Diagram of Tau-Jitter Loop

The normalized mean square delay error was shown to be

$$\sigma_T^2 = \left[0.905(\rho_i)^{-1} + [0.453 - T_d B_i/10]\left(\frac{N}{N-1}\right)^2(\rho_i)^{-2}\right]\frac{B_L}{B_i}, \qquad (35)$$

where the dithering frequency $f_d = 1/(2T_d)$ is usually taken in the range $B_i/8$ to $B_i/4$. The assumptions concerning the ideal rectangular filter and no signal distortion caused by the filter were also part of Hartmann's results. Again Simon shows that for optimized parameters and real filters, Hartmann's results in (35) are about 0.9 dB optimistic. Figure 25 shows the comparison between the DLL and TJL for N=4 as a function of input signal-to-noise ratio P_s/N_0. The loop bandwidth (B_L) is taken as a parameter. The value of B_i was chosen for the highest data rate of 2400 bps (i.e., 9600 MCSK chips per second). Therefore, the performance could be improved for lower data rates by narrowing the bandwidth B_i as a function of data rate. Equations (34) and (35) can be used to calculate the performance for these other data rates.

The code tracking performance presented in Figure 25 shows that the percent tracking filter, $\sigma_T\%$, decreases with the increase of input signal-to-noise ratio P_s/N_0 as expected. Furthermore, the performance of the TJL is approximately 3 dB worse than that of the DLL because of the time-sharing between the early and late channels. This result does not take into account the performance degradation due to gain and bandwidth imbalance in DLL channels which tends to negate the difference in performance between the two loops.

The remaining blocks in Figure 16 that have not been discussed are the deinterleaver, the binary feedback decoder, and the symbol and deinterleaver synchronization logic. The deinterleaver is just the inverse of the interleaver in the modulator. The deinterleaver disperses error by separating data bits on a single frequency hop with 22 data bits from other frequency hops to achieve the full power of the binary feedback decoder. When the hop rate is faster than the MCSK symbol rate, then the deinterleaver is programmed to separate data bits from the same MCSK symbol by 22 data bits from other MCSK symbols to achieve the full power of the binary feedback decoder.

The binary feedback decoder is illustrated in Figure 26. The top shift register is a replica encoder which is used to form estimates of the parity checks from the received information bits. These estimates of the parity checks are modulo 2 added to the received parity checks to form syndrome bits.

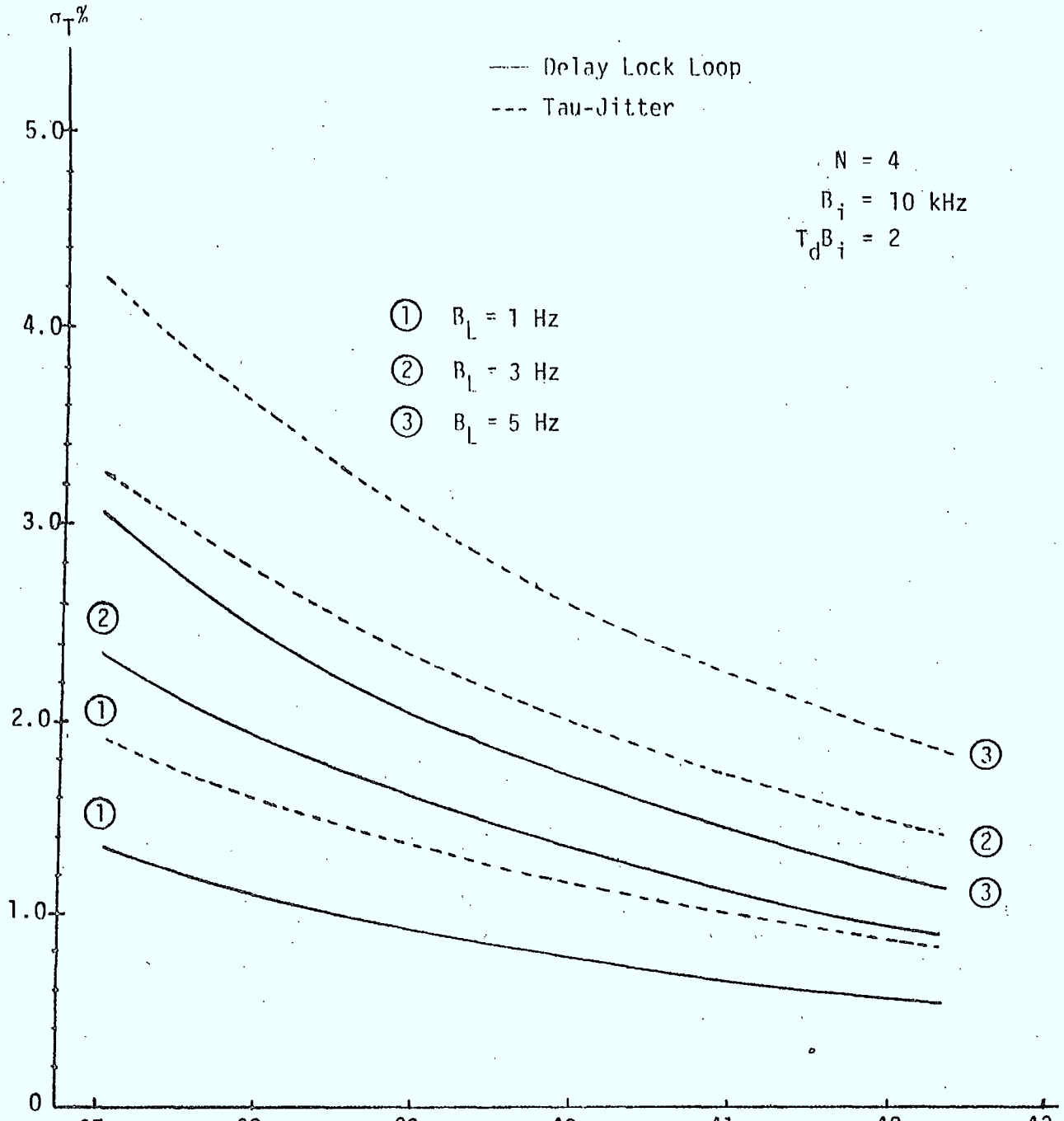

Figure 25. Percent Jitter Versus Signal-to-Noise Ratio (B_i = 1 MHz)

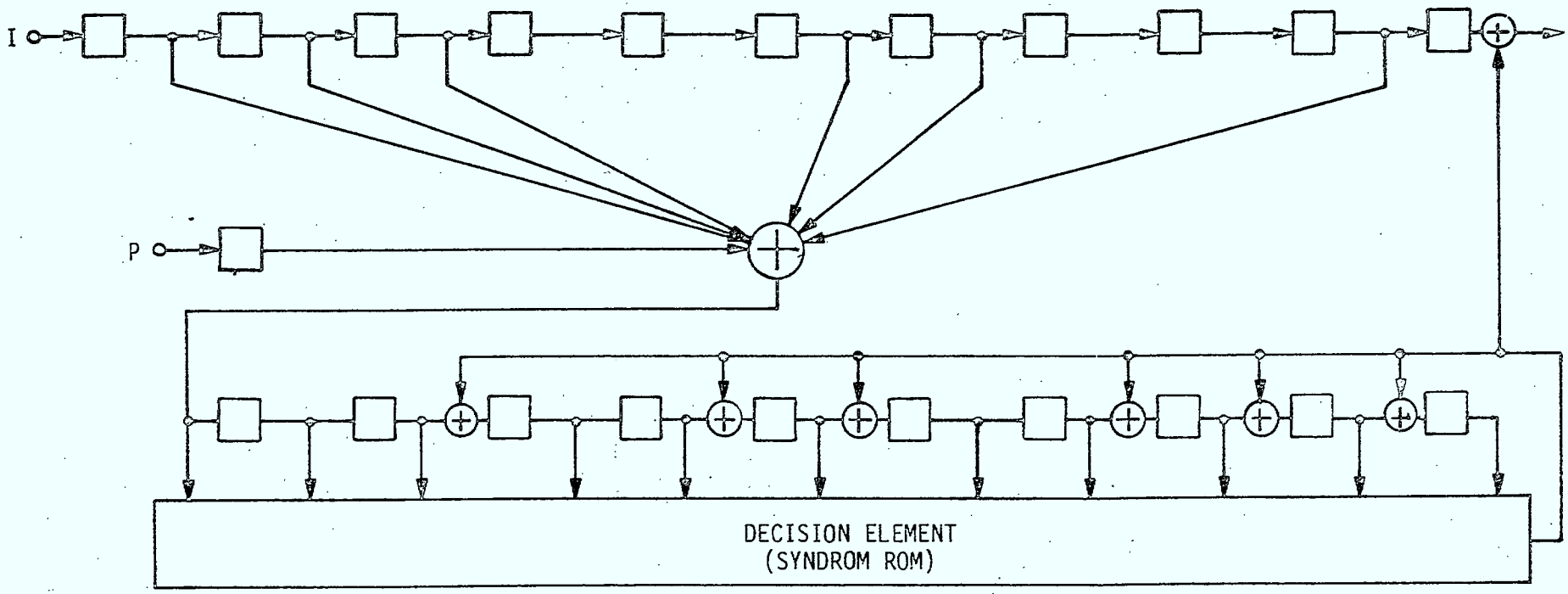

Figure 26. Rate 1/2 Constraint Length 10 Feedback Decoder

If no errors are made, the syndrome bits will be zero. If a parity check is in error, then a single syndrome bit will be equal to one, but if an information bit is in error, there will be six syndrome bits that will be equal to one. The decision element (i.e., a 2048 by 1 Read Only Memory) looks at patterns of syndrome bits to determine if an information bit is in error. If the syndrome pattern indicates that the next bit to be output from the replica encoder is in error, then the decision element has a one as an output to be modulo 2 added to the information bit to correct the error. Also, the other six syndrome bits that would be one due to the information bit error are complemented to negate the effect of the error in the syndrome register. The performance of the binary feedback decoder is presented in Figure 5 and throughout the report.

Synchronization of the MCSK demodulator, deinterleaver, and decoder can be performed in a number of ways. The two most common techniques used to synchronize these functions are to frame the data and use a frame synchronization word such as a Barker code or short PN code to identify the beginning of a frame or to use the decoder to identify synchronization. Using a frame synchronization word requires extra overhead in the message as well as requiring a matched filter for detection. The frame synchronization is not interleaved; however, it may be distributed throughout the frame. Distributed frame synchronization words provide added protection against pulse jammers, but the implementation becomes much more complex. Note that using the MCSK code in Table 11 results in the four different frame synchronization words (i.e.,one for each shift of the MCSK code) since the MCSK code is cyclic. Therefore, the matched filter for the frame synchronization word must be able to identify each of the possible words, or the MCSK demodulator synchronization must be shifted as each symbol is received to find the correct frame synchronization word. To provide probability of synchronization equal to 0.9 to 0.99 with a reasonably small probability of false synchronization, the frame synchronization word should be between 24 and 32 bits in length for a coded system.

The binary feedback decoder can also be used to determine synchronization, although probably not as quickly as using an optimum frame synchronization word. Using the binary feedback decoder to determine synchronization is the technique shown as part of the FH-PN/MCSK demodulator in Figure 16. When the MCSK demodulator or the deinterleaver is not synchronized with the received data, the convolutional code words do not match the data at the

input to the decoder. Therefore, the syndrome register indicates a large number of errors that must be corrected. This condition can easily be detected by the decision element if the ROM is slightly modified. When a large number of errors to be corrected occurs, the decoder indicates to the synchronization logic that either the MCSK demodulator or the deinterleaver is out of synchronism. Hence, the synchronization position is advanced one position, and the decoder is checked again. To perform this procedure rapidly, the deinterleaver must have the data stored as it was received before deinterleaving so that the deinterleaving for the new synchronization position can be easily recomputed.

4.0 CONCLUSIONS

This report optimized the signal and system design for a FH-PN spread spectrum system. Section 2 presented a general comparison of the signal design choices to illustrate under what conditions a given signal design is optimum. Section 3 presented a system design of the optimized FH-PN/MCSK signal. A number of system design tradeoffs were identified which need more analysis to refine the design.

APPENDIX A

MATCHED FILTER SYNCHRONIZATION OF PSEUDONOISE SPREAD SPECTRUM

Rapid acquisition of PN modulation is required to be a useful antijam technique if large antijam processing gain is required. Matched filters implemented by surface wave devices or digital techniques are the most feasible approaches to rapid acquisition that maintain high antijam protection. In theory, the matched filter correlator, which stores the PN waveform replica internally, and the active correlator, which accepts an externally generated replica, have similar characteristics for implementing a spread spectrum receiver. The distinction is that the active correlation requires synchronization of the external generator be acquired by a serial (or parallel) search of the time and frequency uncertainty. The matched filter reduces the acquisition to that of a frequency search. Alternately, the active correlator is more efficient in the tracking mode than the matched filter due to inherent implementation losses.

1. THE MATCHED FILTER

To begin the discussion a brief review is given of the use of a matched filter (MF) for initial synchronization of a spread spectrum receiver. The operational problem is that the time of arrival, or epoch, of the desired spread spectrum signal is unknown at the receiver due to the clock error and propagation delay. Hence, the concept of acquiring synchronization with the MF is to extract the epoch so that the PN code in the receiver can be properly aligned to start a conventional active correlation process which tracks synchronization and demodulates data. Figure 1 shows this concept in an elementary functional block diagram.

The segregation of the acquisition and tracking modes into distinct functional implementations has a fundamental advantage. During acquisition, degradation due to processing can be accepted if there is a net overall reduction in the time to acquire synchronization. For example, a degradation of 3 dB due to integration losses in a digitally implemented matched filter can, in principle, be made up by increasing the length of the matched filter by a factor of two. Hence, except indirectly through complexity and side effects like reduced doppler tolerance, the 3 dB degradation is not inherently a system performance loss. In contrast, in the tracking mode, any degradation is directly reflected as a reduction in data rate (or a reduction in tolerable jamming), and it is therefore imperative to implement the correlation process with a small loss.

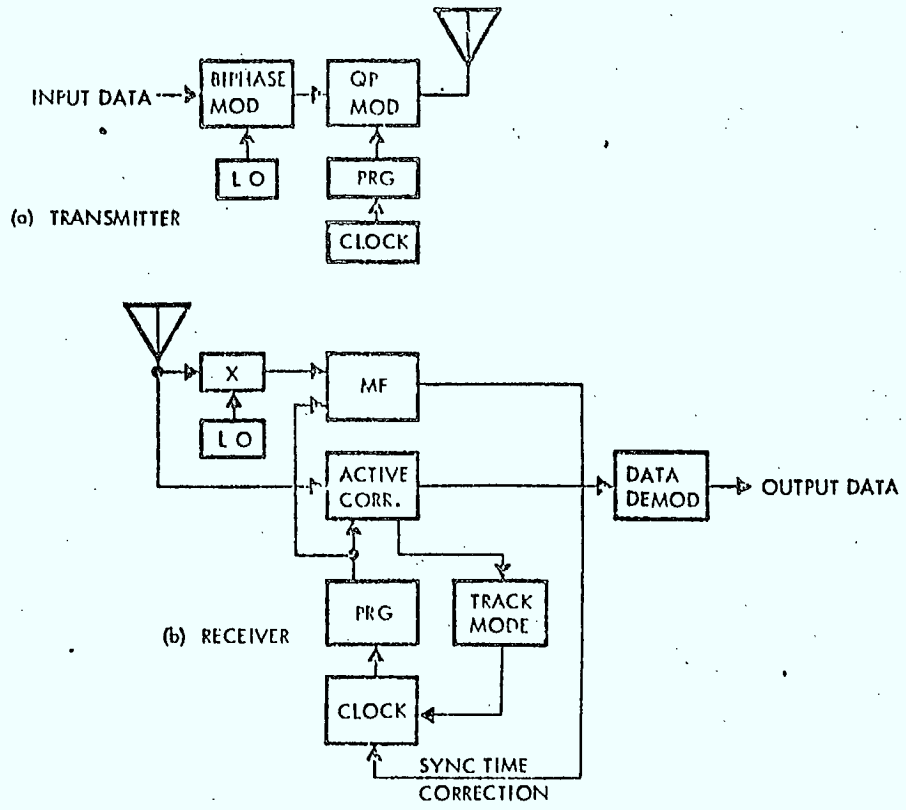

Figure 1. Functional Concept of a MF Synchronizer in a Spread Spectrum System

The basic concept of the MF acquisition circuit is shown in Figure 2, where the quantization is used when digital implementation is employed. Two parameters are of significance: (1) the bandwidth B, and (2) the time duration T of the matched filter. The product BT is often termed the "processing gain " and is a meaningful system parameter interpreted as an ideal signal-to-noise ratio improvement factor, so that

$$(S/N)_{output} = BT\ (S/J)_{input} = E/N_0 \qquad (1)$$

In the last equality, E is the received signal energy over the time duration T and N_0 is defined as the average jamming power per unit bandwidth.

The processing gain ideally is proportional to the number of PN bits stored in the MF; hence, the processing gain is loosely interchangeable

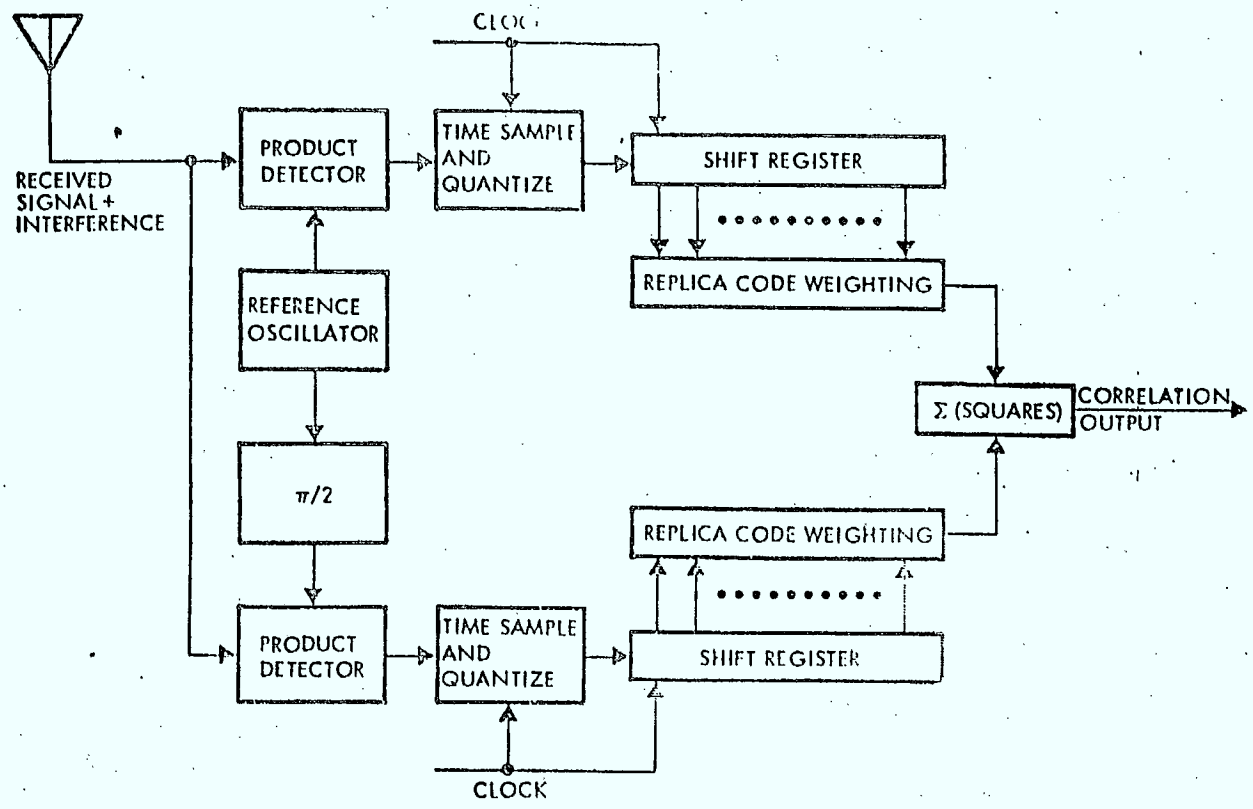

Figure 2. Concept of a Digital Matched Filter

with the length of the MF expressed as number of PN bits. Thus, the first problem is to compute the losses, i.e., degradation from the ideal of Equation (1) in a practical MF implementation. The second problem then is to compute acquisition performance as a function of $2E/N_0$ after the losses have been accounted for. These respective problems are treated by way of examples in the following sections.

A source of degradation in a digital MF is the requisite time sampling to obtain the discrete samples for storage. Now, a design parameter is the number of samples per PN bit. The question arises whether randomized aperiodic sampling might be a design strategy which is superior to periodic in the sense of allowing fewer samples to be taken.

Considering jamming by wideband noise, one is led to a low pass filter on the product demodulation output which is matched to the PN bit. The filter output response to a single bit is, then, the triangular correlation function shown in Figure 3. If m samples per bit are taken, the worst

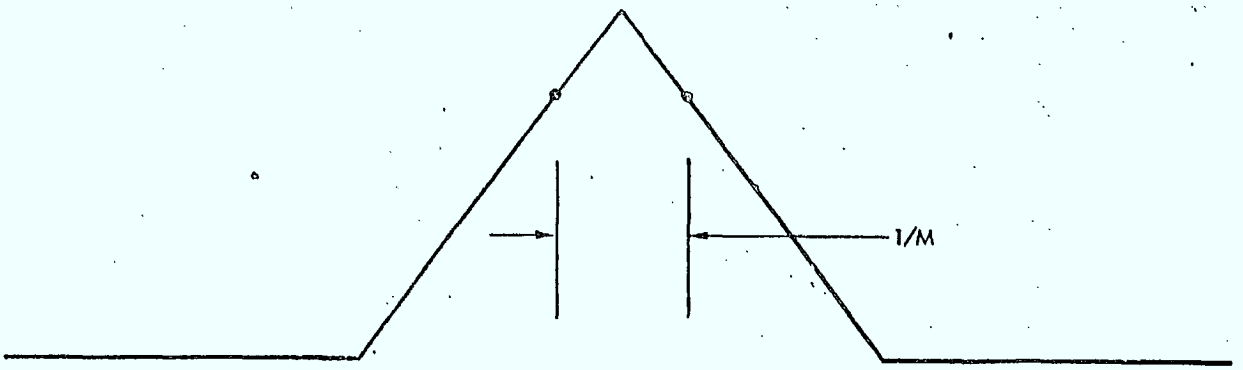

Figure 3. Output of an Ideal Low Pass Filter

case with periodic sampling is as illustrated and produces a maximum output amplitude equal to (2m - 1)/2m of the peak. The worst case degradation using just this maximum amplitude sample is given in Table 1. The most dramatic improvement is observed going from one and two samples per bit.

Table 1. Degradation for Worst Case Sampling

Number of Samples/Bit	Worst Case Degradation
1	6.0 dB
2	2.5 dB
3	1.6 dB

With periodic sampling at a multiple of the PN clock, the m samples per bit should be segregated into separate digital MF summations, as sketched in Figure 4. The best sample in the worst case has the loss given in Table 1.

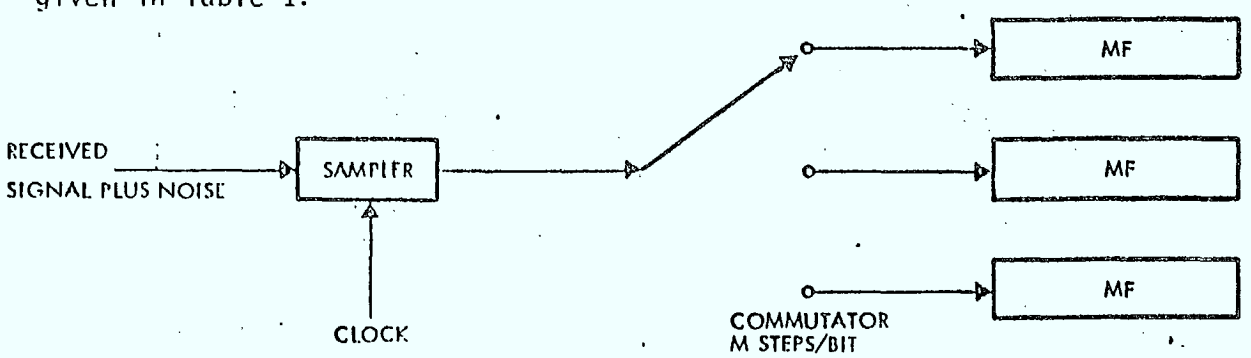

Figure 4. Optimized Periodic Sampling

No scheme of randomized (or jittered) time sampling seems to surpass the above periodic sampling approach. As a simple illustration, suppose one sample is taken per bit at a randomized time uniformly distributed over the bit width. In the worst case, the average amplitude is 0.5, equal to the 6 dB loss noted for the periodic sampling case, and for other timing errors, periodic sampling is superior.

If the carrier frequency on the received signal is offset by an error $\Delta\omega$, the performance of the MF is degraded because of reduction in correlation amplitude by the approximate factor

$$\text{Correlation amplitude} = \frac{\sin(\Delta\omega T/2)}{\Delta\omega T/2} \qquad (2)$$

where T is the length of the integration. Equation (2) predicts a loss of 0.9 dB if $\Delta\omega T = \pi/2$ and 4.0 dB if $\Delta\omega T = \pi$. Thus, the nominally allowed carrier frequency error in Hertz (such as doppler) is $\pm 1/4T$. Equation (2) presumes $\Delta\omega$ is constant and has to be modified when doppler rate of change becomes large.

If the frequency uncertainty exceeds the nominal maximum allowed error, multiple correlation integration must be employed. Then the replica must be matched to the doppler shifted signal. For example, the signal can be written in the general form

$$s(t) = a(t) \cos \omega_0 t + b(t) \sin \omega_0 t \qquad (3)$$

With a phase shift θ and an offset $\Delta\omega$ in the carrier frequency, the representation becomes

$$\begin{aligned} a(t) \cos ((\omega_0 + \Delta\omega)\ t + \theta) + b(t) \sin ((\omega_0 + \Delta\omega)\ t + \theta) \\ = (a(t) \cos \Delta\omega t + b(t) \sin \Delta\omega t) \cos (\omega_0 t + \theta) \\ + (- a(t) \sin \Delta\omega t + b(t) \cos \Delta\omega t) \sin (\omega_0 t + \theta) \qquad (4) \end{aligned}$$

which displays the replica waveforms now needed.

To analyze the detection performance of the matched filter, consider the basic detection problem of discriminating between the presence and

absence of a signal of known waveform and known epoch in the presence of Gaussian noise. Since, realistically, carrier phase is unknown, the receiver operating characteristic (ROC) for this basic problem is shown* in Figure 5. The parameter R is equal to $2E/N_0$.

For example, let us postulate $P_d = 0.9$ and $P_{fa} = 10^{-6}$. Achieving $P_d = 0.9$ requires an output signal-to-noise ratio

$$2E/N_0 = 16 \text{ dB} \tag{5}$$

which demonstrates the difficulties of the simple concept of attempting to recognize a preamble on a single trial.

An example of a more sophisticated verification strategy for sync acquisition may be proposed in the case where the time uncertainty ΔT (corresponding to the distance uncertainty) is small compared with the allowed acquisition time. The objective of the sophistication is to reduce the output signal-to-noise ratio required from the matched filter while still maintaining the goal for acquisition reliability. The basic strategy is to insert a portion of the PN code as a replica and to hold the replica for ΔT. During this interval, the times at which all threshold exceedances occurred are stored. During the next ΔT interval, all new threshold exceedences are stored, and all previous ones are rejected unless verified by a second occurrence. If verification occurs, sync acquisition is declared.

The advantage of this simple strategy can be seen by way of a numerical illustration. Let P_{fa} be 10^{-6} and $P_d = 0.9$. Then, for each trial, we can set $P_{fa1} = P_{fa2} = 10^{-3}$ and $P_{d1} = P_{d2} = 0.949$, since detection is declared after two trials. From Figure 5, the required signal-to-noise ratio is $2E/N_0 = 14$ dB, compared with 16 dB required for acquisition on a single trial. It can be seen by direct computation that little, if any, improvement is achieved in this numerical case by setting the thresholds differently for verification.

---

*DiFranco and Rubin, Radar Detection, Prentice-Hall, 1968.

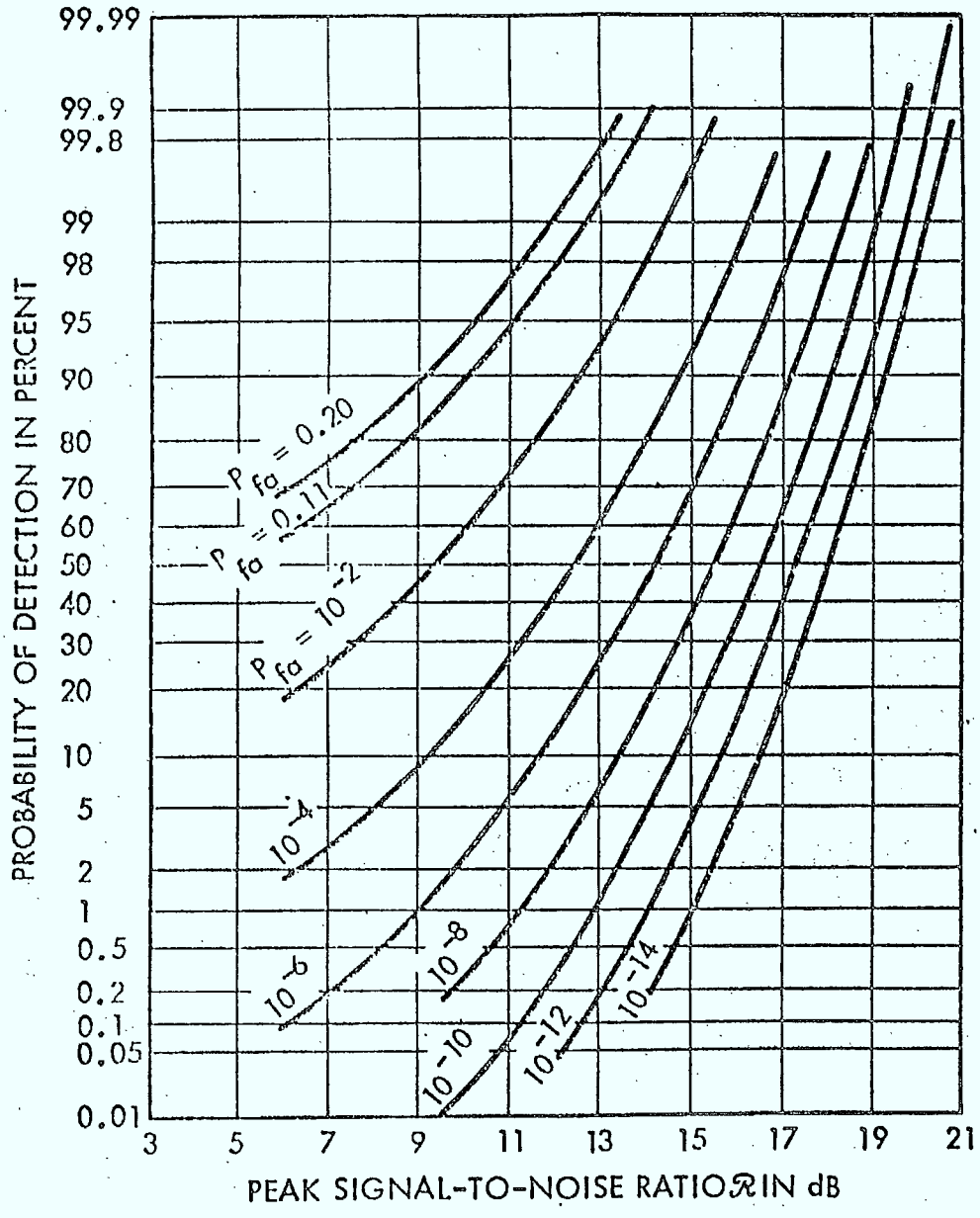

Figure 5. Detection Characteristic for Signal of Unknown Phase

A significant impact on performance will arise from the method of gain control. In an analog matched filter, gain is related to the threshold setting which defines the false alarm and detection probabilities; hence, gain control is critical. In a digital matched filter, the problem arises primarily with respect to quantization. In fact, with binary quantization, the false alarm and detection probabilities are determined from a binomial distribution and are independent of signal levels. However, the detection probablity still is affected by the method of amplitude quantization, optimization of which still requires measurement of interference power to define the randomized quantization process.

A practical implementation requires that the threshold be controlled relative to the interference power level, and Figure 6 is an illustration of a self-referencing correlation detection technique for AGC. As illustrated in Figure 6, the responses of two parallel channels are compared. One channel is the usual signal channel in which the received signal is correlated with a replica of itself stored as the impulse response of the matched filter. The other channel correlates the received signal with an orthogonal function of itself which is also stored as the impulse response of a matched filter. The purpose of the reference channel is to provide a reference threshold level which depends mainly on the uncorrelated signal and interference level. This scheme provides a variable decision threshold level for a relatively wide dynamic range. The gain factor of k, shown in the reference channel, provides for a differential or bias between the reference and signal channel outputs. The value of k can be varied to adjust false alarm and false dismissal probabilities.

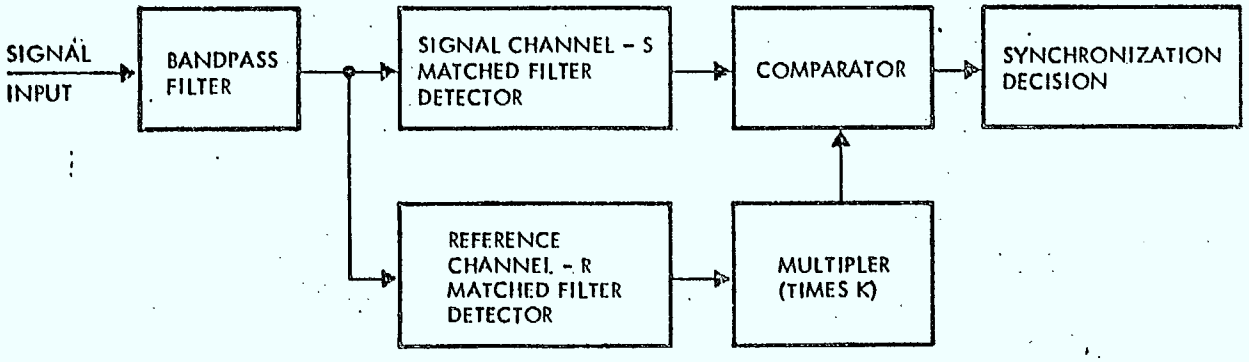

Figure 6. Block Diagram of a Self-Referencing Correlation Detector

2. SURFACE ACOUSTIC WAVE DEVICES

Surface acoustic wave devices (SAWD) are ideally suited for analog matched filtering of direct sequence PN. Chip rates from 50-500 MHz are of small size and weight. Chip rates below 50 MHz can be handled with increasing size and weight for reasonable time-bandwidth products, but it is of debatable practicality to consider chip rates below 2 MHz. However, below 2 MHz, charge coupled devices make excellent match filters for PN.

Surface acoustic wave devices provide wide dynamic range (in excess of 100 dB). The inherent performance of these multi-tap delay lines depends on the accuracy of the tap placement. Tap placement accuracy of ±1 micron of required position ($\pm 14^{0}$ phase error at 120 MHz) can be obtained. Larger phase errors cause partial cancellation between signals from different taps which results in output signal-to-noise degradation. Temperature also presents problems in these lines and a temperature-controlled enclosure of the crystal-oven type must be used.

Single crystal SAWD with delays as much as 120 microseconds and as many as 1000 taps can be implemented.* Note that, for a 10 MHz chip rate, 1000 taps requires 100 microseconds. For delays up to 250 microseconds, the propagation loss becomes significant. For example, at a delay of 250 microseconds and a center frequency of 300 MHz, there is a 3 dB propagation loss and this loss increases as the square of the carrier frequency. As an example of size, a 50-tap delay line has been fabricated on quartz at a center frequency of 120 MHz and a 3 dB bandwidth of 5 MHz. This delay line can be packaged in about eight cubic inches.

3. CHARGE COUPLED DEVICES

The charge coupled device (CCD) was first announced in 1970.** The basic concept is to transfer charge in packets through the device like a bucket brigade. This idea leads naturally to a shift register organization

---

*C.F. Vasile and R. LaRosa, "1000 Bit Surface Wave Matched Filter," Electron. Lett., Vol. 8, 1972, pp. 401-402.

**W.S. Boyle and G.E. Smith, "Charge Coupled Semiconductor Devices," Bell System Technical Journal, BSTJ Briefs, April 1970, pp. 588-593.

shown in Figure 7. Two phase clocks can be used to transfer each individual charge packet from the input to the output circuit. Each packet can be of arbitrary size (within certain limits) and therefore such a shift register represents a true analog sampled data system. The taps in Figure 7 are set to match the PN sequence. Thus, the output signal is correlation function.

In practical terms, the CCD is not simply an ideal analog delay. The transferral of charge from one storage site to the next does not occur with 100 percent efficiency. The small amount of charge lost from a given packet at each transfer introduces an amplitude and phase effect that is dependent on the total number of transfers in the shift register and the charge transfer efficiency. These phase and amplitude effects limit the time delay at a given clock frequency that can be achieved. Figure 8 indicates the typical range of clock frequencies and time delays that are achievable with present day devices. The maximum clock frequency is primarily a function of the device design; charge carrier transit time from one storage device to another will severely limit transfer efficiency for clock frequencies that do not allow sufficient time for the charge to

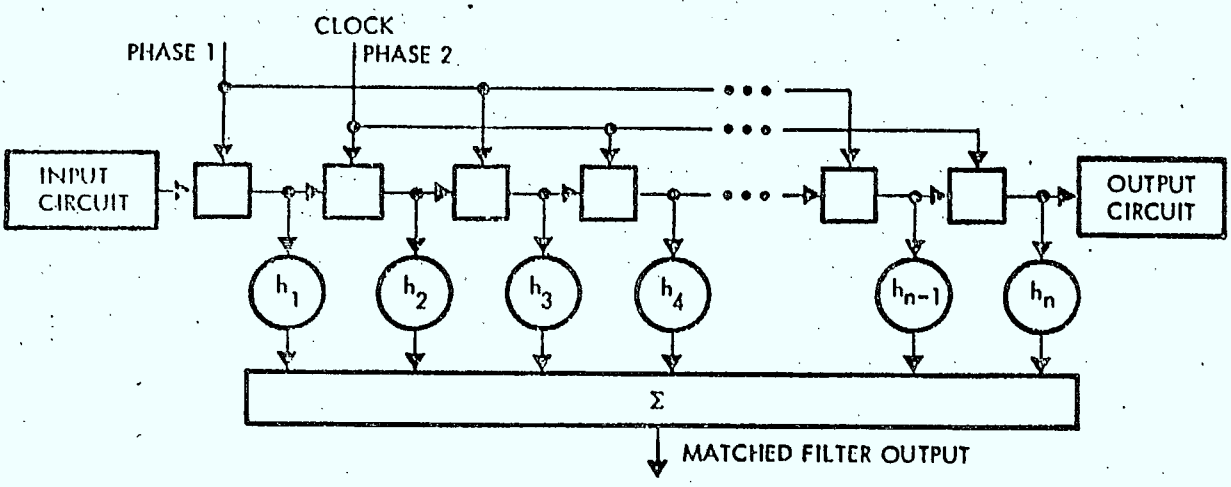

Figure 7. Charge Coupled Device Tapped-Delay Line Matched Filter

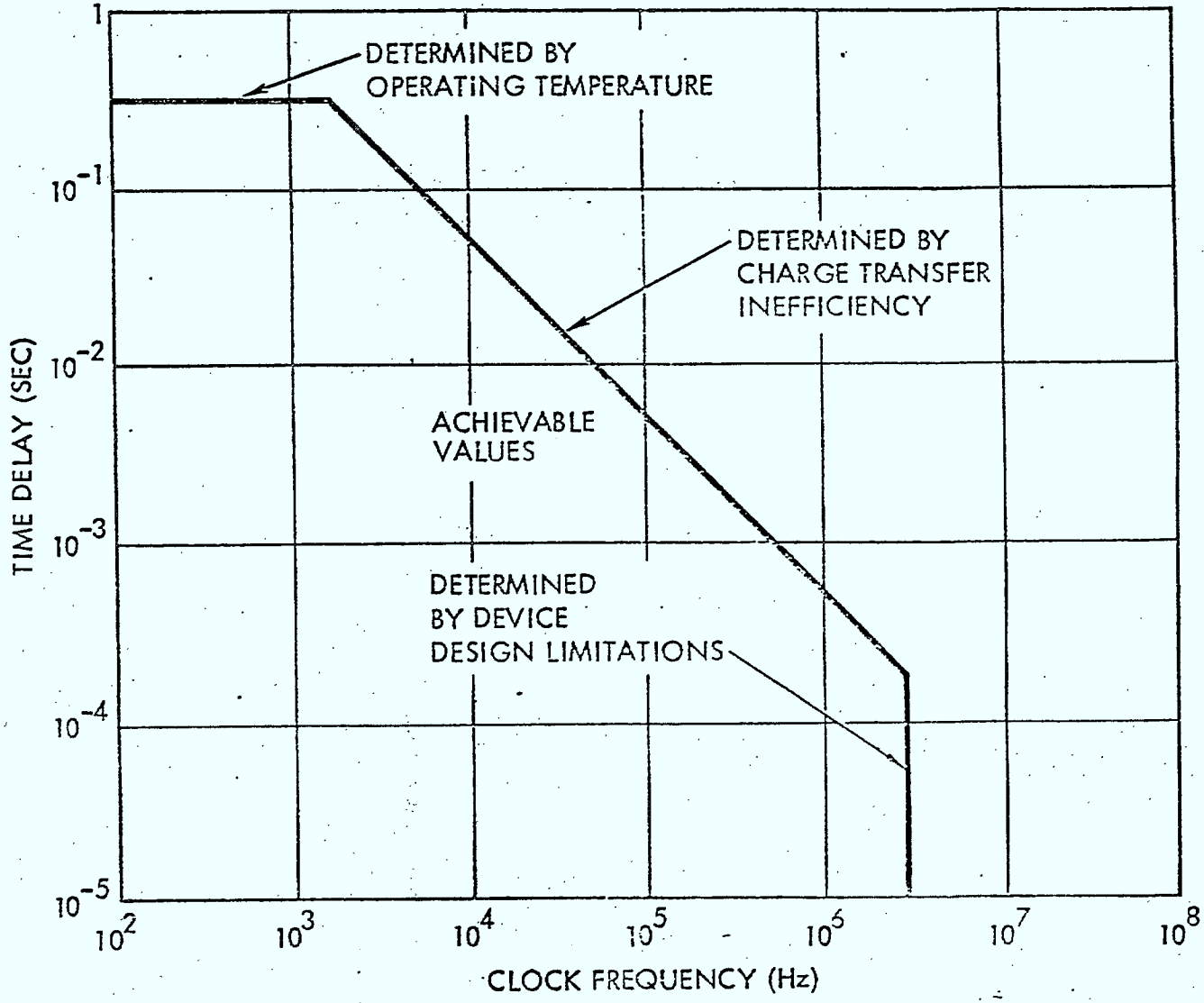

Figure 8. Typical Range of Achievable Time Delay and Clock Frequency Values for Charge Coupled Devices

move equal to the gate length. The maximum delay time limit is mainly a function of temperature. The remaining boundary is due to the phase and amplitude effects introduced by charge transfer inefficiency.

The performance of the CCD is identical to the active correlator except for time sampling. Thus, if a single time sample is made per chip, the worst case loss of 6 dB from the active correlator performance can result. Using a pair of time samples per chip, the worst case degradation is 2.5 dB, but two CCD's must be used in both the in-phase and quadrature channels to handle the two time samples.

4. DIGITAL MATCHED FILTER

Development of large scale integration (LSI) in the microelectronics industry has made a high-speed, low-cost, low-power-consuming, digital matched filter possible. One such development contains 32 stages each of the data register and the reference register (replica code shift register) with the exclusive-OR connecting each stage on a single chip. All 32 exclusive-OR outputs are tied together, providing an analog signal to an external resistor which is proportional to the number of matches (or correlation) between the contents of the two registers. The correlator utilizes the CMOS/SOS technology and can handle chip rates in excess of 50 MHz. A 1024 stage correlator (for 30 dB processing gain) would require 32 each of the 32-bit LSI chips. Such correlator circuits are eminently suited for multi-chip hybrid packaging, with 16 chips in a single one inch by one inch flat pack.

Hard limiting can be used to obtain two levels of quantization (±1). Implementation of a two-level correlator requires the least circuitry but produces the largest degradation in signal-to-noise ratio. Compared with a linear (unquantized) correlation process, the S/N loss is only 2 dB if the accompanying noise is Gaussian distributed with zero mean. While the S/N loss due to Gaussian noise is relatively small, complete loss of correlation can occur whenever the noise or a jamming signal dominates the quantization amplitude (i.e., a random binary waveform whose polarity exceeds that of the quantized signal). Complete loss can be prevented by adding a noise perturbation (dither) prior to the amplitude limiting

process. Alternatively, one is forced to higher quantization levels and a consequent increase in DMF complexity.

If the additive noise distribution is unknown, a minimax dither strategy based on game theory may be used to reduce the signal-to-noise degradation of hard limiting.* For the minimax strategy, the shifting of the quantization level can be controlled by a probability density which is designed to minimize the probability of error for the worst-noise-distribution case. Consequently, while minimizing the effects of a worst-case noise distribution, the degradation effects from the best-case noise distribution become more severe. For a two-level correlator, the minimax loss of S/N ratio is 4.8 dB, regardless of the actual distribution of the noise. This is an additional loss of 2.8 dB when compared to the optimized performance against Gaussian noise of the same power.

In general, the dither signal must conform to the following conditions:

a) Be statistically independent of the signal to which the dither is added.

b) Have zero mean so as not to introduce a bias.

c) Contain no spectral components lower in frequency than the most significant signal component.

d) Periodic-dither frequencies must be incommensurable with the sampling frequency.

e) The dither signal must be at least as great as the quantization interval size, Δ_q.

5. DOPPLER DEGRADATION

For a MF, the immediate question is how best to implement the summations in Equation (4) called for by the doppler shifted replica. In a tapped delay line MF, it is most convenient to restrict the replica to a binary code. However, even if a(t) and b(t) are binary, the doppler shifted replica waveforms are not. Two possibilities may be studied. In the first, the replica waveforms are hard limited to be

*C.R. Cahn, "Performance of Digital Matched Filter Correlator with Unknown Interference," IEEE Trans. on Comm. Tech., Vol. COM-19, December 1971, pp. 1163-1172.

$$\begin{aligned} a(t) &\quad \text{sign } (\cos \Delta\omega t) \\ a(t) &\quad \text{sign } (\sin \Delta\omega t) \\ b(t) &\quad \text{sign } (\cos \Delta\omega t) \\ b(t) &\quad \text{sign } (\sin \Delta\omega t) \end{aligned} \qquad (6)$$

The hard limiting can be performed as the replica is generated. The loss of this convenient approximation must be evaluated accurately. A simple estimate is that the correlation is proportional to the amplitude of the fundamental harmonic in a square wave, corresponding to a power loss of $8/\pi^2$, or 1.0 dB.

The second possibility is to break the summation over the length of the DMF into subparts, in each of which sin $\Delta\omega t$ or cos $\Delta\omega t$ can be assumed constant as a good approximation. The summation result for each subpart at time $t = t_0$ is then weighted by the assumed constant values cos $\Delta\omega t_0$ and sin $\Delta\omega t_0$. Figure 9 shows the conceptual implementation of this approach for a typical weighting.

A different approach to accommodating doppler offset with summation over subparts is to combine noncoherently by performing an envelope

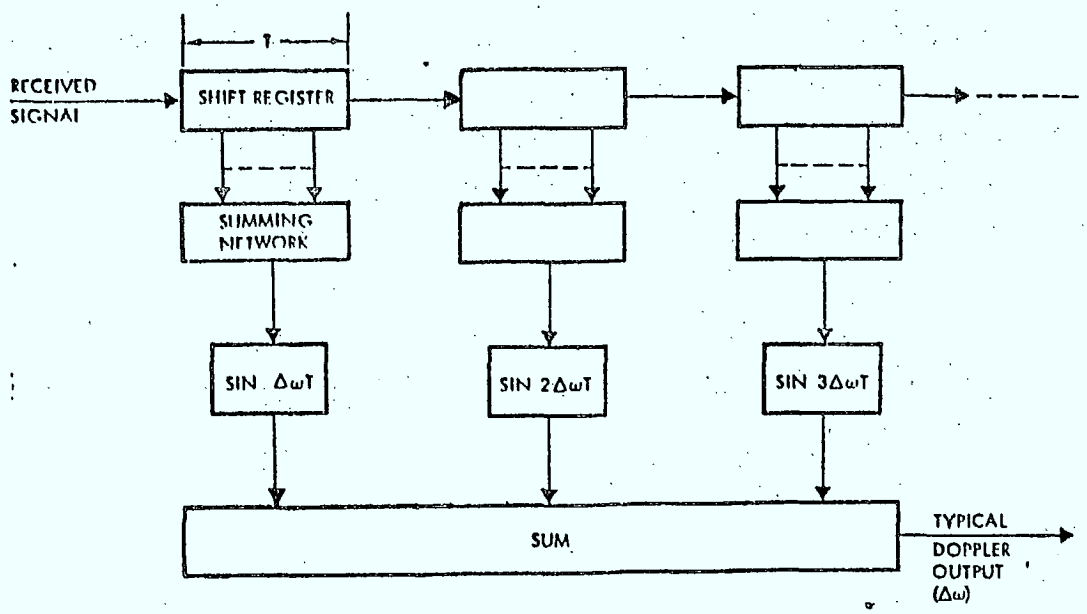

Figure 9. Doppler Weighted Summation of Partial Integration

detection prior to combining the subparts, as shown in Figure 10. The doppler tolerance is increased in direct proportion to the number of subparts; however, there is a detection loss resulting therefrom. Figure 11 shows an estimate of this detection loss as a function of the number of subparts integrated.

An incidental advantage of the noncoherent summation over subparts is that PSK data modulation is directly tolerated with little degradation. Suppose that a single data bit transition on the signal occurs near the center of the integration. The resulting correlation is close to zero. However, with noncoherent summation over subparts, only one of the subparts is lost. The phase reversal is not seen except within a single subpart.

6. CONCLUSIONS

Discussions of the degradation in practical tapped line matched filters have been given. It was shown that the SAWD has only a degradation due to doppler offset but SAWD's for large antijam processing gain are impractical since only a maximum of 1000 taps can be implemented. Even for this number of taps, the SAWD could not be programmable which implies a short PN code for a synchronization preamble. Short PN codes are susceptible to jamming by other short PN codes due to poor cross-correlation properties. Therefore, long PN codes would need to be used which would require a programmable tapped delay line. With programmable taps, SAWD's are limited to 50 taps which severely limits the antijam processing gain.

To obtain longer delays, charge coupled devices and digital matched filters were discussed. The CCD tapped delay line has a degradation due to doppler offset and in addition, a degradation due to time sampling of from 2.5 to 6 dB. Digital matched filters have those degradations as well as a 4.8 dB degradation due to amplitude quantization.

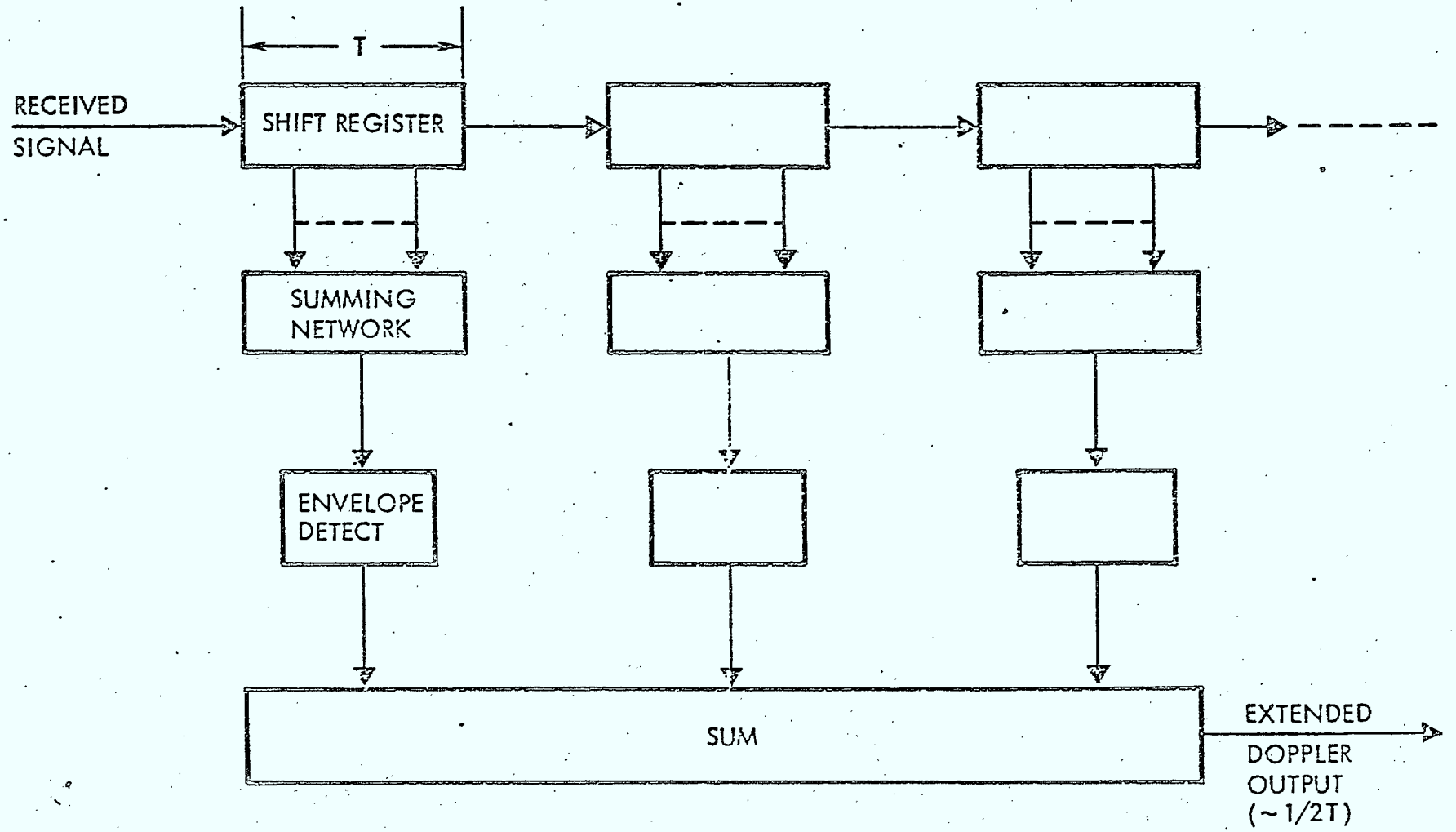

Figure 10. Noncoherent Summation of Partial Integration

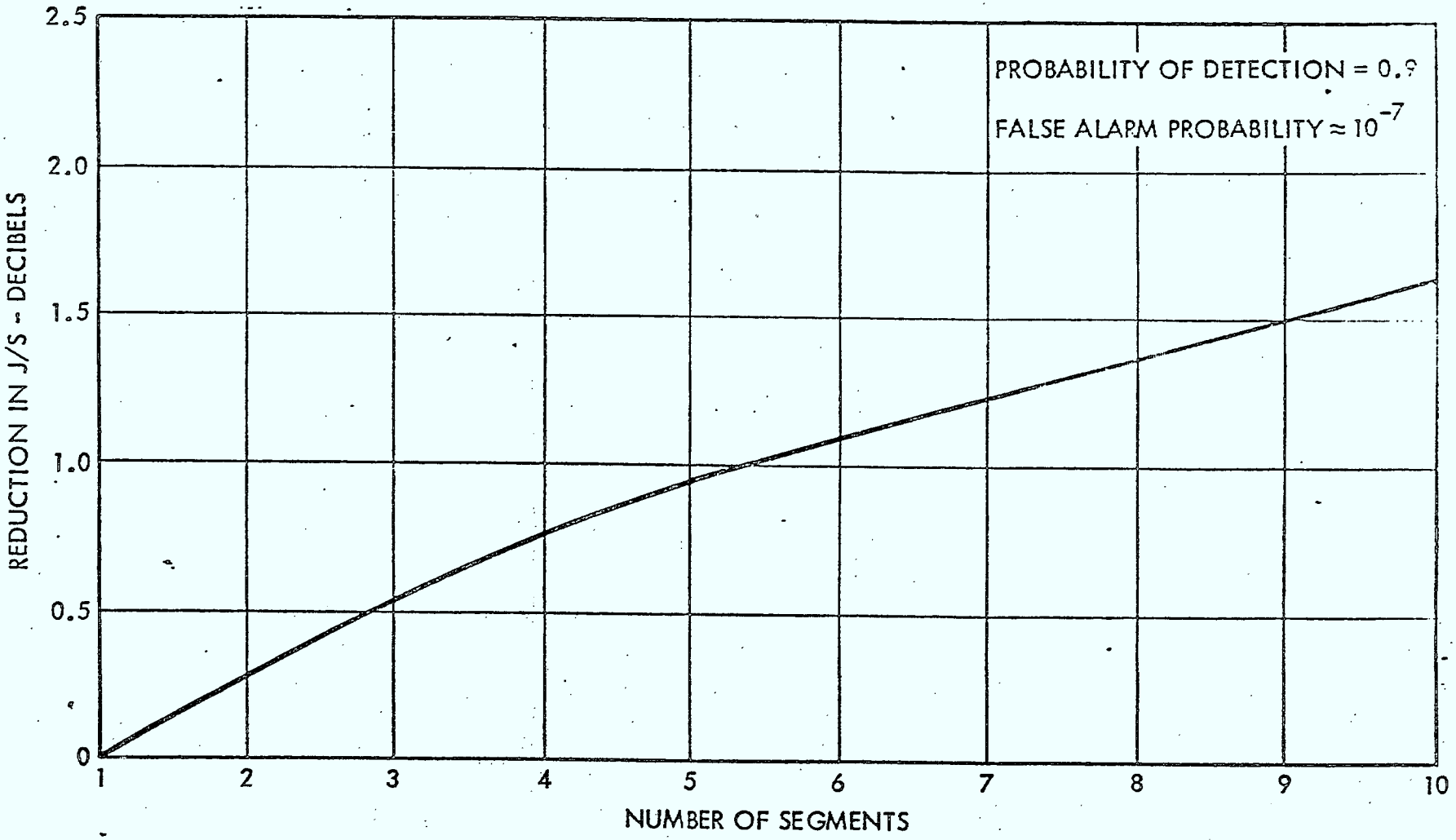

Figure 11. Integration Loss with Noncoherent Summation

APPENDIX B

PERFORMANCE OF DIRECT SEQUENCE PSEUDONOISE/PHASE-SHIFT-KEYING (PN/PSK) MODULATION WITH PULSE JAMMING

PERFORMANCE OF DIRECT SEQUENCE PSEUDONOISE/PHASE-SHIFT-KEYING (PN/PSK) MODULATION WITH PULSE JAMMING

The worst case jammer against PN/PSK spread spectrum modulation is a tone at the carrier frequency that is pulsed with duty cycle α. It is assumed that the jammer chooses the duty cycle to maximize the probability of error for the communication system. It is also assumed that a jammer with average power J can pulse with duty cycle α and achieve a peak power of J/α.

The PSK bit error probability P_b with no pseudonoise spreading is given by[1].

$$P_b = Q(\sqrt{2E_b/N_0}) \tag{1}$$

where

$$Q(x) = \int_{-\infty}^{x} \frac{\exp(-y^2/2)}{\sqrt{2\pi}} dy \tag{2}$$

A jammer tone centered at the carrier frequency will be multiplied by the PN code in the receiver producing a spectrum of the form

$$S_J(f) = \frac{J}{\alpha W} \frac{\sin^2(\pi f/W)}{(\pi f/W)^2} \tag{3}$$

where W is the PN chip rate. If the bit rate is small compared to the PN chip rate, then the jammer appears to the PSK demodulator as approximately white Gaussian noise with spectral density $J/(\alpha W)$. Therefore, when the receiver is jammed, the effective E_b/N_0 is

$$(E_b/N_0)_{eff} = \frac{S/R_b}{N_0 + J/(\alpha W)} \tag{4}$$

where N_0 is the single-sided noise spectral density and R_b is the bit rate. Note that if $J/(\alpha W)$ is much larger than N_0, then

$$(E_b/N_0)_{eff} = \alpha(\frac{S}{J})(\frac{W}{R_b}) = \alpha G \tag{5}$$

1. 1. A.J. Viterbi, Principles of Coherent Communications, McGraw-Hill New York, 1966.

where the ratio (W/R_b) is called the processing gain of the spread spectrum receiver and G is called the performance measure.

The probability of bit error for the pulsed jammed PN/PSK system is

$$P_b = \alpha Q(\sqrt{2(E_b/N_0)_{eff}}) + (1-\alpha)Q(\sqrt{2E_b/N_0}) \qquad (6)$$

where the first term corresponds to the period when the receiver is jammed and the second term corresponds to the unjammed period. It has been assumed that the duration of the jamming pulse is an integer number of information bits. If the jammer pulse duration is less than a single bit, the expression becomes somewhat more complicated, and the jammer is less effective. If $J/(\alpha W)$ is much larger than N_0, then equation becomes

$$P_b = Q(\sqrt{2\alpha G}) \qquad (7)$$

APPENDIX C

PERFORMANCE OF FH-PN/MCSK MODULATION WITH PARTIAL BAND JAMMING

PERFORMANCE OF FH-PN/MCSK MODULATION WITH PARTIAL BAND JAMMING

The worst case jammer against FH-PN/MCSK spread spectrum modulation is multiple tones centered at the hop frequencies and with spacing equal to the PN code rate. The reason this type of jamming is so deleterious is that a CW tone at the hop frequency causes the PN code to spread the jammer energy over the smallest bandwidth of any narrowband interference. However, assuming a large ratio between the MCSK symbol rate and the PN code rate, the Central Limit Theorem can be applied which effectively shows that the noise of the baseband demodulator is wideband Gaussian.

Consider the MCSK symbol probability of error with no frequency hopping and a CW tone of power J at the center of the PN spectrum. Assuming that the MCSK symbol rate is small compared to the PN code rate, let the symbol energy to jamming energy at the output of the PN correlator be denoted by

$$\frac{E_s}{N_0} = \frac{ST_s}{JT_p} = \left(\frac{S}{J}\right)\left(\frac{B}{R_s}\right), \tag{1}$$

where S is the signal power, J is the jammer power, T_s is the symbol duration equal to the inverse of the symbol rate R_s, and T_p is the PN chip duration equal to the inverse of the PN code rate B. Then the probability of symbol error is given by

$$P_E(M,E_s/N_0) = \frac{1}{M}\sum_{i=2}^{M}(-1)^i\binom{M}{i}\exp\left(-\frac{(i-1)}{i}\frac{E_s}{N_0}\right). \tag{2}$$

The probability of bit error for orthogonal signaling is

$$P_B(M,E_s/N_0) = \frac{M}{2(M-1)}P_E(M,E_s/N_0)$$

$$= \frac{1}{2(M-1)}\sum_{i=2}^{M}(-1)^i\binom{M}{i}\exp\left(-\frac{(i-1)}{i}\frac{E_s}{N_0}\right). \tag{3}$$

For partial band jamming with FH-PN, the available jamming power J is divided among q tones of the n possible hop frequencies. The total possible hop frequencies is

$$n = \frac{W}{B} , \tag{4}$$

where W is the total hopping bandwidth and B is the PN code rate. Let α be the fraction of the total hopping bandwidth jammed, that is,

$$\alpha = \frac{q}{n} = \frac{qB}{W} . \tag{5}$$

Note that since the jamming power J is divided into q tones

$$\begin{aligned} \alpha\left(\frac{E_s}{N_0}\right) &= \left(\frac{S}{J/q}\right)\left(\frac{B}{R_s}\right) \\ &= q\left(\frac{S}{J}\right)\left(\frac{B}{R_s}\right) . \end{aligned} \tag{6}$$

Substituting for q from (5),

$$\begin{aligned} \alpha\left(\frac{E_s}{N_0}\right) &= \alpha\left(\frac{W}{B}\right)\left(\frac{S}{J}\right)\left(\frac{B}{R_s}\right) \\ &= \alpha\left(\frac{W}{R_s}\right)\left(\frac{S}{J}\right) . \end{aligned} \tag{7}$$

The symbol energy can be written in terms of the bit energy for uncoded or error correction coded channels as

$$\frac{E_s}{N_0} = \ell\left(\frac{E_b}{N_0}\right) = \frac{\ell}{R}\left(\frac{W}{R_c}\right)\left(\frac{S}{J}\right), \tag{8}$$

where ℓ is $\log_2 M$, the channel data rate is R_c, and the code rate is R. The performance measure used to compare different spread spectrum modulation techniques is given by

$$G = \left(\frac{W}{R_c}\right)\left(\frac{S}{J}\right)\left(\frac{1}{R}\right) . \tag{9}$$

The probability of MCSK symbol error with partial band jamming is

$$P_E(M,\ell GR,\alpha) = \alpha P_E(M,\alpha\ell GR) . \tag{10}$$

The probability of bit error is then

$$P_B(M,\ell GR,\alpha) = \frac{\alpha}{2(M-1)} \sum_{i=2}^{M} (-1)^i \binom{M}{i} \exp\left(-\frac{(i-1)}{i}\alpha\ell GR\right) . \tag{11}$$

The worst case jammer can be found by maximizing P_B with respect to α. Differentiating (11) with respect to α results in

$$\frac{\partial P_b}{\partial \alpha} = \frac{1}{2(M-1)} \sum_{i=2}^{M} (-1)^i \binom{M}{i} \exp\left(-\frac{(i-1)}{i} \alpha \ell GR\right)$$

$$- \frac{\alpha \ell}{2(M-1)} \sum_{i=2}^{M} (-1)^i \binom{M}{i} \left(\frac{(i-1)}{i}\right) GR \exp\left(-\frac{(i-1)}{i} \alpha \ell G\right)$$

$$= 0. \tag{12}$$

Equation (12) can be rewritten as

$$\frac{y-1}{y} = \frac{\sum_{i=2}^{M} \frac{(-1)^i}{i} \binom{M}{i} e^{y/i}}{\sum_{i=2}^{M} (-1)^i \binom{M}{i} e^{y/i}}, \tag{13}$$

where $y = \alpha \ell GR$. The value of y that maximizes the bit error probability is denoted by y_0 and has been evaluated for several values of M. The results are

$$\begin{aligned} &M = 2 && y_0 = 2.0 \\ &M = 4 && y_0 = 2.34 \\ &M = 8 && y_0 = 2.79 \\ &M = 16 && y_0 = 3.49 \\ &M = 32 && y_0 = 3.99 \end{aligned} \tag{14}$$

If α is chosen so that $\alpha \ell GR$ equals y_0, then

$$P_B\left(M, \frac{E_s}{N_0}, \alpha_0\right) = \frac{y_0}{2(M-1)\ell GR} \sum_{i=2}^{M} (-1)^i \binom{M}{i} \exp\left(-\frac{(i-1)}{i} y_0\right)$$

$$= \frac{k}{GR}, \tag{15}$$

where k is equal to a constant calculated from the known values of y_0. Evaluation of k for various values of M results in

$$\begin{aligned} &M = 2 && k = 0.3679 \\ &M = 4 && k = 0.2329 \\ &M = 8 && k = 0.1954 \\ &M = 16 && k = 0.1803 \\ &M = 32 && k = 0.1746 \end{aligned} \tag{16}$$

Note that α is constrained to be less than 1 and so α cannot be chosen so that $\alpha \ell GR$ equal y_0 for all values of G. When α must be chosen equal to 1, then the probability of bit error is given by (11) with $\alpha = 1$. A further restriction on α being chosen optimally is that q and n are integers and only discrete values of α can be obtained. This restriction has little effect as long as q and n are large numbers; but, for q small or n and q small, α must be chosen as the closest possible value to the optimum α and then (11) must be used to calculate the bit error probability.

To reduce these excessive degradations to more reasonable levels requires either fast frequency hopping or coding, or a combination of the two. With a single receiver, transmission of one bit can be broken up into N independent transmissions, each of duration 1/Nth of the bit time. Each such transmission is commonly referred to as a chip. Fast frequency hopping involves transmitting each chip on a different pre-established center frequency, with the N center frequencies widely spaced to cover the available bandwidth. For a channel perturbed by partial band interference, fast frequency hopping provides for independent interference statistics for successive chips.

The demodulator for fast frequency hopping combines the outputs of the M envelope detectors for the N chips. That is, the squared match filter envelope detector outputs for each chip are summed to form the decision statistic. Thus, the statistics based on N hops per M-ary symbol will be

$$z = \sum_{k=1}^{N} (x_k^2 + y_k^2), \tag{18}$$

where x_k is the in-phase correlator and y_k is the quadrature correlator output for the kth chip. The error probability is then

$$P_E = \Pr (z < z'), \tag{19}$$

where z corresponds to the output statistic for the correct signal detector which responds to signal plus noise, and z' to the incorrect signal detector output which responds only to noise. This, of course, assumes as before that the two signals are orthogonal—the optimum case. While the exact expression for this error probability is known,

it involves the integral of special functions and consequently is too cumbersome to yield any insight.* On the other hand, an upper Chernoff bound on P_E is easily obtained. This bound, which is asymptotically exact in exponent when the Chernoff bound parameter λ is optimized, has been shown to be**

$$P_B(\underline{a}) < \frac{M}{4} \prod_{k=1}^{N} \frac{\exp\left[-\frac{\lambda}{1+\lambda}\frac{\ell GR}{N} a_k^2\right]}{1-\lambda^2}, \quad \text{for } 0<\lambda<1, \tag{20}$$

where $\underline{a} = (a_1, a_2, \ldots, a_N)$ are the chip amplitudes and λ is the arbitrary Chernoff parameter.

For partial band noise jamming, a particular chip is perturbed by noise density $J/\alpha W$ with probability α and not perturbed with probability $1-\alpha$. Thus, a_k^2 equals α with probability α and infinity with probability $1-\alpha$. Thus, from (20),

$$P_B(\alpha) < \frac{M}{4} \prod_{k=1}^{N} \frac{\alpha \exp\left[-\frac{\lambda}{1+\lambda}\frac{\ell GR}{N}\alpha\right]}{1-\lambda^2} = \frac{M}{4}\left[\frac{\alpha \exp\left[-\frac{\lambda}{1+\lambda}\frac{\ell GR}{N}\alpha\right]}{1-\lambda^2}\right]^N,$$

$$\text{for } 0<\lambda<1 \text{ and } 0<\alpha<1. \tag{21}$$

The worst case partial band jamming is

$$\max_{0<\alpha<1} P_B(\alpha) < \frac{M}{4} \max_{0<\alpha<1} \min_{0<\lambda<1} \left[\frac{\alpha \exp\left[-\frac{\lambda}{1+\lambda}\frac{\ell GR}{N}\alpha\right]}{1-\lambda^2}\right]^N \tag{22}$$

$$\max_{0<\alpha<1} P_B(\alpha) < \frac{M}{4}\left[\frac{4N}{e\ell GR}\right]^N \tag{23}$$

where the worst choice of α is $\alpha = \frac{3N}{\ell GR}$, and $\lambda = 1/2$ gives the tightest Chernoff bound. The optimum choice of N which minimizes the bit error probability is

$$N = \frac{\ell GR}{4}. \tag{24}$$

---

*C. W. Helstrom, Statistical Theory of Signal Detection, 2nd Ed., Pergamon Press, London, 1968.

**I. M. Jacobs, "Probability-of-Error Bounds for Binary Transmission on the Slowly Fading Rician Channel," IEEE Transactions on Information Theory, Vol. IT-12, October 1966, pp. 431-441.

Using the optimum choice of N with all values of G,

$$\min_{N} P_B = \frac{M}{4} \exp\left[-\frac{\ell G R}{4}\right] . \tag{25}$$

Thus, by fast frequency hopping at N hops per M-ary MFSK symbol, the probability of bit error decreases exponentially with G instead of linearly as with normal frequency hopping. However, the values N must be integers and there is a linear variation with G for a fixed N. Again note there are restrictions on α to be less than 1 and α may not be exactly equal to the optimum, due to the possible values of q and n. When α is not equal to the optimum, then the probability of bit error is given by

$$P_B(\alpha) = \frac{M}{4}\left[\frac{4}{3}\alpha \exp\left[-\frac{\ell G R}{3N}\alpha\right]\right]^N . \tag{26}$$

The FH-PN/MCSK antijam performance for various values of N and M are presented in Table 1 for bit error probability of 10^{-3}. The rate 1/2 coding is a convolutional code with constraint length 10 and the decoding is binary feedback. The optimum partial jam band α in Table 1 is given in percent where there has been no restriction placed on α to take on any discrete ratio of q to n. Therefore, the results in Table 1 provide a first cut at the worst case jammer for any FH-PN/MCSK system. The next step is to choose an allowed value of α and use equations (11) or (26). The results in Table 1 show that increasing the number of hops per symbol and employing rate 1/2 coding increases the optimum jam band, while increasing the bits per symbol decreases the optimum jam band. Note, however, that with M = 16, N = 8 and rate 1/2 coding, the jammer is forced to jam the total band.

Table 1. Anti-jam Performance for Multiple Code Shift Keying

Hops/Symbol	Bits/Symbol	Code Rate	Percent Partial Jam Band	Performance Measure G (dB)
1, 1/2, 1/3, 1/4, 1/6, 1/12, 1/24	2	1	0.50	23.7
		1/2	13.4	12.4
	3	1	0.48	22.9
		1/2	12.7	11.7
	4	1	0.48	22.6
		1/2	12.9	11.3
2	2	1	6.40	16.7
		1/2	33.0	12.6
	3	1	4.60	16.4
		1/2	23.6	12.3
	4	1	3.24	16.7
		1/2	16.6	12.6
4	2	1	36.2	12.2
		1/2	83.2	11.6
	3	1	30.4	11.2
		1/2	69.6	10.6
	4	1	25.6	10.7
		1/2	58.4	10.1
8	4	1	72.4	9.2
		1/2	100.0	10.4